To the Graduate Council:

I am submitting herewith a thesis written by Mussie Wossene entitled "Corrosion of Zinc and Iron-Zinc Galvanic Couples in $HCO_3^-$, $CO_3^=$, $NO_3^-$ and $Cl^-$ Environments." I have examined the final copy of this thesis for form and content and recommend that it be accepted for the degree of Master of Science, with a major in Metallurgical Engineering.

E.E. Stansbury

E.E. Stansbury, Major Professor

We have read this thesis
and recommend its acceptance:

Charlie R. Brooks

Roy O. Vanderveen

Accepted for the Council:

C.W. Minkel

The Graduate School

# CORROSION OF ZINC AND IRON-ZINC GALVANIC COUPLES IN $HCO_3^-$, $CO_3^=$, $NO_3^-$ AND $Cl^-$ ENVIRONMENTS

A Thesis

Presented for the

Master of Science

Degree

The University of Tennessee, Knoxville

Mussie Wossene

June 1984

# DEDICATION

The author would like to dedicate this thesis to his family, particularly his fiancée, Elizabeth Getachew. Without their support, research of this nature would not be possible.

# ACKNOWLEDGEMENTS

The author would like to express his deep gratitude to his major professor, Dr. E.E. Stansbury, for his kindness, perserverance and patience. Through many discussions he has clarified for the author many of the complexities of electrochemical corrosion.

The Department of Chemical, Metallurgical, and Polymer Engineering has provided excellent laboratory facilities, materials and a competent, helpful staff. Mr. Ted A. Long, Sr. and his electronics group, Mr. Stephen A. Steiner, Mr. Ronald L. Johnson and Mr. Michael R. Neal, for their work maintaining the corrosion lab equipment.

Thanks are also extended to the departmental machine shop led by Mr. H.B. Thompson and his staff for their help with assorted sample preparations.

Special thanks are due to Mr. Bob L. McGill for his help with scanning electron microscopy and to Mr. Albert W.J. Carter and Mrs. Aileen Cagle for distributing many of the materials necessary to this research.

Financial support provided by the Department of Chemical, Metallurgical and Polymer Engineering are gratefully acknowledged.

The support of the ladies in the department office, Mrs. Sancy Hail, Mrs. Betty Frazier and particularly the author's typist, Mrs. Phyllis Davis, is most gratefully acknowledged.

Last but not least, the author would like to thank his fellow graduate students who provided a congenial work atmosphere.

# ABSTRACT

The general corrosion and electrochemical behavior of zinc and iron-zinc couples was explained in water and aqueous solutions containing $HCO_3^-$, $NO_3^-$, $CO_3^=$, and $Cl^-$ environments within the temperature range 30-60°C under stagnant, aerated and deaerated conditions.

Bicarbonates, nitrates and carbonates cause the potential of the zinc to increase. This results in a potential reversal of iron-zinc couples which is accelerated by higher temperature (60°C) and is promoted by the presence of oxygen. The increasing potential of the zinc is due to a very compact film of zinc corrosion products. The film does not appear to be associated with the typical transition to a passive state. It is proposed that the effect may relate to the semiconducting properties of the film and the progressively decreasing anode/cathode area ratio as it forms.

For zinc in chloride solutions, a potential reversal does not occur. The galvanic current remains high and constant. The electrode potential of the iron is depressed well below its equilibrium value and the surface remains bright and free from corrosion product throughout the test period of the weeks.

The morphology of the corrosion product film and the substrate were investigated with a scanning electron microscope. The surface morphology was very dependent on the environmental conditions. In the bicarbonate solutions, most of the oxide film, before removing the corrosion product, revealed a dense cellular type structure with protrusions. However, in chloride solutions, the corrosion deposit

appears to be flaky, and does not show any cellular structure. Upon removing the corrosion product formed, in both bicarbonate and chloride solutions, the highly localized and crystallographic nature of attack was observed.

X-ray analysis was used to examine the corrosion product. A moist film examined immediately following removal from the environment, results in a broad diffraction pattern indicating amorphous or poorly developed crystalline material. Dried films showed well defined diffraction peaks for zinc oxide.

Polarization measurements were undertaken in an attempt to provide insight into the corrosion mechanisms responsible for the weight loss, potential-time behavior and surface morphology observations. Although schematic polarization curves could be developed which were consistent with the experimentally measured polarization curves, a satisfactory understanding of the corrosion behavior, particularly the cathodic reactions supporting the corrosion was not developed. Rather these measurements served to demonstrate that the corrosion mechanisms are quite complex and the present results shed some light on the information available in the literature.

TABLE OF CONTENTS

# LIST OF TABLES

# LIST OF FIGURES

FIGURE PAGE

FIGURE PAGE

FIGURE PAGE

# CHAPTER 1

## INTRODUCTION

Cathodic protection is a widely accepted method of corrosion control. In cathodic protection, the corrosion rate of a metal is decreased by decreasing the half-cell potential of the metal from $E_{corr}$ to some lower value and in the limit to $E_{M,M^+}$, the open circuit or thermodynamic equilibrium potential of the metal. At this potential, $I_o = \vec{I}_M = \overleftarrow{I}_M$ and net transfer of metal to the solution no longer occurs (1). Here Io is called the exchange current density, $\vec{Im}$ is the anodic component, and $\overleftarrow{Im}$ is the cathodic component of the equilibrium $M \rightarrow M^+ + e$ (1,2,3).

Cathodic protection is generally accomplished by one of the following two methods:

1. cathodic protection by impressed current;
2. cathodic protection by sacrificial or galvanic anodes.

It is the purpose of this study to investigate some of the variables controlling cathodic protection by coupling zinc to iron. The principal information to be derived from the research is a better understanding of the following:

1. The zinc-iron potential reversal which is observed under certain environmental conditions. This is done through measurements to determine the effect of electrolyte composition and temperature on the electrochemical relationship between zinc and iron. Electrolytes to be studied include

those based on bicarbonates, nitrates, carbonates and chlorides.

2. Determination of the polarization characteristics of the metals coupled and uncoupled, including both open circuit potential measurements and potentiostatic polarization measurements.
3. Measurement of the galvanic current density and relation of the local corrosion current density, $i_{corr}$, to the polarization curves of iron, zinc and the zinc-iron couple.
4. Other variables include pH, solution resistivity, and degree of aeration.

The potentiostat is employed in this investigation as it enables a variety of practical environmental conditions to be simulated in the laboratory. The potentiostat maintains a constant potential with reference to a standard electrode and the resultant current flow may be related to the rate of electrochemical reactions on the sample at that potential (2,3). By altering the applied potential, changes in oxidizing or reducing conditions may be experimentally produced. By plotting potential versus current, a "polarization curve" is obtained. Such a curve indicates how a material behaves when exposed to various environments, and on the basis of this, comparison may be made between materials for use in particular types of environments, i.e., an estimate of corrosion rate can be made. Other techniques include $E_{corr}$ vs. time using electrometer measurements recorded by a microprocessor and galvanic current measurements using a zero resistance ammeter.

Two other important experimental techniques, SEM and X-ray diffraction were used in an attempt to better understand the nature of the corrosion product film formed.

# CHAPTER 2

## LITERATURE REVIEW

This chapter provides a brief summary of the significant results of published papers relating to the research.

### Galvanic Coupling

Zinc is one of the metals most widely used as a protective coating for iron and steel. Aside from economic advantages there is one important factor which accounts for the widespread use of zinc, which is the electrochemical protection afforded to the iron or steel at bared areas. When contacting zinc and iron are exposed to an electrolyte, a galvanic cell is formed in which the iron usually is cathodic and is protected by the galvanic current from the anodic zinc into the environment (electrons flow from zinc to the iron). Because of this protection, certain zinc coated steel products have come to be known as "galvanized steels" (4,5).

Coupling is associated with corrosion potentials and corrosion current densities which change significantly from the values for the two metals in the uncoupled condition (5,6). This necessary condition was demonstrated very simply by Farady who experimented with zinc, or rather zinc-coated, nails and small steel plates. Placing both in small vessels containing fresh and salt water he showed that when the zinc and iron were in electrical contact in sea water the iron did not corrode. When the zinc was not in electrical contact with the iron and also when there was electrical contact between

them in fresh water, the iron corroded. The galvanic effects are influenced by the relative areas of anode and cathode, the resistance of the electrochemical circuit including the resistance that exists at the junction between the two metals, oxygen supply, electrolyte composition, the presence of ionic species such as bicarbonate, nitrate and carbonate which can lead to potential reversal, and as well as several other factors that normally influence corrosion processes (1).

The electrochemical behavior of iron and zinc is important to the understanding of the effects of coupling. Considerable information exists on iron but review of the literature indicates relatively little basic information on the mechanism of corrosion of zinc, in the pH range of "neutral" environments (pH = 4-9). An extensive literature exists for strongly alkaline solutions in which the electrochemical behavior is important in battery technology.

## Overview of Electrochemistry of Corrosion

Before reviewing the literature on the corrosion behavior of iron-zinc couples and iron and zinc as they relate to coupling, an overview is given of the electrochemical principles involved. The overview is presented in terms of what Fontana and Green have called the "Modern Theory" (4). This theory is actually based on the theory of Wagner-Traud (4,7) referred to as the mixed-potential theory.

The electrochemical theory of corrosion was proposed as a result of observations on the behavior of zinc in aqueous media. This can

be illustrated by the oxidation reaction:

$$Zn \rightarrow Zn^{++} + 2e \qquad (1)$$

This occurs at areas called anodes, defined as sites where oxidation occurs. The rate of this reaction is found to be dependent upon the rate of cathodic reactions, hence the corrosion rate is "cathodically controlled," depending on pH and dissolved oxygen typical reactions at cathode areas are:

$$2H_{ADS} + 2e \rightarrow H_2 \qquad (2)$$

$$2H_2O + 2e \rightarrow OH^- + H_2 \qquad (2a)$$

$$2H_{ADS} + 1/2O_2 + 2e \rightarrow H_2O \qquad (3)$$

$$1/2O_2 + H_2O + 2e \rightarrow 2OH^- \qquad (3b)$$

Reaction 2 is fairly rapid in acids, but is very slow in alkaline or neutral media. Reaction 1 can be speeded up by dissolved oxygen according to reactions 3 and 3b. The cathodic reaction rate, and the overall corrosion rate for these reactions is proportional to the rate of diffusion of oxygen to the metal surface. The diffusion rate in turn is proportional to the concentration of dissolved oxygen in the aqueous environment (1).

If a metal is placed in a solution containing its ions, a potential difference exists between the metal and the solution. This potential can be measured with a high impedence voltmeter or electrometer relative to a reference electrode placed in the solution, providing that no other electrochemical reactions occur. This potential

is called a "half-cell potential" because it is for an electrochemical reaction that must be accompanied by another half-cell reaction, with corresponding half-cell potential, in order to have a net chemical change producing a cell potential. The value of the reference electrode potential is determined relative to the standard hydrogen electrode (SHE) and hence the half-cell potentials may be corrected to the SHE scale. By convention, the hydrogen reaction, $2H^+ + 2e \rightarrow H_2$ is assigned a standard half-cell potential of zero volts, at $PH_2 = 1$, $aH^+ = 1$. All other half-cell potentials are measured reported to that of hydrogen.

A half-cell potential depends on the concentration of the ions in the solution. If metal ions are present in the amount of 1 gram-atom/l. (i.e., unit activity), the half-cell potential is called a "standard half-cell potential." If the latter is known, then the half-cell potential at any concentration can be calculated from the Nernst equation (3,4,8). For the half-cell reaction:

$$V_1\ \text{red1} + V_2\ \text{red2} + \ldots V_i \text{redi}\ V_1\ \text{oxid1} + V_2\ \text{oxid2} + \ldots V_j\ \text{oxidj} + ne$$

$$E = E_o + 2.3\ (RT/nF) \log\ II[\text{oxid}]_i^{\nu} / II[\text{red}]_j^{\nu} \qquad (4)$$

where: E is electrode potential

$E_o$ is equilibrium electrode potential

2.3 is conversion factor

R is gas constant

T is absolute temperature

n is number of charges carried

F is Faraday

II[oxid] is the product of variable species on the oxidized side of the half-cell reaction (electron produced) raise to coefficient, $V_i$.

II[red] is the product of variable species on the reduced side of the half-cell reaction (electron consumed) raise to coefficient, $V_j$.

Polarization

When the cell is short-circuited or connected to an external voltage or current source such that net oxidation and reduction processes occur at the electrode interfaces, then the electrode potentials are no longer at the equilibrium values, and the electrodes are said to be polarized (3,4,8). The magnitude of polarization of a half cell is frequently measured in terms of its overvoltage $\eta$, which is the value of the polarized electrode potential relative to the equilibrium potential of the electrode, that is,

$$\eta = E_{pol} - E_{eq} \qquad (5)$$

Where $\eta$ is the overpotential, $E_{pol}$ is the polarized potential, $E_{eq}$ is the equilibrium potential.

Electrochemical polarization can be divided into two main types: (1) activation or charge transfer polarization, and (2) concentration, or diffusion controlled polarization. When a metal is in a solution containing its ions, the system is said to be in its

equilibrium state when the rate of oxidation is equal to the rate of reduction. Since ions are transferred, the movement can be expressed in terms of charges transported per unit time, or in terms of current density, i. Positive ions going into solution are said to constitute an anodic current density, $\vec{I}_M$, where ions passing from the solution constitute a cathodic current, $\overleftarrow{I}_M$. Hence at equilibrium, $\vec{I}_M = \overleftarrow{I}_M = I_{o,M}$, where $I_{o,M}$ is called the exchange current density (4,8). (See Figure 1.)

If the rate of both partial reactions occurring at an electrode are determined by a slow electrochemical step, at the interface, then the reaction said to be activated and the rates are under charge transfer control. Polarization which is controlled by this type of process is called charge transfer polarization. Charge transfer polarization, $\eta$, of any kind increases with current density, i in accord with the Tafel equation (3,4).

$$\eta = \pm \beta \log i/i_o \qquad (6)$$

Where i is the rate of oxidation or reduction in terms of current density, and $\beta$ is frequently called the Tafel constant; the positive value applies to the anodic and the negative value to the cathodic polarization of the respective directions of the partial electrochemical reactions.

When the reaction rate or the applied external current is so large that the species being oxidized or reduced cannot reach the surface fast enough, then the system is said to be under concentration, or diffusion controlled polarization. The solution adjacent

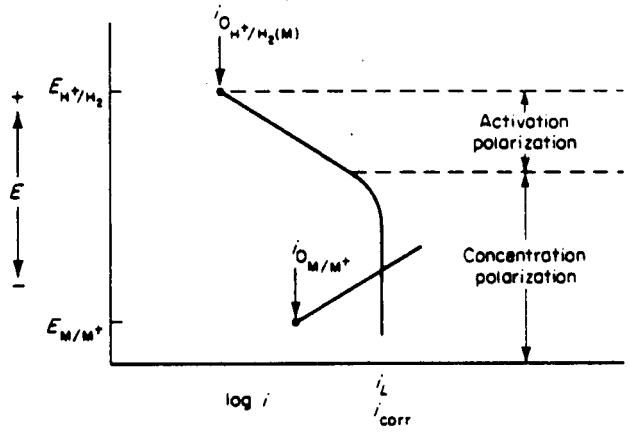


Figure 1. Combined polarization curve activation and concentration polarization.

Source: Fontana, M.G., and Green, N.D., "Corrosion Engineering," McGraw-Hill Book Co., 1967.

to the electrode surface becomes depleted of the reacting ions, and the reaction is then controlled by the rate at which the reacting species can diffuse to the surface. This limiting rate may be expressed as the limiting diffusion current density, $i_D$. It represents the maximum rate of reduction possible for a given system, and is given for limiting diffusion of a single species (1,7):

$$i_D = DnFc/x \tag{7}$$

where D is diffusion coefficient of the reacting specie, c is the concentration of the reacting species, x is the thickness of the diffusion layer, and $\eta$ is the number of electrons involved in the discharge process. The effect of concentration polarization on overvoltage can be given as:

$$\eta c = -2.3\ RT/\eta F\ \log(1-i/i_D) \tag{8}$$

Both charge transfer and concentration polarization usually occur at an electrode. At low current densities, charge transfer polarization usually controls, while at higher current densities concentration polarization becomes controlling. The total polarization of an electrode is the sum of the contribution of charge transfer polarization and concentration polarization.

During reduction processes such as hydrogen evolution or oxygen reduction, concentration polarization becomes important as the reduction rate approaches the limiting diffusion current density. The overall reaction for a reduction process is given by (3)

$$\eta red. = -\beta \log i/i_o - 2.3\ RT/\eta F \log(1-i/i_D) \qquad (9)$$

Equation 9 is graphically illustrated in Figure 2. Equation 9 applies to any reduction reaction where one species is diffusion rate controlling. An equivalent equation applies close to the early stages of all anodic dissolution reactions. However, exceptions occur for metals which demonstrate active-passive behavior. The kinetics of most cathodic reactions can be described (3,4,8) using only these basic parameters, namely, $\beta$, $i_o$ and $i_D$.

Polarization measurements must take into account a potential drop measured between the electrode and the reference electrode; it includes the potential drop across the electrolyte and any corrosion products (i.e., surface films). This resistance polarization is important only at high current densities or in high resistance solutions (7,8).

## Mixed-Potential Theory

> The mixed-potential theory consists of two simple hypotheses: 1. Any electrochemical reaction can be divided into two or more partial oxidation and reduction reactions. 2. There can be no net accumulation of electrical charge during an electrochemical reaction (4).

From the above hypotheses, the corrosion of a physically isolated metal requires that the overall rate of oxidation must equal the overall rate of reduction. The mixed potential theory is easily shown by considering mixed electrodes. A mixed electrode is defined as an electrode or metal which is in contact with two or more oxidation-reduction systems. The theory is briefly discussed by reference to figures based on the treatment by Fontana and Greene (4).

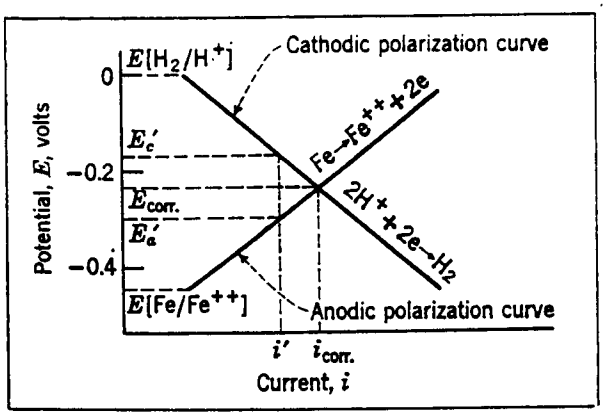


Figure 2. Polarization for iron in acid solution.

Source: Henthrone, M., "Corrosion and the Process Plant," J. Chemical Engineering, 1971-1972.

Figure 3 represents schematically the polarization of zinc immersed in hydrochloric acid, and shows that zinc is rapidly corroded by hydrochloric acid (4). A steady potential is achieved when the second hypothesis of the mixed potential theory is satisfied; that is, when the total rate of oxidation equals the total rate of reduction. This intersection represents the only point where the total rate of oxidation and reduction are equal and is identified as the mixed potential or $E_{corr}$. This is the point where the zinc dissolution i is equal to the hydrogen evolution which is expressed in terms of current, and called the corrosion current, $I_{corr}$, and represents the rate of zinc dissolution. The corrosion current, $I_{corr}$, divided by the corroding metal area is the corrosion current density, $I_{corr}$, which is directly related to penetration rate, providing corrosion is uniform.

A schematic diagram from Fontana and Green for the corrosion behavior of iron in dilute hydrochloric acid solution is shown in Figure 3. The iron dissolution and hydrogen evolution on iron are shown. Similar polarization curves for zinc were shown in Figure 4. In each case, the metal dissolution and hydrogen evolution represents steady state corrosion. It should be noted that although the free energy for iron is smaller than that of zinc, the corrosion rate of iron is greater than that of pure zinc when exposed to identical concentrations of hydrochloric acid. Comparisons of the figure indicate that "this is due to the very low exchange current density for the hydrogen-evolution reaction on the zinc surface."

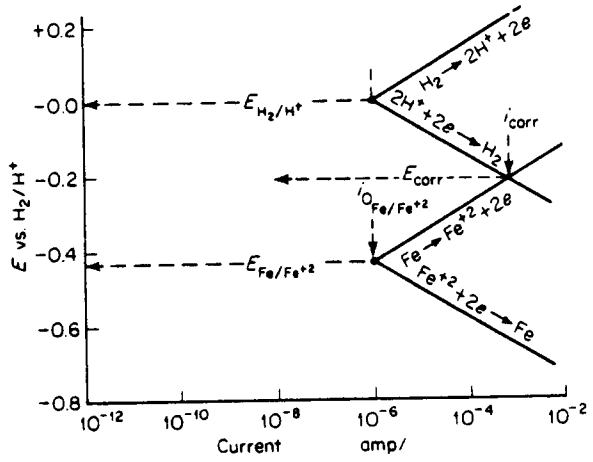


Figure 3. Electrode kinetic behavior of pure iron in acid solution.

Source: Fontana, M.F., and Greene, N.D., "Corrosion Engineering," McGraw-Hill Book Co., 1967.

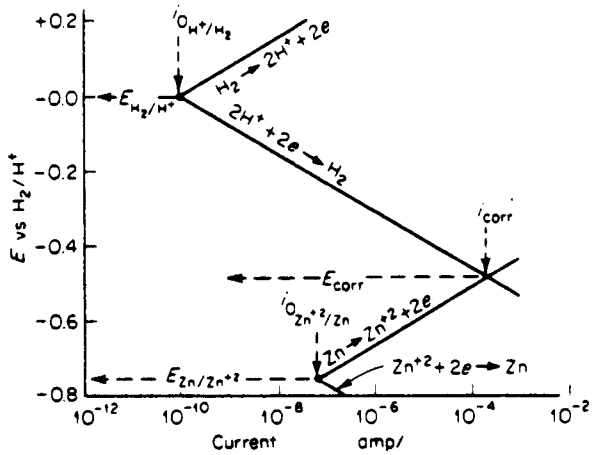


Figure 4. Electrode kinetic behavior of pure zinc in acid solution.

Source: Fontana, M.G., and Greene, N.D., "Corrosion Engineering," McGraw-Hill Book Co., 1967.

The schematic diagram in Figure 5 illustrates the corrosion behavior of a metal in acid containing ferric salts (4). Again, the concept of mixed-potential theory can be applied to this type of more complex systems. At steady state, "the total rate of oxidation is determined by summing the individual oxidation currents corresponding to metal dissolution, hydrogen-gas oxidation, and ferrous ion oxidation at constant potentials." Similarly, "the total rate of reduction is determined by summing the total reduction currents corresponding to ferric ion reduction, as is shown in Figure 5." The only point in this system where the total rate of oxidation and reduction are equal is at the intersection represented by the mixed or corrosion potential, $E_{corr}$.

Electrochemical Behavior of Active-Passive Metals

From an electrochemical viewpoint, the phenomenon of passivity may be described by the schematic, anodic polarization curve shown in Figure 6 (3,4,7,10) a logarithmic scale permits the presentation of a wide range of current densities. As the potential is made increasingly more noble, the dissolution rate of a typical active-passive metal passes through a maximum and then remains essentially independent of potential. At very noble potentials, dissolution rates again increase. As shown in Figure 6, the behavior of an active-passive metal can be divided into three different regions: active, passive and transpassive. Almost all metals and alloys which demonstrate active-passive behavior can be characterized by an S-shaped curve such as Figure 6. The most important parameters describing the

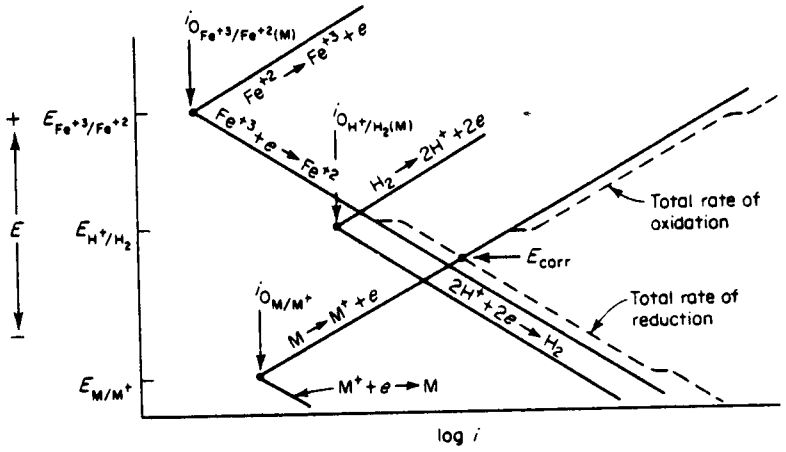


Figure 5. Behavior of metal M in acid solution containing ferric salts showing determination of $E_{corr}$ .

Source: Fontana, M.G., and Greene, N.D., "Corrosion Engineering," McGraw-Hill Book Co., 1967.

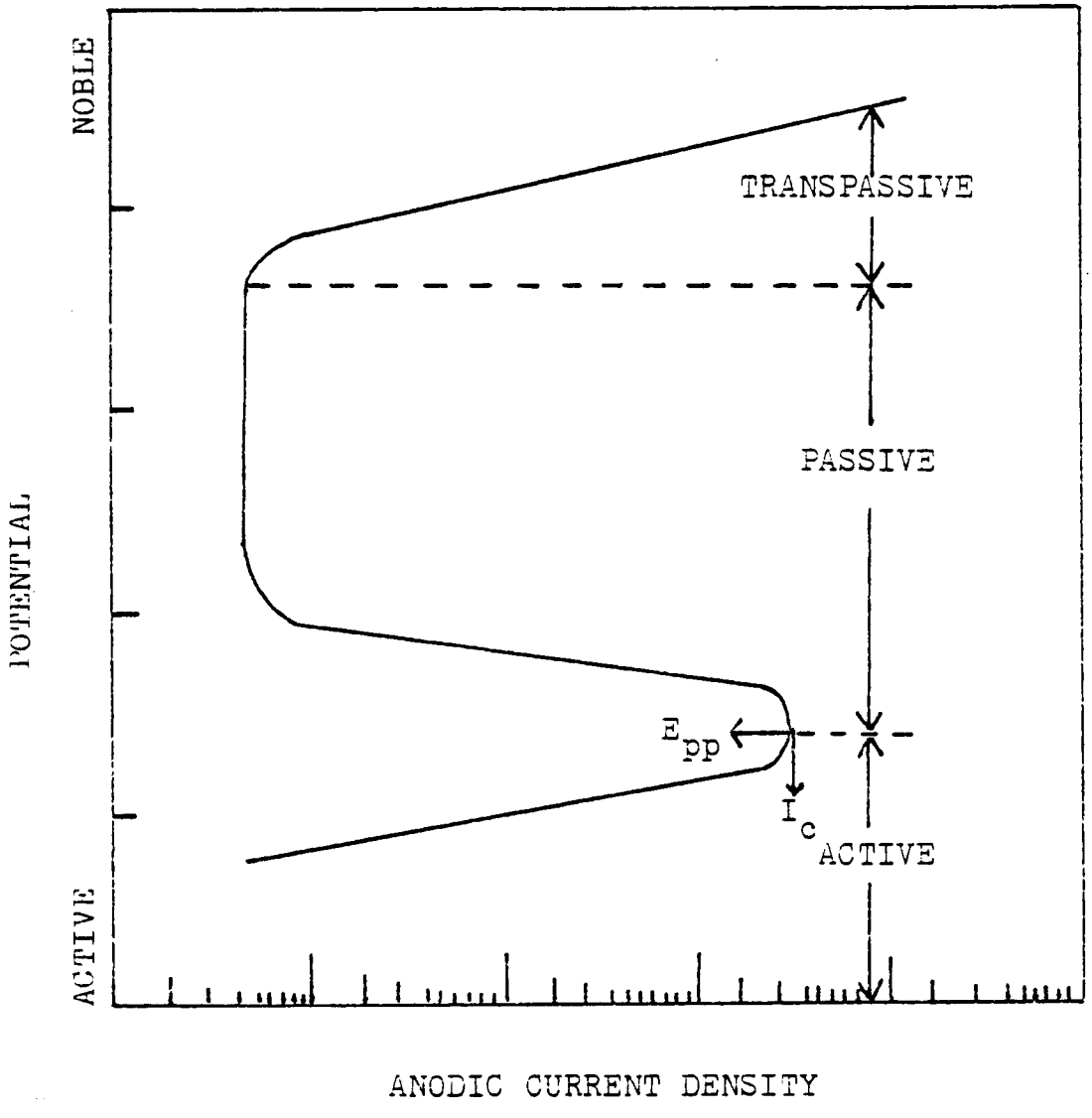


Figure 6. Typical anodic dissolution behavior of an active passive metal.

behavior of an active-passive metal are the potential and current corresponding to the current maximum. Here, these are temred the primary passive potential, $E_{pp}$, and critical anodic current density, $I_{crit}$.

A polarization curve such as Figure 7 provides a unique means of describing and predicting the dissolution or corrosion behavior of a metal which demonstrates an active-passive transition (10). For example, it is possible to determine:

1. the passive potential region;
2. the passive corrosion rates;
3. the relative stability of the passive state;
4. the conditions necessary for achieving passivity.

Furthermore, it is possible to compare the behavior of two different elements on the basis of these properties.

When a metal is exposed to a corrosive media, two processes occur on its surface--oxidation and reduction. For a metal which demonstrates an active-passive transition, this can be illustrated by superimposing a cathodic reduction polarization curve. Figure 7 illustrates three different conditions which can arise when a cathodic process is superimposed. The three curves represent different activation control reduction processes with different exchange current densities. For case 1 there is only one stable corrosion potential and current at A. That is, at point A, the condition that total rate of oxidation equals the total rate of reduction is fulfilled. In case 2 there are three points (B, C and D) where the rate equality

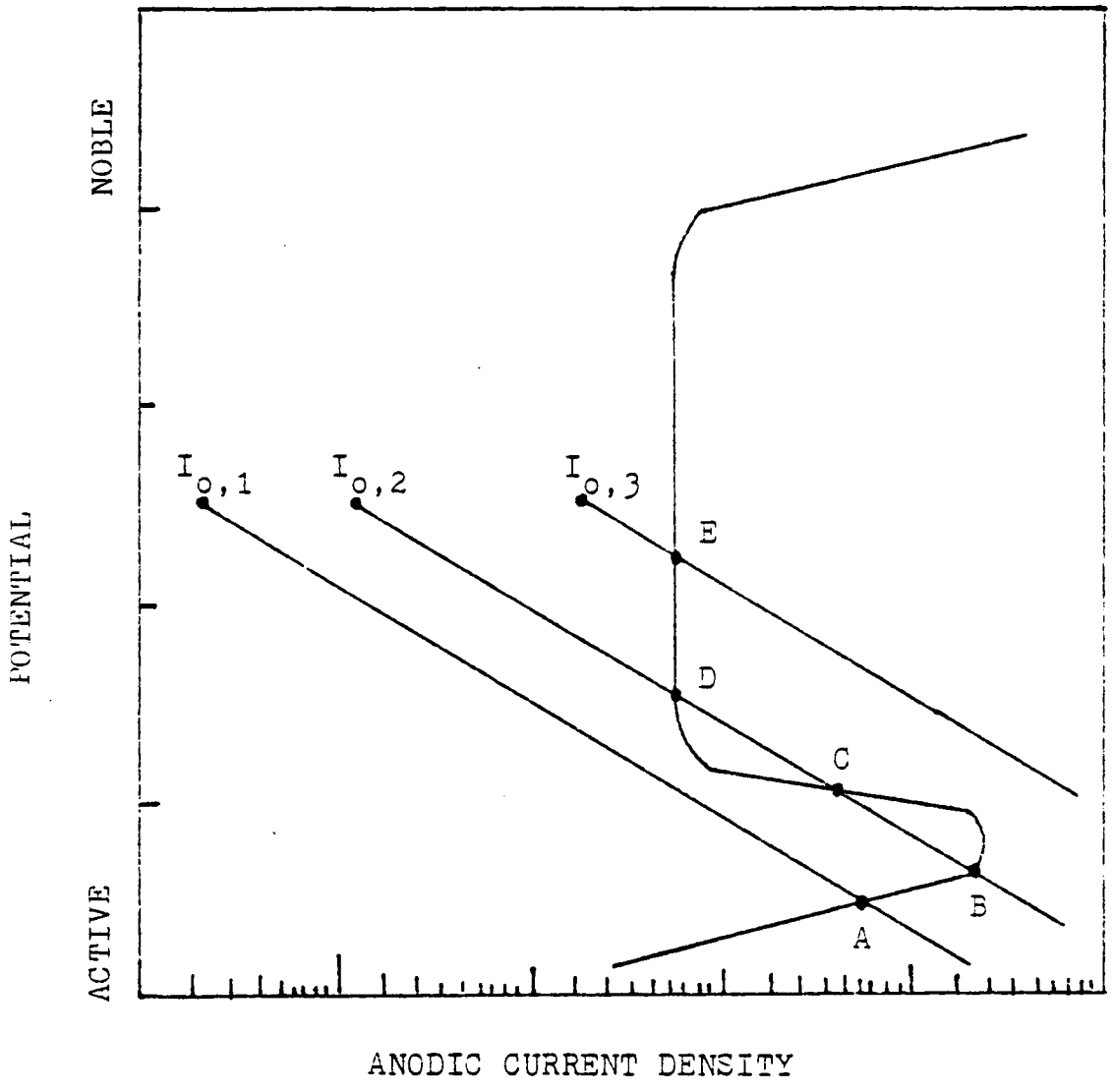


Figure 7. Behavior of an active passive metal under corrosive conditions.

criteria is fulfilled. However, point C does not represent a stable state. Hence, only points B and D are stable. There is only one stable point, E, for case 3. The above examples indicate there are three distinct possibilities: (1) the metal is stable only in the active state, (2) the metal is stable in either the active or the passive states, or (3) only the passive state is stable. From the standpoint of practical corrosion resistance, case 3 is desirable since a metal-corrosive system illustrating these characteristics will spontaneously passivate.

Methods for Determining Applied Current-Potential Curves

There are two methods commonly used for determining applied current-potential curves (9,10). In the first method called the galvanostatic method, the applied current is held constant and the value of the electrode potential is measured relative to some standard potentials. The disadvantage in using the galvanostatic technique is that the active-passive transition in metals cannot be examined in detail. When the critical anodic current density is reached, the potential changes spontaneously to the transpassive region, since this is the next stable potential. This is shown in Figure 8.

In the second method called the potentiostatic method, the potential of the electrode is held constant and the value of the resulting current is measured. A potentiostat functions by monitoring the potential between the working electrode and auxiliary electrode and using the difference to activate a power supply to

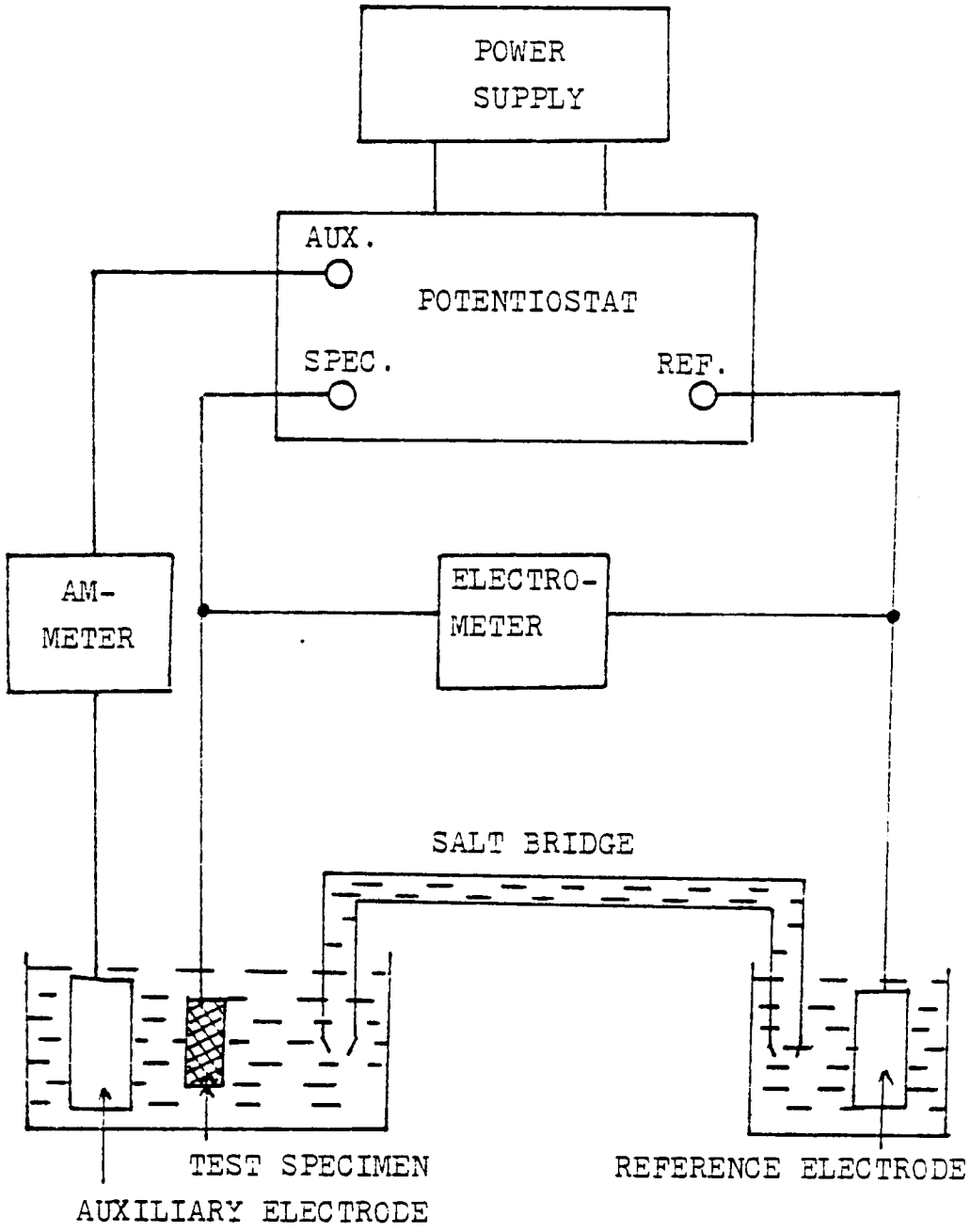


Figure 8. Potentiostat measures polarization.

maintain this potential constant. Thus, a potentiostat is a three-terminal device; there are terminals for the working, auxiliary and reference electrodes. Figure 8 shows a potentiostatic polarization circuit. In this diagram, a potentiostat with an external power supply is connected to the appropriate electrodes. An ammeter is placed in the lead to the auxiliary electrode and a short, low resistance lead is used to connect the working electrode to the potentiostat. The potential of the working electrode is measured by a potentiometer-electrometer combination.

There are two general ways of conducting potentiostatic polarization measurements; manually and automatically. In the manual method, potential is increased in a stepwise fashion and current is measured after a predetermined time at each potential setting. Automatic potentiostatic polarization is accomplished by continuously varying potential while simultaneously recording current.

Potentiostatic anodic polarization measurements of metals and alloys possessing active-passive transitions require several special precautions. Most active-passive metals demonstrate strongly time-dependent polarization behavior and therefore, it is necessary to control time parameters for maximum accuracy and reproducibility. Electrodes should be pre-exposed to the electrolyte solution for constant time periods and potential step size, transverse rate and time at each potential setting must be carefully and reproducibility controlled. It is recommended that polarization be conducted in the anodic or positive direction starting at the mixed or corrosion potential. Cathodic pretreatment of the electrode is not recommended

as it tends to distort the polarization curve shape. Oxygen and other oxidizers should be excluded from the electrolyte as their presence complicates the analysis of the resulting polarization curves (10).

Metal Evaluation by using Potentiostatic Anodic Polarization Curve

Many commercial metals and alloys depend on the achievement of passivity for their corrosion resistance, and there are two general ways for achieving passivity (4). First, the environment may be made sufficiently oxidizing to cause spontaneous passivation, or in special instances, galvanic coupling can be used to achieve passivity as in the case of titanium. Both methods depend on establishing potentials in the passive range. One of the most common oxidizers encountered in practice is dissolved oxygen. Oxygen is slightly soluble in water and aqueous solutions and, as a result, its reduction is usually under diffusion control (1). In air-saturated non-agitated solutions, the limiting diffusion current density for oxygen reduction is approximately 100 $\mu a/cm^2$. If an active-passive metal is exposed to an aerated corrosive medium it spontaneously passivates if its critical anodic current density is equal to or less than approximately 100 $\mu a/cm^2$. Thus, if the anodic dissolution behavior of a metal or alloy is known, it is possible to predict whether or not it will passivate in an aerated solution. To illustrate some of these concepts, Fontana and Greene showed (4) the anodic polarization behavior of several metals as is shown in Figure 9. This figure represents experimental data measured in dilute sulphuric acid. The anodic polarization curves of iron, chromium, and nickel were shown in

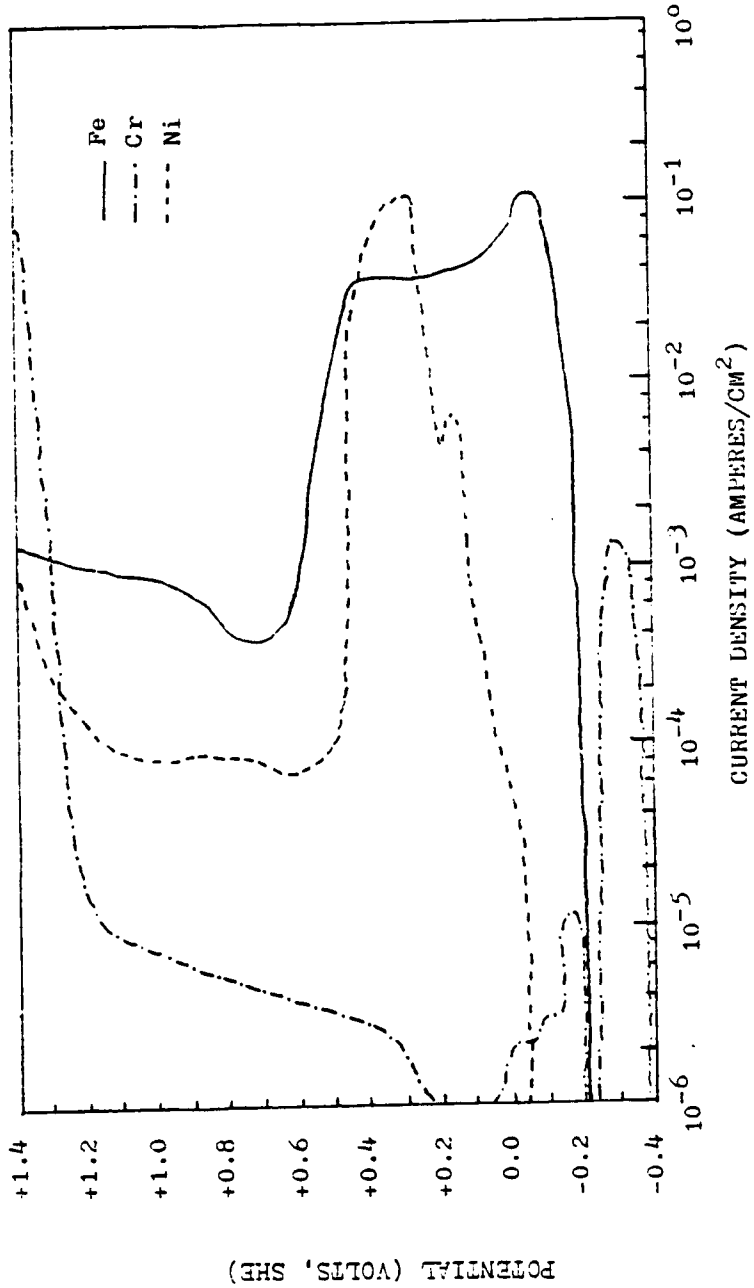


Figure 9. Anodic polarization curves of iron, chromium and nickel in 1N$H_2SO_4$ at 25°C.

Figure 9. Because iron has a very large critical anodic current density and relatively noble primary passive potential, it is difficult to passivate in acid solution. It is obvious that a limiting oxygen diffusion current density of 100 $\mu a/cm^2$ is insufficient to cause its passivation. The addition of chromium to iron increases the ease of passivation by reducing critical anodic current density. The addition of both chromium and nickel to iron markedly increases the ease of passivation.

Cathodic Protection by Sacrificial Anodes

Metals commonly used as sacrificial anodes to iron are zinc and magnesium. Cathodic protection by galvanic coupling to zinc is shown in Figure 10. Zinc is anodic with respect to iron and corrodes preferentially when galvanically coupled. The anode in this case is called a sacrificial anode since it is consumed during the protection of the iron structure (3,6,11).

Plates of iron and zinc are joined by a variable resistance connection which can be varied from Rzinc-iron = 0 to Rzinc-iron=$\infty$, the latter corresponding to two individual, uncoupled pieces of metal. When the two metals are directly coupled, Rzinc-iron = 0, there will be negligible resistance between them and the metal will be at a single potential (3,6). A flux of current, however, will pass from the zinc to the iron in the solution as shown. The current density at the surface will diminish with increasing distance from the iron-zinc junction because of the progressively larger resistance of fluid elements shown by dashed lines away from the junction between the

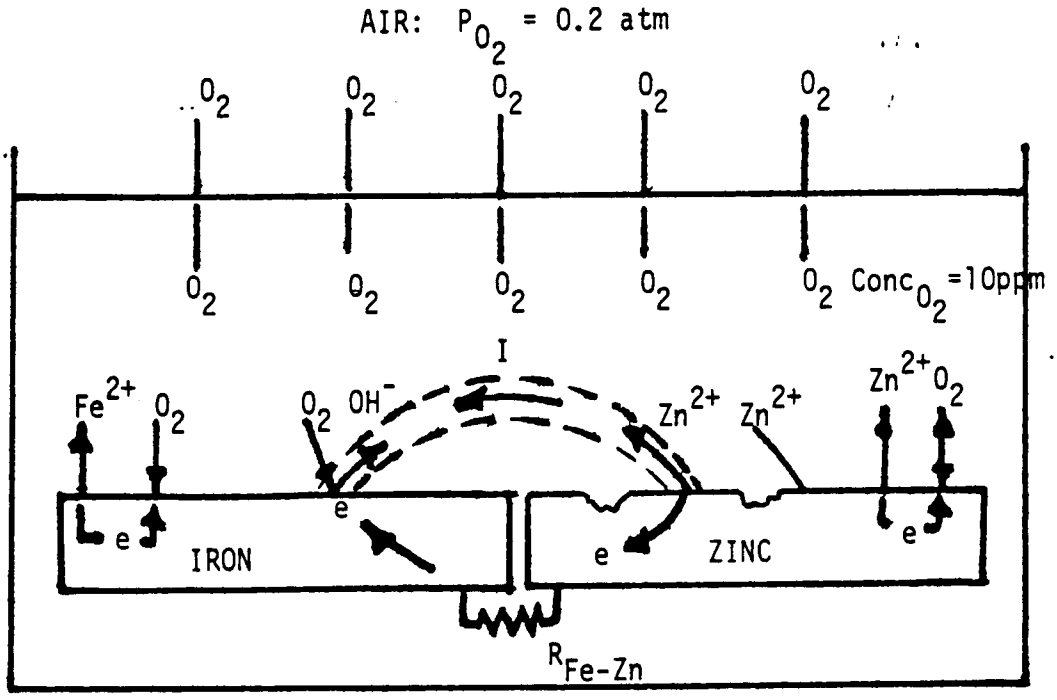


Figure 10. Iron and zinc in an aerated environment.

metals. Near the junction, current path length and hence solution resistance will approach zero and the potential at the junction will approach Ecouple, however, progressively away from the zinc-iron junction, the length of fluid elements increases and the current density decreases. When the current density is decreased to a value that no longer polarizes the iron surface to $E_{Fe,\ Fe^{++}}$, the required potential for protection, corrosion of the iron will occur. As a consequence, in the arrangement of Figure 10 the zinc will protect the iron until a certain distance from the metal junction beyond which corrosion will be observed. The larger the specific resistivity of the environment, the shorter the distance over which the iron will be protected (6). Figure 11 shows polarization curves for the reactions involved are such that $E_{corr.A}$ has been reduced to or below $E_{A,A^+}$. Hence, the requirements for cathodic protection is thus met. It has been mentioned that $E_{couple}$ depends not only on the electrochemical parameters of the system ($E_o$,$I_o$, and $\beta$ for each reaction) but also on the electrolyte composition relating size, shape and distance between anode and cathode areas, the resistivity of the environment, the metallic path resistance between anodes and cathodes and the fluid velocity. In Figure 10 and 11 the total resistivity is assumed to be negligibly small. This allows establishing $E_{couple}$ in terms of the intersection of the curves representing $I_{ox}$ and $I_{red}$. If (B) is decreased, the polarization curves for both reactions associated with (B) will be more to the left or to the lower values of current--the shift being proportional to the decrease in area. As a result,

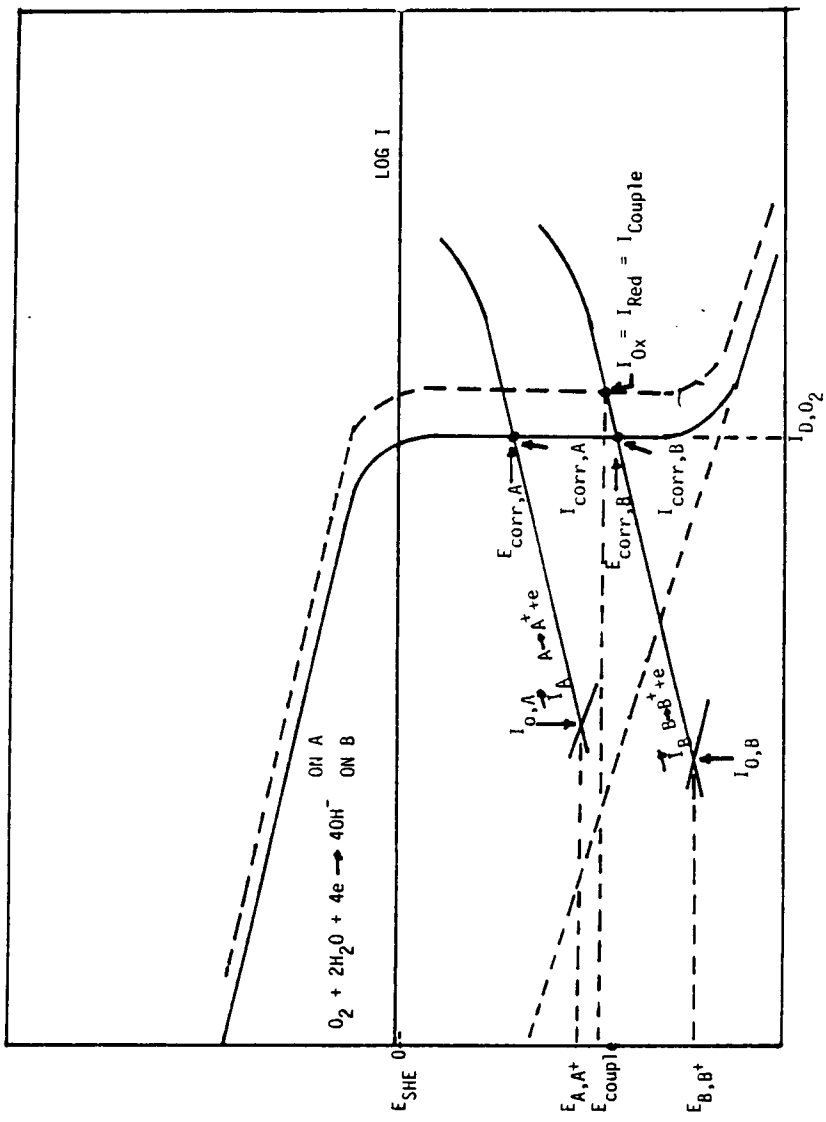


Figure 11. The effects of galvanic coupling under conditions of oxygen diffusion control.

$E_{couple}$ will increase and if $E_{couple}$ $E_{A,A^+}$, metal A is no longer completely protected. Naturally, the values of $I_o$, $\beta$, $\beta b$, $I_o$, H on B and BH on B will govern for a given area A/Area $\beta$ ratio, the value of $E_{couple}$ and therefore whether cathodic protection can become accomplished. It is also evident that the influence of the geometry and spacing of metals A and B, and the circuit resistance on the ability of $\beta$ to cathodically protect A is complicated (3,11).

Polarization of Zinc

It is evident that an understanding of the behavior of iron-zinc galvanic couples depends on the polarization characteristics of the individual metals. While there is a large literature on the polarization of iron, it is surprising to find that relatively little has been published on the polarization of zinc in near neutral environments. Since the electrochemical behavior of the zinc appears to be the controlling factor in determining its ability to galvanically protect iron, a brief review of the literature on zinc as it pertains to the present research is given.

Recently Alvarez and Galvele (12) reported the passivity breakdown of high purity zinc in aqueous solutions containing different aggressive anions. Samples were prepared from 99.9995% zinc rods. The zinc coupons were annealed for two hours at 370°C in argon atmosphere. Before the electrochemical measurements the specimen were chemically polished in an aqueous solution of 320 g/l of $CrO_3$ plus 18 g/l of $Na_2SO4$, for about two minutes at room temperature. Alvarez and Galvele showed that when zinc is exposed in alkaline solutions,

pH=9 it exhibits passive behavior with current density as low as $10^{-6}$ A/cm$^2$. In acid solution (pH = 5), no passive region was found. In the more alkaline solution and with 1 and .1M NaCl pitting potential of about -700mV was also observed.

Hurlen (13) and Dirkse (14,15) reported on the electrochemistry of zinc in acidic and alkaline environments. Dirkse's paper gives experimental values of $i_o$,Zn. His values are larger when compared to values for other metals reported by West (16).

Leidheiser, Momose and Granata (17) and Leidheiser and Suzuki (18) showed typical cathodic polarization curves obtained in aerated and deaerated 3% NaCl at pH=6.4. The curves reported in the aerated solution differed slightly in shape for different samples, but they all had the steep vertical shape characteristics of concentration polarization. They showed a small peak in the lower potential region which was attributed to a reducible oxide or hydrated oxide such as ZnO, $ZnO.xH_2O$, or $Zn(OH)_2$. Neither of these papers propose cathodic reactions responsible for the corrosion of the zinc or for the cathodic polarization curves that they report.

The Zinc-Iron Potential Reversal in Cathodic Protection

Zinc, because of its electrochemical behavior, is one of the metals most widely used to galvanically protect iron. The use of zinc as a sacrificial anode depends upon its potential remaining electrochemically more active than the iron it is to protect (10). The fact that the potential of zinc will change with time at

elevated temperatures in the presence of certain natural water impurities has been documented (6,11). Haney's (19) investigations of the behavior of high purity zinc in dilute aqueous solutions while galvanically coupled to steel reveal that bicarbonates and nitrates promote an increase in the zinc corrosion potential, the rate increasing significantly from room temperature to 90°C.

Hoxeng, et al., (20,21) emphasized that the solution composition is more important than the temperature in its effect on the electrochemical behavior of zinc. The anodic-cathodic behavior of zinc-iron couples in any water will depend on the equilibrium or balance of the various constituents of the water and cannot be determined from the content of any one constituent (22).

Effect of Electrolyte Composition

Many workers have studied the corrosion of zinc in various electrolytes. Bauer and Schiker (21) found that, in distilled water, the loss in weight of zinc decreased with increasing carbon dioxide content and attributed this to the production of a protective film on zinc.

Some workers have also shown that the corrosion of zinc in water reaches a maximum at some temperature between 60 and 70°C. La Que and Cox (22) using distilled water found maximum penetration at 65°C, which they attributed to a change in the nature of the corrosion product at about 53°C. Hoxeng and Prutton, (20) found the addition of increasingly greater amounts of bicarbonate caused progressively more positive corrosion potentials.

Maconachie (23) also carried out measurements of the corrosion of zinc specimens in aerated distilled water at various temperatures, and for varying periods of immersion. He confirmed that there was a maximum rate of corrosion at about 60°C for all times of immersion tested, but found that there were variations in the rate of corrosion with time at constant temperature. However, Gilbert (24) summarized Maconachies work by stating that a more plausible mechanism is as follows:

$$Zn + H_2 \rightarrow Zn(OH)_2 + 2H_{ADS} \quad (10)$$

$$2H_{ADS} \rightarrow H_{2\ (gas)} \quad (11)$$

or $$2H_{ADS} + 1/2O_{2\ (diss)} \rightarrow H_2O \quad (12)$$

He stated that as the overvoltage is high, reaction 10 is almost completely polarized and 11 proceeds very slowly. Dissolved oxygen can cause depolarization according to reaction 12 and the rate of reaction 12 can correspondingly increase, its speed being controlled by the supply of dissolved oxygen. With increase in temperature and consequent decrease in the rate of reaction 12, however, as Maconachie points out, the maximum in the corrosion rate can only be partially accounted for on the basis of change of oxygen solubility. Based on the above statement, the use of the term depolarization implies that the rate of hydrogen gas evolution is decreased markedly by the addition of oxygen or oxidizing agents to acid solutions. The rate of the cathodic reaction however is increased as the result of

interactions between the oxidizing agents and hydrogen adsorbed on the surface.

It should be pointed out that at the time of this investigation, electrochemical measurements were limited to corrosion potentials and polarization measurements were not made to help identify the cathodic reactants and the kinetics of either the anodic or cathodic reactions. In fact the research just reviewed was done prior to the Wagner-Traud mixed potential theory. This theory questions depolarization in the sense of reaction 12. Specifically West (16) states "It is sometimes asserted that the role of oxygen in solution is to 'depolarize' hydrogen ion reduction by removing adsorbed hydrogen atoms from the surface (see equation 12) and so allowing access of fresh protons to the surface. There is no evidence for this."

## Electrical Resistivity

One of the most important parameters in corrosion and cathodic protection is the electrical resistivity of the electrolyte. This is a property which is defined as the resistance between the opposite faces of a specific cube of a material. The usual units are the ohm-cm. This property of the electrolyte is intrinsic in that it depends entirely upon the substance and not upon its dimensions.

The common electrolytes vary considerably in resistivity from sea water at 20 to 30 ohm-cm to "pure" water which has a resistivity of about 20,000,000 ohm-cm. The distilled water that is obtainable in most laboratories has a resistivity of about 500,000 ohm-cm (6). Rain water that has collected in lakes, and melted ice, has a

resistivity of the order 20,000 ohm-cm, though tap water varies from 1,000 to 5,000 ohm-cm. If pure water, or near it, is contaminated with small quantities of salt, the change in conductivity, the inverse of resistivity is that shown in Figure 12. This indicates that a few parts per million of some salts can greatly reduce the resistivity of pure water. Solutions of higher concentration give resistivities of 1 ohm-cm but are rare. The variation of resistivity with chlorinity for sea water is shown in Figure 13. Ocean water has a chlorinity of 19 parts per thousand and its resistivity varies from 16 ohm-cm to 35 ohm-cm (6).

Effect of pH

The acidity of a solution is a function of the hydrogen ion concentration ($H^+$), and is designated by pH which is defined as:

$$pH = -\log[H^+]$$

The higher the hydrogen ion concentration, the greater the acidity (25,26,27). pH is a very important factor in corrosion and corrosion control. The effect of pH on corrosion of zinc at room temperature is shown in Figure 14. It is well known that zinc in acid solution dissolves by a hydrogen evolution type attack, and that this process is strongly affected in the range pH 1-4 (27,28).

It is important to represent the effect of pH on a metal-water system by the potential -pH diagram, which represents the conditions of thermodynamic equilibrium. The diagram for the system zinc-water, at 25°C is shown in Figure 15. Figure 16, which can be deduced from

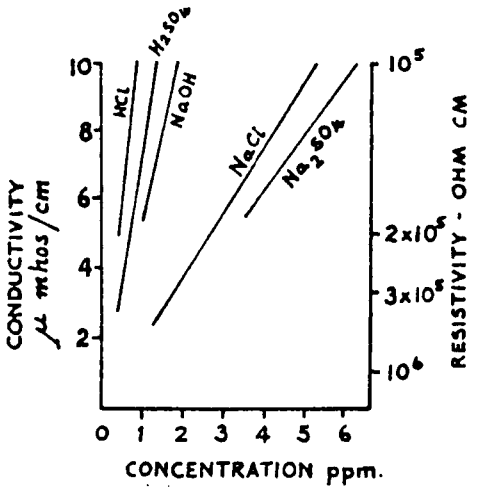


Figure 12. Conductivity of water as a function of added impurity salts.

Source: Morgan, J.H., "Cathodic Protection," Leonard Hill Limited, N.W.1., 1959.

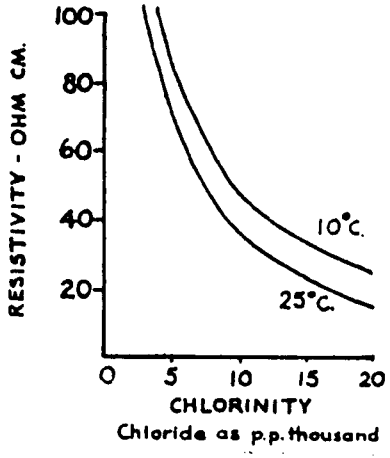


Figure 13. Resistivity of sea water as a function of chlorinity.

Source: Morgan, J.H., "Cathodic Protection," Leonard Hill Limited, N.W.1., 1959.

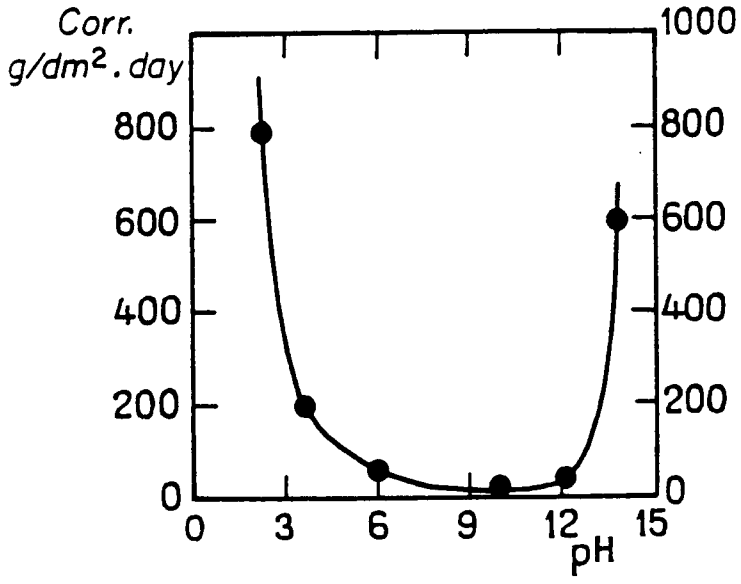


Figure 14. Influence of pH on the corrosion of zinc.

Source: Pourbaix, M., "Atlas of Electrochemical Equilibria in Aqueous Solution," NACE, 1974.

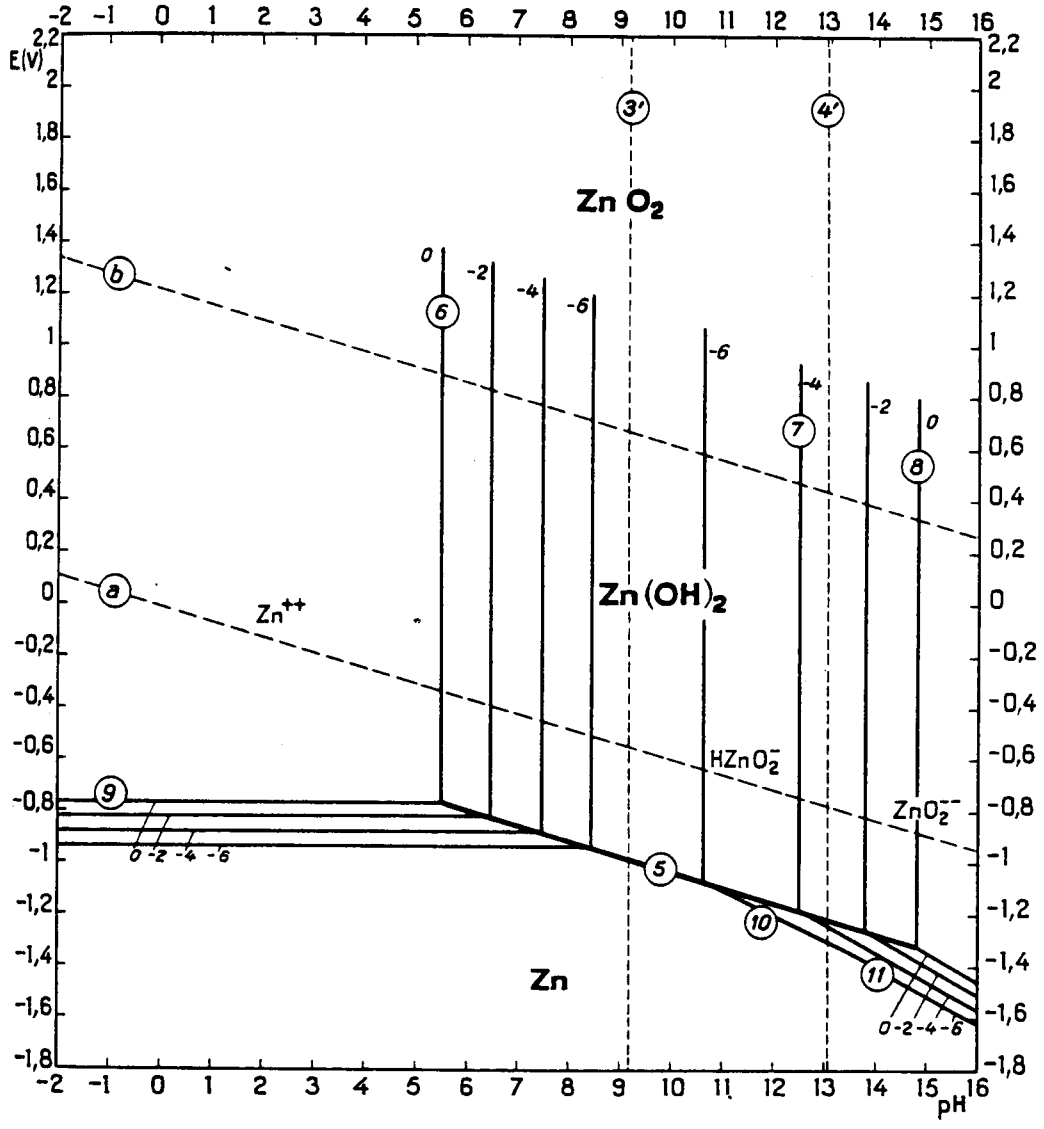


Figure 15. Potential-pH equilibrium diagram for the system zinc-water, at 25°C.

Source: Pourbaix, M., "Atlas of Electrochemical Equilibria in Aqueous Solutions," NACE, 1974.

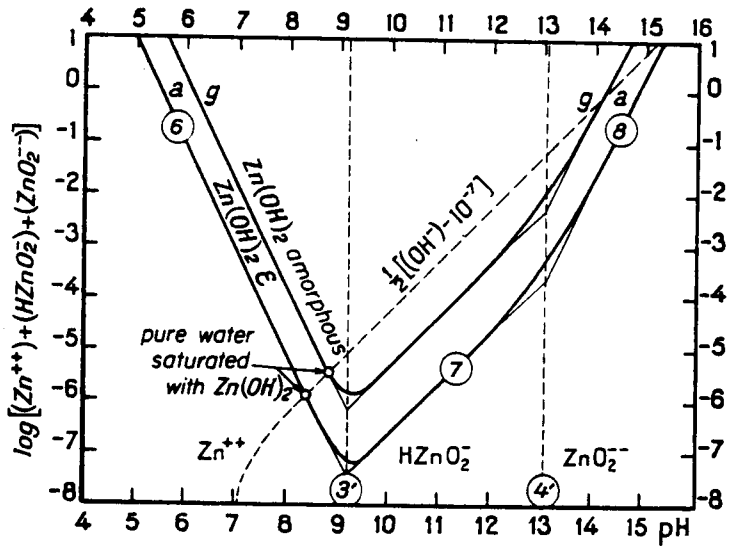


Figure 16. Influence of pH on the solubility of the zinc hydroxides, at 25°C .

Source: Pourbaix, M., "Atlas of Electrochemical Equilibria in Aqueous Solutions," NACE, 1974.

Figure 15, represents the influence of pH on the solubility of the stable hydroxides of zinc (27). Note the presence of the dotted line shown as 3' and 4' in both figures. These lines define the pH ranges over which $Zn^{++}$, $HZnO_2^-$ and $ZnO_2^=$ are the dominant ionic species in solution. The vertical solid lines in Figure 15 show the activities of these ions, in their respective pH ranges of dominance, at saturation with crystalline $Zn(OH)_2$. The two solid curves in Figure 16 refer to $Zn(OH)_2(\varepsilon)$, the crystalline form, and to the amorphous form of $Zn(OH)_2$, which are respectively the least soluble and the most soluble.

Figures 15 and 16 are based on the research of Delahay, Pourbaix and Rysselberghe (29) who also considered the influence of carbonate and bicarbonates in controlling the precipitating species. Figure 17, taken from their work, is a representation of the solubility limits of the stable crystalline $Zn(OH)_2(\varepsilon)$, the unstable amorphous $Zn(OH)_2(\alpha)$ and of zinc carbonate in terms of total $CO_3^=$. The curves are in terms of the total zinc concentration in solution as $Zn^{++}$ + $ZnOH^+$ + $ZnO_2^=$ as a function of pH. These curves are interpreted as follows: for example, at pH = 9, the solubility of zinc hydroxide in terms of total zinc in solution is equal to $10^{-6}$ for the relatively soluble form, $Zn(OH)_2(\alpha)$ (line 5$\alpha$); on the other hand, for the relatively insoluble form, $Zn(OH)(\varepsilon)$(line 5$\varepsilon$); the solubility is lower, about $10^{-7}$. They (29) have observed that both these varieties of $Zn(OH)_2$ are formed in the corrosion of zinc by aqueous solutions. Pourbaix also showed some evidence (7), although not with complete certainty, that a protective coating with a solubility

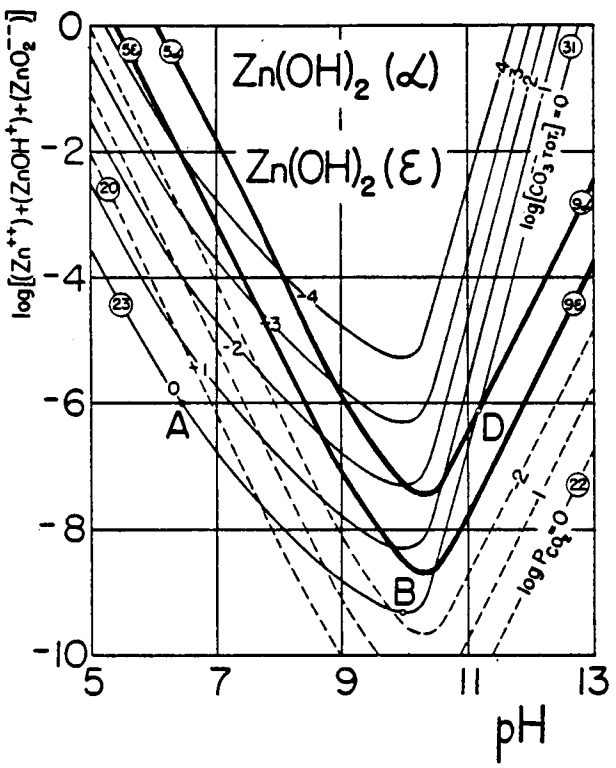


Figure 17. Solubilities of zinc hydroxides and carbonate as a function of pH.

Source: DeLay, P., Pourbaix, M., and Rysselberghe, P.V., "Potential-pH Diagram of Zinc and Application to the Study of Zinc Corrosion," Corrosion, Vol. 98, Page 101, 1951.

comparable with that of $Zn(OH)_2$ (29) and consisting of a mixture of zinc oxide and carbonate is formed when there is an intensive relative motion between zinc and aerated distilled water. This would point toward a real possibility of passivation of zinc at pH values between about 8.5 and 11.9, and account for the low corrosion rate shown in Figure 14 (page 38).

Delahay, Pourbaix and Rysselberghe (29) interpret Figure 17 as follows: on Figure 17, the variation of solubility of $ZnCO_3$ with pH for two series of cases is shown (1): saturated $CO_2$ solutions under partial pressure of $CO_2$ varying from 0.01 to 1 atmosphere [lines (20) - (22)] and solutions containing total concentrations of $H_2CO_3 + HCO_3^- + CO_3^=$ varying from 0.0001 to 1 mole of $CO_2$ per liter [lines (23), (31)].

> Figure 17 shows that when the sum $H_2CO_3 + HCO_3^- + CO_2^=$ is equal to 1 and the total zinc concentration is $10^{-6}$ gram atom of zinc per liter, a gradual increase of pH causes a separation of solid $ZnCO_3$ at pH = 6.45 (point A of Figure 17). If the pH is still increased the solubility of $ZnCO_3$ varies along the curve AB and is minimum for pH = 10.0. At still higher pH values $ZnCO_3$ constitutes the only stable solid phase according to curve BD up to a pH of about 11.2 (point D) at which there is simultaneous stability of $ZnCO_3$, of different varieties of $Zn(OH)_2$ and ZnO and also, most likely, of certain basic zinc carbonates which are not considered here. On the basis of the views expressed in this paper one may expect that, in the presence of solutions 1 molar in total $CO_2$, the domain of passivation of zinc pictured on Figure 18B will extend to the left to pH = 6.5. The region between pH - 10.5 and pH 11.3 corresponds to the formation of films containing chiefly $Zn(OH)_2$. By repeating the above reasoning for other concentrations of dissolved $CO_2$, as well as for different equilibrium partial pressure

of gaseous $CO_2$, one can, on the basis of Figure 17, predict the probably circumstances of passivation of zinc by carbonates and bicarbonates. One can thus establish Figure 18B which represents the total concentration ($H_2CO_3 + HCO_3^- + CO_3^=$) and therefore the influence of $H_2CO_3$ and its ions on the corrosion and passivation of zinc.

By comparing Figure 18A and B one sees that the threshold of concentration ($H_2CO_3 + HCO_3^- + CO_3^=$) above which these substances could exert passivating action on zinc would be in the neighborhood of $10^{-2.4}$ moles per liter. When ($H_2O_3 + HCO_3^- + CO_3^=$) is larger than $10^{-2.4}$ the domain of passivation zinc at slightly alkaline pH values, but there seems to be no possibility of protecting the metal at pH values larger than about 11.3.

Effect of Dissolved Oxygen

Experience with corrosion of metallic materials in aqueous solutions of electrolytes, indicates that dissolved oxygen has a marked effect on corrosion in acids (30) as well as in nearly neutral solutions (31,32). An understanding of the mechanism of the reactions involved in such systems is of interest not only in general electrochemical theory but also in developing methods for minimizing corrosion.

Deficiency of oxygen due to decrease in solubility with increase of temperature makes itself felt at higher temperatures. According to Gilbert (24), zinc specimens were found to show maximum positive potentials at about 70°C and above this temperature the potential became somewhat more negative again. It has also been found that zinc specimens in boiling tap water have a much more negative

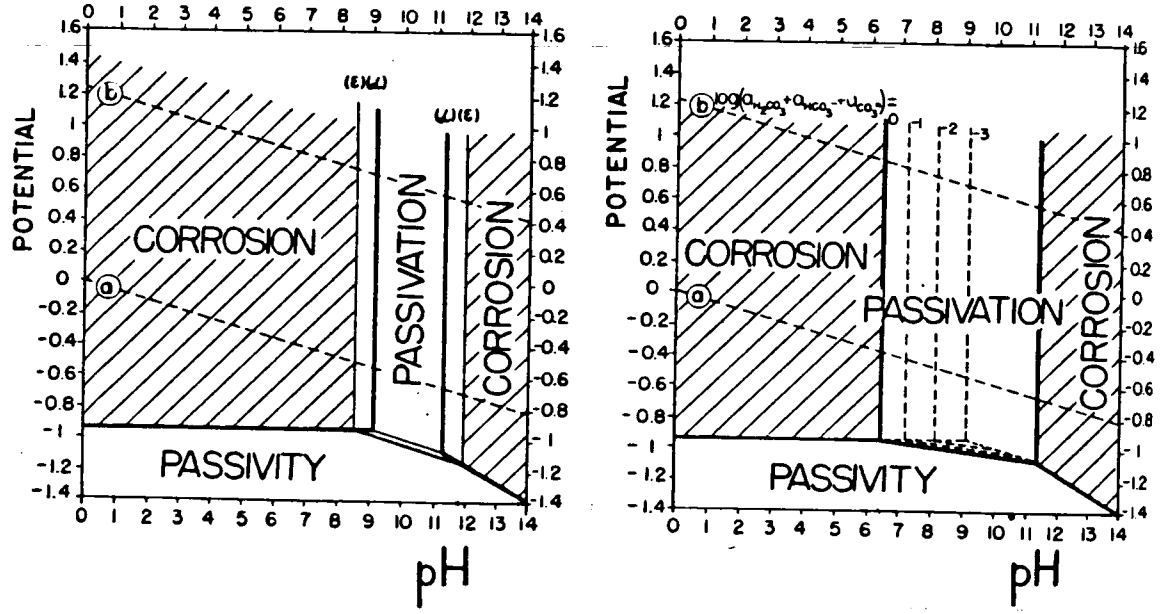


a) For solutions free from $CO_2$ b) For solutions containing $CO_2$

Figure 18. Conditions of corrosion, passivity, and passivation of zinc as determined from the potential-pH diagram. Potential, in volts, referred to the normal hydrogen electrode. In a) passivation is due to ppt. of $Zn(OH)_2$ and in b) it is due to $ZnCO_3$.

Source: DeLay, P., Pourbaix, M., and Rysselberghe, P.V., "Potential-pH Diagram of Zinc and Application to the Study of Zinc Corrosion," Corrosion, Vol. 98, Page 101, 1951.

potential than specimens at 85°C. (Boiling water no doubt approximates to deaerated conditions.) He also pointed out that decreasing solubility above 70°C also explains why the reversal of polarity, in the case of zinc-steel couples in water at 85°C was usually observed when fresh water was introduced into the cells. The oxygen supply was thus temporarily replenished but such reversal of polarity generally only lasted for some hours after the introduction of fresh water.

The opinion of Gilbert (22,25,33) and others, who have studied the effect of oxygen on the corrosion of zinc, is that the initial corrosion behavior of zinc in oxygenated water is rationalized in terms of electrochemical kinetics by taking into consideration both the anodic and cathodic partial reactions, and that together these give rise to the mixed type of corrosion potential.

In the absence of reducible substances other than hydrogen ions and dissolved oxygen, the partial electrode processes operating during corrosion of zinc in water can be described in general by equations 13-15.

$$Zn \rightarrow Zn^{++} + 2e \qquad (13)$$

$$2H_2O + 2e \rightarrow 2H_2O + H_2 \qquad (14)$$

$$2H_2O + 2e \rightarrow 2OH^- + H_2 \qquad (14b)$$

$$O_2 + 2H_2O + 2e \rightarrow 4OH^- \qquad (15)$$

For the case of deoxygenated water, the prevailing cathodic reaction is Equation 14b, whereas, in the case of oxygenated water, Equation 15 is the predominant cathodic partial reaction. On zinc-iron coupling, in hot waters, oxygen leads to a more positive potentials, since it causes cathodic depolarization, but the effect of oxygen can not alone account for the much more positive potentials occuring in hot waters. The supply of oxygen is greater at room temperature than in hot solutions, and if oxygen were the only factor, the most positive potentials would be expected to occur in cold solutions. On the other hand, deficiency of oxygen will lead to more negative potential.

## The Behavior of Zinc in Alkaline Solutions

Many workers (12,14,34) have studied the corrosion of zinc in alkaline solution. Recently, Dirkse (14,15) has dealt with the kinetics and mechanisms of the zinc electrode in alkaline solutions, containing high and low concentrations of hydroxyl ions. His work has shown that the exchange current density value and the Tafel region are only slightly affected by change in ionic strength except that as the ionic strength increases, the result tends to become more erratic. A likely reason, he points out, is that at these higher ionic strengths, normal hydration numbers of the ions cannot be satisfied and the physical nature of the solution is changing.

Similarly, Nagy and Bockris (35) carried out tests on pourous zinc electrodes in potassium hydroxide solutions. They also investigated the morphology of the zinc oxide film which exhibited a

dendritic appearance, with all the needles pointing towards the solution; the oxide film was identified to be ZnO. Their argument for this mechanism is: the dissolving zinc supersaturates the solution with zincate until a concentration is reached when oxide nucleation suddenly begins. This happens at the surface of the metal where the zincate concentration is the highest; once nucleation occurs, crystallization proceeds very fast and a concentration gradient is set up, creating a diffusion layer. In addition to the above results, the current distribution evidence indicates that the reaction in a pourous zinc electrode proceeds through the soluble zincate intermediate. Their studies on anodic zinc electrodes show that the oxide film was formed by a dissolution precipitation mechanism, which is supported by the morphology of the zinc oxide film. They also stated that the observed exchange current density is as high as 80 $mA/cm^2$.

Powers, et al., (34) also investigated the behavior of zinc in alkaline solutions. Using a very slow potential scan with simultaneous microscopic observations they identified a precipitated coating of ZnO particles (type I film) which overlies a more coherent film of ZnO (type II film). To gain a better understanding of the phenomenon under consideration, they cited the electrode potentials of the zinc: for zinc in equilibrium with 0.25M zincate the potential was -1.36V when measured against Hg/HgO reference electrode in the same alkaline solutions. For equilibrium between zinc and a solution saturated with respect to either zinc hydroxide or zinc oxide, the potential was -1.34V, and hydrogen evolution was observed.

Similar experimental results were observed by Hurlen (36) working with dilute solutions of NaOH and $NaHCO_3$. Furthermore, Hurlene confirmed the existence of an electroreducible film on zinc, presumed to be zinc oxide at potentials slightly more positive than that formed by others.

# CHAPTER 3

## EXPERIMENTAL PROGRAM

In this chapter a brief discussion of the experimental procedure used in the course of this investigation is presented.

### Materials

The zinc and iron used in this investigation was supplied with the analyses shown in Table 1 and 2.

### Preparation of Specimens

Two types of specimens were prepared. One set of zinc and iron specimens (2cm x 2cm) was mounted in Marglass epoxy to permit metallographic polishing for both microscopic examination and to allow electrochemical measurements in various environments by electrical contact to the specimen within the mount thus insulating conducting wires from the solution. A second set of zinc samples had exposed dimensions of 1.8 cm wide x 10 cm long and were mounted with one end in Marglass to allow electrical contact. Surface preparation consisted of polishing with emery paper down to 600 grade, followed by a washing with distilled water and a rinse with alcohol.

This technique was found to be very satisfactory, permitting uniform surface preparation. Furthermore, it allowed repeated use of each sample, thus ensuring uniformity of material throughout the series of experiments.

TABLE 1

ZINC ANALYSIS

| Element | Percent |
|---|---|
| Cu | <0.0001 |
| Pb | 0.0015 |
| Cd | 0.005 |
| Fe | 0.0017 |
| Al | <0.0001 |
| Mg | <0.0001 |
| Ti | <0.0001 |
| Cr | <0.0001 |
| Ni | <0.0001 |
| Zn | 99.9963 |

TABLE 2

IRON ANALYSIS

| Element | Percent |
|---|---|
| C | 0.007 |
| Mn | 0.010 |
| P | 0.002 |
| S | 0.0015 |
| Cu | 0.13 |
| Ni | 0.042 |
| Cr | 0.003 |
| Cb | 0.005 |
| V | 0.000 |
| Mo | 0.006 |
| Si | 0.001 |
| Co | 0.009 |
| Pb | 0.001 |
| Sn | 0.010 |
| Al | 0.003 |

## Preparation of Solutions or Electrolytes

In preparing the test solutions, the various salts were added gravimetrically to distilled water. The electrolytes were prepared from reagent grade sodium chloride, sodium nitrate, calcium carbonate, and calcium bicarbonate.

## Potentiostatic Polarization Measurements

The potentiostat used in this investigation was characterized by an input impedence of 100 megohms, a maximum output current of ±5 amperes and an output voltage of ±30 volts; the set point range was ±2 volts. In addition the instrument was equipped with a differential amplifier and logarithmic converter capable of plotting a continuous polarization curve through five decades of log current. Figure 19 shows a circuit diagram of the electronic potentiostat used in this investigation.

The potentiostat was calibrated using a dummy cell at which the current and potential could be measured. The X-Y plotter was then calibrated directly in terms of the current and potential indicated by the potentiostat.

## Electrochemical Measurement Cells

Two types of cells were used--a round cell containing 2 liters of solutions and a larger cell containing 7 liters. The top of the two-liter cell is shown in Figure 20. It consisted of a PVC plate containing several drilled and tapped holes for various electrodes

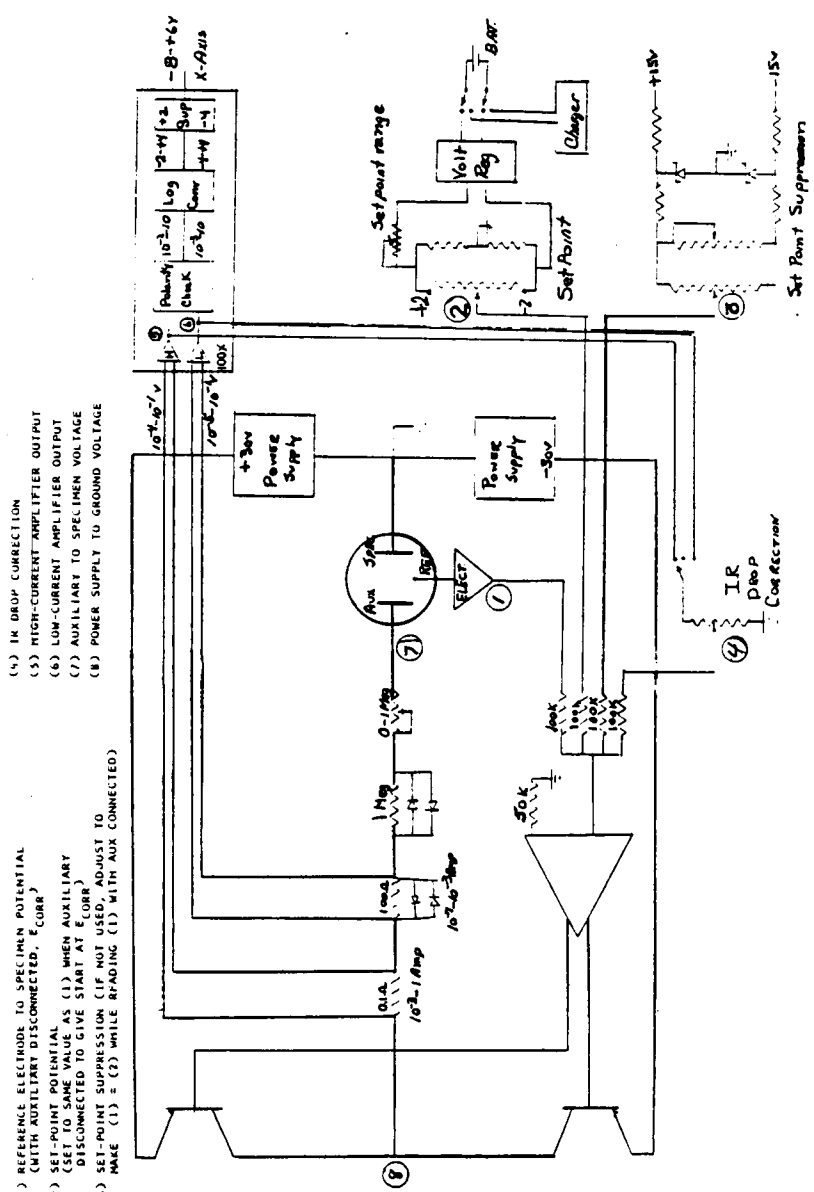


Figure 19. Circuit diagram of electronic potentiostat as used in this investigation.

and to allow auxiliary devices such as a thermometer and sparging tubes to be introduced into the test cell as indicated in the sketch of Figure 20.

Brass screws near the edge of the top were used to compress an O-ring between the top and the flange of the two-liter vessel, thus sealing off the test cell from the atmosphere. The smaller samples were studied in this two liter assembly. The test solutions investigated contained by weight 600 mg/l $HCO_3^-$, 73 mg/l $NO_3^-$, 20 mg/l $CO_3^=$ or 10,000 mg/l NaCl. The seven-liter cell was used for polarization measurements on zinc, iron and iron-zinc couples. It was also used for potential-time measurements. The arrangements for introducing leads and gases was similar to that of the two-liter cell. Heating tapes were wrapped around both types of cells for measurements at 60°C.

The reference electrode used was a saturated silver-silver chloride electrode contained in a capillary tipped glass tube with the tip positioned about 1-2 mm from the surface of the specimen. The reference electrode was checked with respect to a standard saturated calomel electrode before use in the polarization cell.

Immediately prior to testing, the pretreatment of the zinc and iron electrodes involved polishing through the 600 grade emery, decreasing with alcohol and finally washing with running distilled water.

The initial and final pH of the electrolytes were regularly recorded. The resistivity at room temperature of the electrolyte

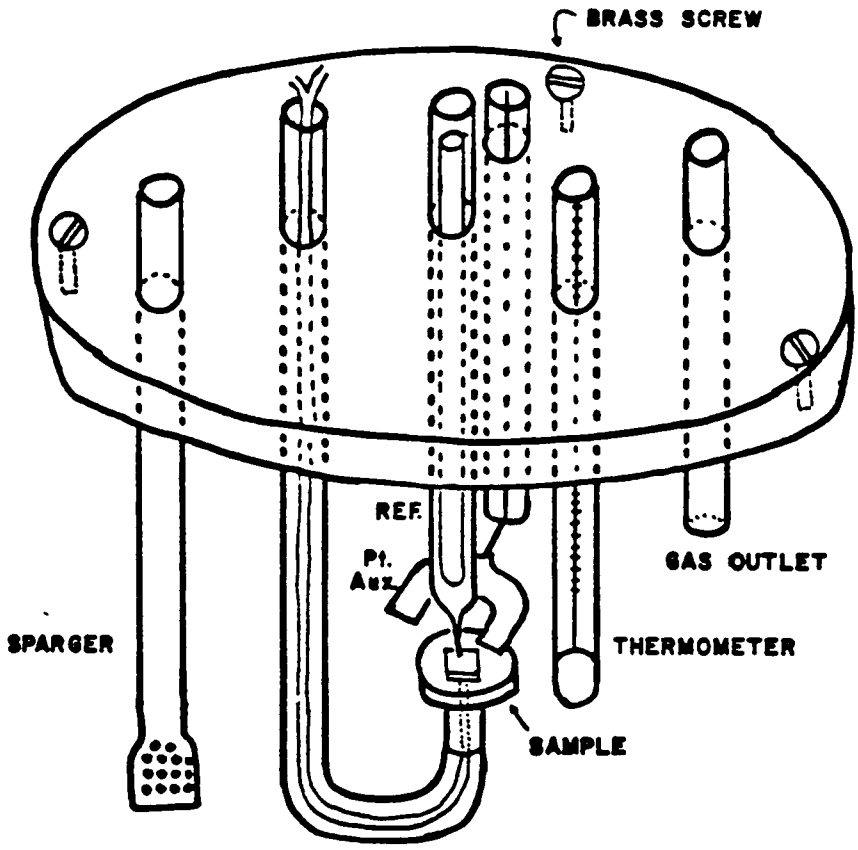


Figure 20. Schematic of polarization cell.

and to allow auxiliary devices such as a thermometer and sparging tubes to be introduced into the test cell as indicated in the sketch of Figure 20.

Brass screws near the edge of the top were used to compress an O-ring between the top and the flange of the two-liter vessel, thus sealing off the test cell from the atmosphere. The smaller samples were studied in this two liter assembly. The test solutions investigated contained by weight 600 mg/l $HCO_3^-$, 73 mg/l $NO_3^-$, 20 mg/l $CO_3^=$ or 10,000 mg/l NaCl. The seven-liter cell was used for polarization measurements on zinc, iron and iron-zinc couples. It was also used for potential-time measurements. The arrangements for introducing leads and gases was similar to that of the two-liter cell. Heating tapes were wrapped around both types of cells for measurements at 60°C.

The reference electrode used was a saturated silver-silver chloride electrode contained in a capillary tipped glass tube with the tip positioned about 1-2 mm from the surface of the specimen. The reference electrode was checked with respect to a standard saturated calomel electrode before use in the polarization cell.

Immediately prior to testing, the pretreatment of the zinc and iron electrodes involved polishing through the 600 grade emery, decreasing with alcohol and finally washing with running distilled water.

The initial and final pH of the electrolytes were regularly recorded. The resistivity at room temperature of the electrolyte

solutions ranged from 200,000 ohm-cm for distilled water containing calcium carbonate to around 20,000 ohm-cm for solutions containing 600 mg/l calcium bicarbonate; and 100 ohm-cm for solutions containing 1% NaCl ohm-cm. The resistivity measurements were made with a conductivity cell (K = 1.0) and a conductivity bridge.

Before an initial run was made, the specimen was left in the polarization cell for at least thirty minutes to ensure that a stable corrosion potential was reached. The potentiostat was then set at the open-circuit or corrosion potential of the samples. Final connection between the cell and potentiostat was made through a 1 megohm resistor to reduce current surge through the specimen during the time (a few milliseconds) required for the potentiostat to come to a steady state. The resistance was then reduced to either zero or to a small enough value such that the resistance did not limit the current from potentiostat at its maximum voltage output of ±30V. The potentiostatic polarization curve was recorded by scanning at preselected rates over the desired potential range with respect to the reference electrode.

Corrosion potentials of uncoupled specimens of iron and zinc, the individual potentials of each when coupled and measurements of the direction and the value of the current generated by a couple throughout a test period were recorded. The current was measured with a zero resistance ammeter. The galvanic currents were converted to voltage signals and these along with the potentials of the corroding specimens were fed to an electrometer through a multiplexing switch. The potentials were measured with the electrometer and

recorded as output on a teletype. As described previously, the system was operated by a microprocessor which selected the signal to be processed and the time interval between measurements and translated electrometer output to input to the teletype.

Weight Loss Test

The zinc specimens, having an area of about $3cm^2$ were polished initially with fine emery paper and finished with 9 micron diamond paste. The specimens were suspended from glass hooks in flasks containing 1000 cc of bicarbonate or sodium chloride solutions. Tests were performed in duplicate.

After exposure for up to three weeks, specimens were cleaned by immersion for a short time in 10% HCL with inhibiting 0.5% Rodine 213 and rinsed with distilled water followed by alcohol. It was shown that this inhibited acid cleaned the zinc with negligible chemical attack on the metal ($<0.0001$ mg/$cm^2$ in three days).

# CHAPTER 4

## RESULTS AND DISCUSSION

The use of zinc as a sacrificial anode depends upon its potential remaining more electrochemically active (4,6) than the iron it is to protect. However, it is observed that potential of zinc does change to higher values with time at elevated temperature in the presence of bicarbonates, nitrates and carbonates (inhibiting anions) but this higher potential is offset by the presence of chlorides (19,33).

Although the initial emphasis of this research was on the behavior of iron-zinc couples in selected environments, problems of understanding the behavior of the couples led to shifting the major emphasis on zinc itself. Some measurements were also made on iron. The following discussion therefore deals largely with the corrosion behavior of zinc in bicarbonate, nitrate, carbonate and chloride bearing environments. Results of weight loss measurements and electron microscopy will be discussed later in this chapter. Throughout this section all potentials are referred to the standard hydrogen electrode (SHE).

### Corrosion Potential-Time Behavior

Corrosion potentials as a function of time for zinc under several environmental conditions are shown in Figures 21 and 22. The bicarbonate solutions contained 600 ppm bicarbonate with exposure being made at room temperature and 60°C under stagnant, aerated and deaerated conditions. Figure 21 shows that the corrosion

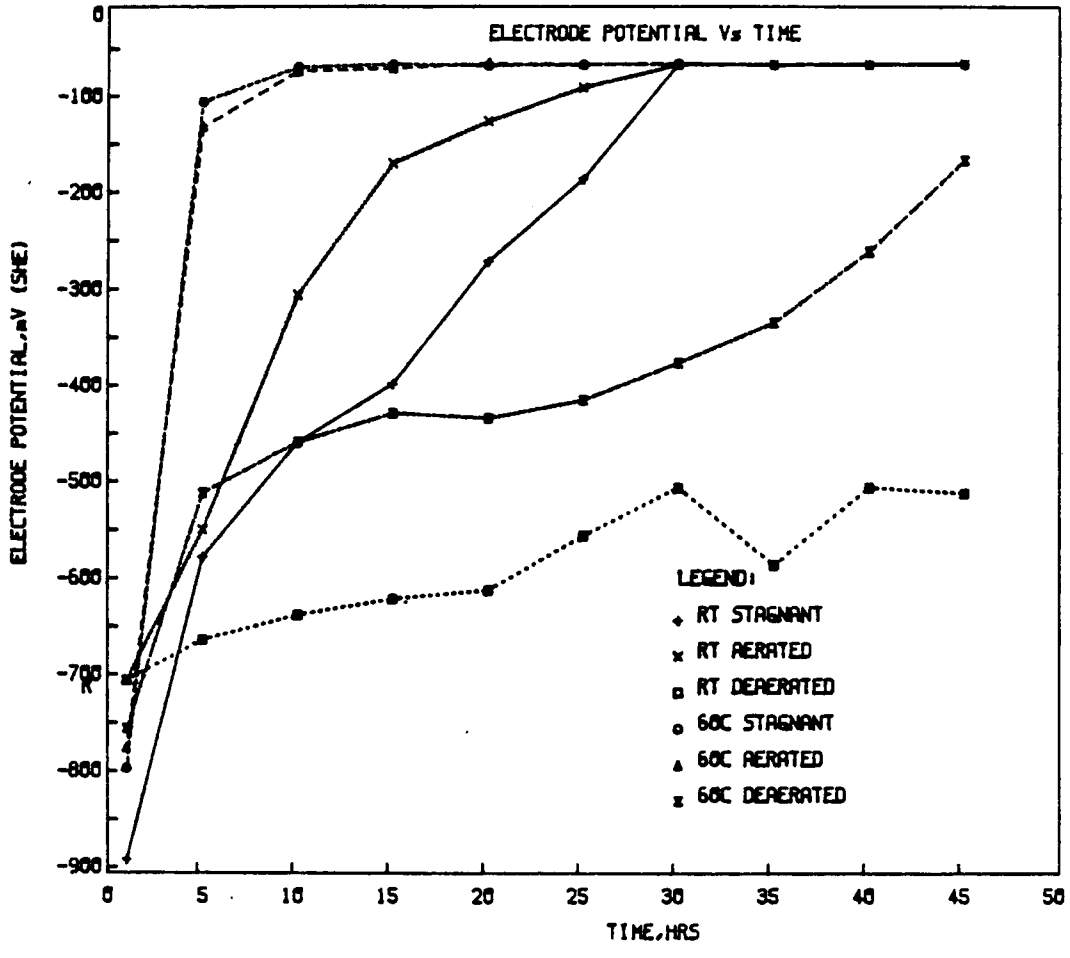


Figure 21. The behavior of zinc in 600PPM $HCO_3^-$ solutions and different environments.

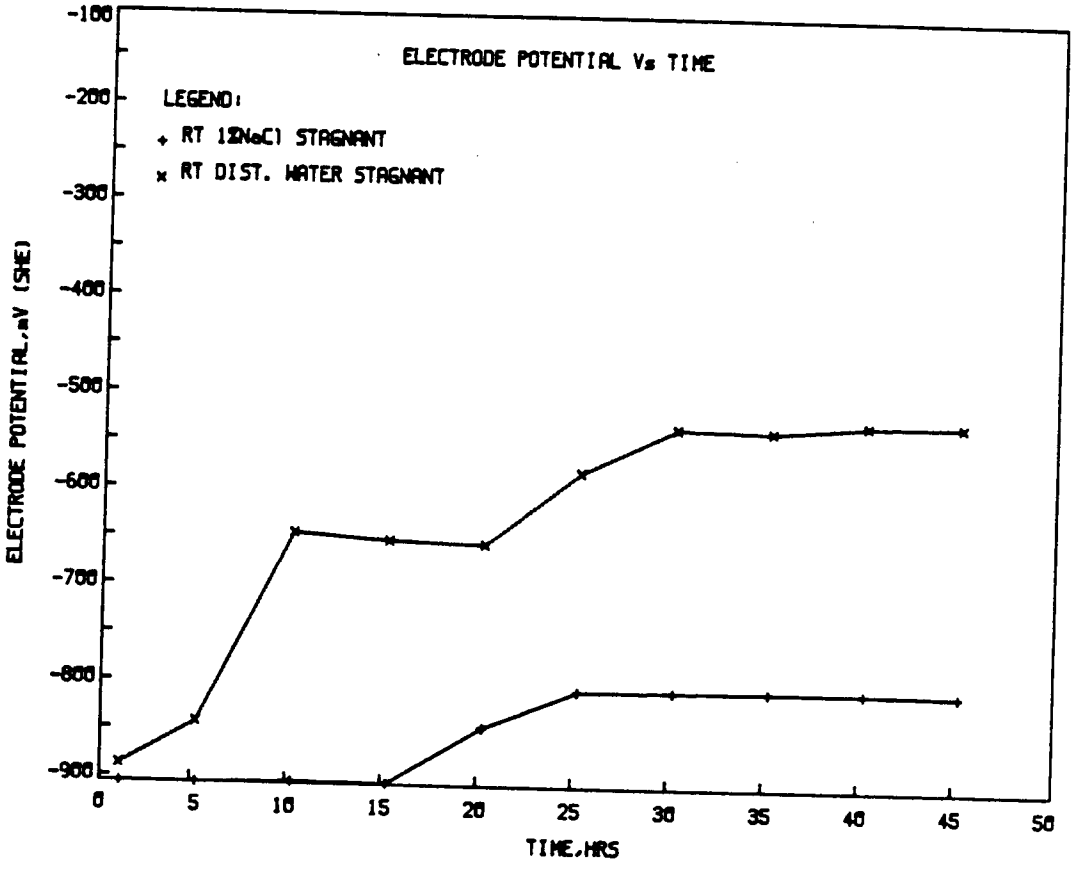


Figure 22. The behavior of zinc in 1% NaCl and distilled water and different environments.

potential of zinc at room temperature in aerated and stagnant conditions increases from approximately -850 mV to -50 mV in 30 hours and remains essentially constant thereafter. When the temperature is increased to 60°C, however, the potential increases rapidly to about -100 mV under both aerated and stagnant conditions. In contrast, the increase in potential in deaerated conditions for both room temperature and 60°C was significantly less than the increase observed in aerated and stagnant solutions. As would be expected, the zinc potential in deaerated and room temperature conditions showed the least increase. This is in agreement with the findings of Haney, et al., and others (19,20,23).

To further elucidate the effects of electrolyte composition, corrosion potential measurements were made in distilled water with a pH of approximately 4.3 due to dissolved carbon dioxide. Figure 22 shows that the initial potential was approximately -890 mV, increased rapidly to -650 mV and then became relatively constant at -500 mV after 30 hours. These potentials are considerably more negative when compared to solutions containing bicarbonates.

Environments containing 1% NaCl in distilled water showed the lowest initial potentials, Figure 22, and these remain low, not exceeding -800 mV over the exposure time of 50 hours. The comparative effects of nitrate, carbonate and the combination of nitrate + carbonate + bicarbonate are shown in Figure 23. The data show that the corrosion potential of zinc in carbonate containing environments started at approximately -790 mV and increased gradually to -687 mV

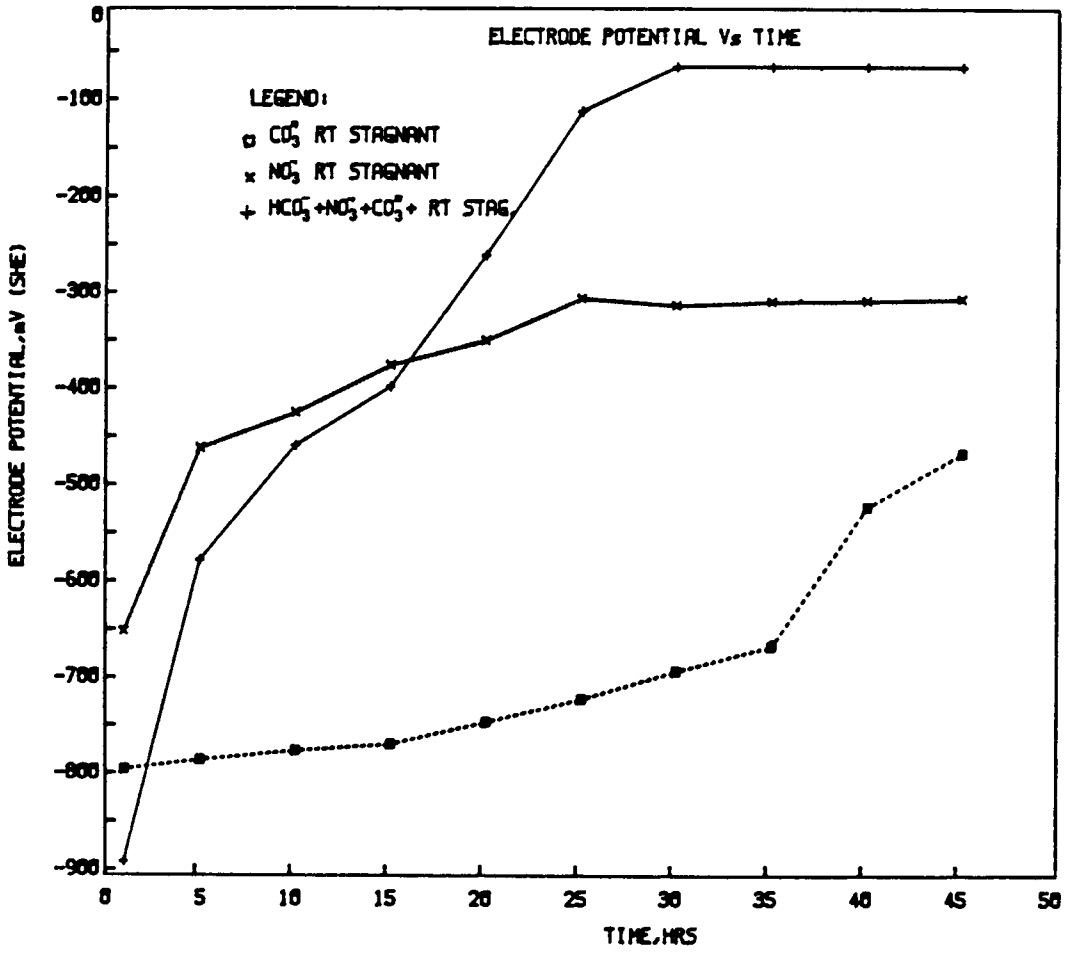


Figure 23. The behavior of zinc in different environments at room temperature.

in 35 hours; the potential increased more rapidly to -440 mV in 45 hours.

The effects of the nitrate ion are somewhat different relative to that observed with carbonate. The data presented in Figure 23 show that the initial potential was approximately -646 mV, increased rapidly to -307 mV within 30 hours, and became constant through the rest of the test period.

The combined effects of 600 mg/l $HCO_3^-$ + 20 mg/l $CO_3^=$ + 73 mg/l $NO_3^-$ on the time dependence of the zinc potential is shown as a third curve in Figure 23. Note the combination of these ions resulted in a similar behavior in the zinc potential to that plotted in Figure 21 for the environment contain 600 mg/l $HCO_3^-$, also under stagnant conditions. The initial potential was approximately -900 mV and reached a value of -50 mV within about 30 hours and essentially remained constant for the remainder of the test period.

The significant difference in the behavior of zinc in the 1% NaCl compared to the other environments can be related to the tendency of the respective environments to form different corrosion product films. It appears therefore that films which form in the presence of chloride do not result in a significant increase in potential but remain near -800 mV as shown in Figure 22. Evans, et al., (33) reported that the chloride ion adversely affects passive film formation on zinc (36). These authors reported that the presence of chloride would deter the precipitation in situ of a corrosion product at the anodic areas, thus decreasing the tendency for stifling of the anodic reaction. It has also been shown by Evans (33) that

chloride and sulfate ions, particularly the former, are capable of penetrating metallic oxide films, thus causing an increased number of anodic sites on corroding metallic surface. However, the observation that the higher potential does not occur in the presence of this ion is not fully explained, at least in terms of mechanism, by only commenting that chloride ions produce local damage on a passive film of zinc.

An explanation can be advanced relating the formation of corrosion product films, including effects of temperature and electrolyte composition, to the potential of zinc, which will also suffice to explain, at least qualitatively, the associated corrosion behavior in terms of weight loss. Few investigations have been reported on the identification or morphology of the corrosion products on zinc. Only one publication, by Gilbert (24) using x-ray diffraction, reports ZnO in $HCO_3^-$ solutions; this film was also identified recently by Powers (34) in alkaline solution. Gilbert (24) explained the corrosion rate in terms of the formation of a zinc oxide film, attributing the more positive potentials observed at 60°C to the formation of the oxide at this temperature. No x-ray test results were reported to show the formation of zinc hydroxide at lower temperatures, although theoretical speculations were made proposing that this might be true.

Gilbert (24) concluded that the most logical explanation for the higher potential behavior of zinc in the various environments was that suggested by Maconachie (23,36).

$$Zn + 2H_2O \rightarrow Zn(OH)_2 + 2H \quad (16)$$

$$2H_{ADS} \rightarrow H_{2gas} \quad (17)$$

$$2H_{ADS} + 1/2O_2 \rightarrow H_2O \quad (18)$$

Gilbert summarizes Maconachie's argument as follows:

> As the overvoltage is high, reaction 16 is almost completely polarized and reaction 17 proceeds very slowly. Dissolved oxygen can cause higher potential according to reaction 18 and the rate of reaction 16 can correspondingly increase, its speed being controlled by the supply of dissolved oxygen. The observed decrease in the rate of corrosion above 60°C would then be due to the decreasing solubility of oxygen with increase in temperature and consequent decrease in the rate of reaction 18.

Grubitsch and Illi (23) consider that in addition to reactions 16, 17 and 18 above, one or both of the following could determine the rate,

$$Zn(OH)_2 \rightarrow ZnO + H_2O \quad (19)$$

$$Zn + 1/2O_2 \rightarrow ZnO \quad (20)$$

Grubitsch and Illi propose that the decrease in the corrosion rate in distilled water above 60°C may be due to a transition of a film of zinc hydroxide to one of zinc oxide. Schikor (38) simply stated that the higher potential behavior of zinc at 60°C is probably due to a very compact film of zinc corrosion products produced at these temperatures.

It is apparent therefore that, depending on the composition of the solution, it might be concluded either that temperature was a controlling factor or that temperature had absolutely no effect on

the potential of zinc. Considering all available data, a conclusion can be made that the effect of temperature is to accelerate the formation of those films that increase the corrosion potential of zinc. There is some evidence (36), although no complete certainty, that a protective coating with a solubility comparable with that of $Zn(OH)_2$ and consisting of a mixture of zinc oxide and carbonate is formed in the presence of bicarbonate.

On the basis of analysis previously described by Delahay, Pourbaix and Rysselberghe (29) in Figure 17 (page 42) and 18 (page 45) one can examine in greater detail the probable circumstances of the film formation on zinc by bicarbonates and carbonates. Figure 21 (page 59) shows that when the sum of $H_2CO_3 + HCO_3^- + CO_3^=$ is equal to 1 and the total zinc concentrations is $10^{-6}$ gram atom of zinc per liter, a gradual increase of pH causes a separation of solid $ZnCO_3$ at pH 6.45 (point A, Figure 17). If the pH is increased further, the solubility of $ZnCO_3$ varies along the curve AB and is a minimum for pH = 10.0.

On the basis of the views expressed in this and other papers one may expect that in solutions containing carbonate and bicarbonate film formation of zinc, based on Figure 18, will occur for values of pH down to 6.5. However, according to Figure 17, the region between pH = 6.5 and 10.5 corresponds to the formation of a film containing chiefly $ZnCO_3$ and the activity of $Zn^{++}$ decreases to about $10^{-9}$. Above pH = 10.5 the activity of $HZnO_2^-$ increases as

$ZnCO_3$ starts to dissolve and at pH = 11.3 of a film containing chiefly $Zn(OH)_2$ will be formed.

By applying the above reasoning to the behavior shown in Figure 18 (page 45) one can conclude that the presence of bicarbonate and carbonate in the solutions leads to the higher corrosion potential of zinc at pH values 6.5 and 10.5 (Table 3).

In order to determine whether the reported reversal in potential was attributable to the iron, time-potential measurements were made on uncoupled iron in a solution containing 600 PPM $HCO_3^-$ at room temperature and at 60°C, under stagnant conditions. Figure 24 shows the corrosion potential of iron at room temperature decreased from approximately -230 mV to -500 mV in 20 hours and remained essentially constant thereafter. At 60°C the initial potential was about -240 mV and reaches the steady potential of -500 mV in 20 hours. The only difference between the two curves as shown in Figure 24 is that at 60°C the potential decreased more rapidly during the first 20 hours.

This observed steady lower potential is accounted for by the formation of a uniform corrosion product covering the metal. As in the case of zinc, the oxide layer on the iron acts as a barrier between the underlying metal and the corrosive environment. However, the controlling effect is less oxygen available by diffusion to the surface. This means that the oxygen polarization curve is shifted to lower current densities with a consequent decrease in the corrosion rate and lowering of the corrosion potential.

TABLE 3

pH AND RESISTIVITY OF THE TEST SOLUTIONS

| | Initial pH | Final pH | Initial Resistivity | Final Resistivity |
|---|---|---|---|---|
| $HCO_3^-$ | 8.13 | 8.82 | 20,000 Ω-cm | 12,000 Ω-cm |
| $NO_3^-$ | 5.40 | 6.40 | 5,000 Ω-cm | 2,000 Ω-cm |
| $CO_3^=$ | 8.09 | 8.23 | 40,000 Ω-cm | 17,000 Ω-cm |
| NaCl | 4.92 | 7.68 | 200 Ω-cm | 100 Ω-cm |
| D.W. | 4.29 | 5.96 | 200,000 Ω-cm | 20,000 Ω-cm |
| $HCO_3^-$ + $CO_3^=$ + $NO_3^-$ | 8.29 | 8.63 | 20,000 Ω-cm | 17,000 Ω-cm |

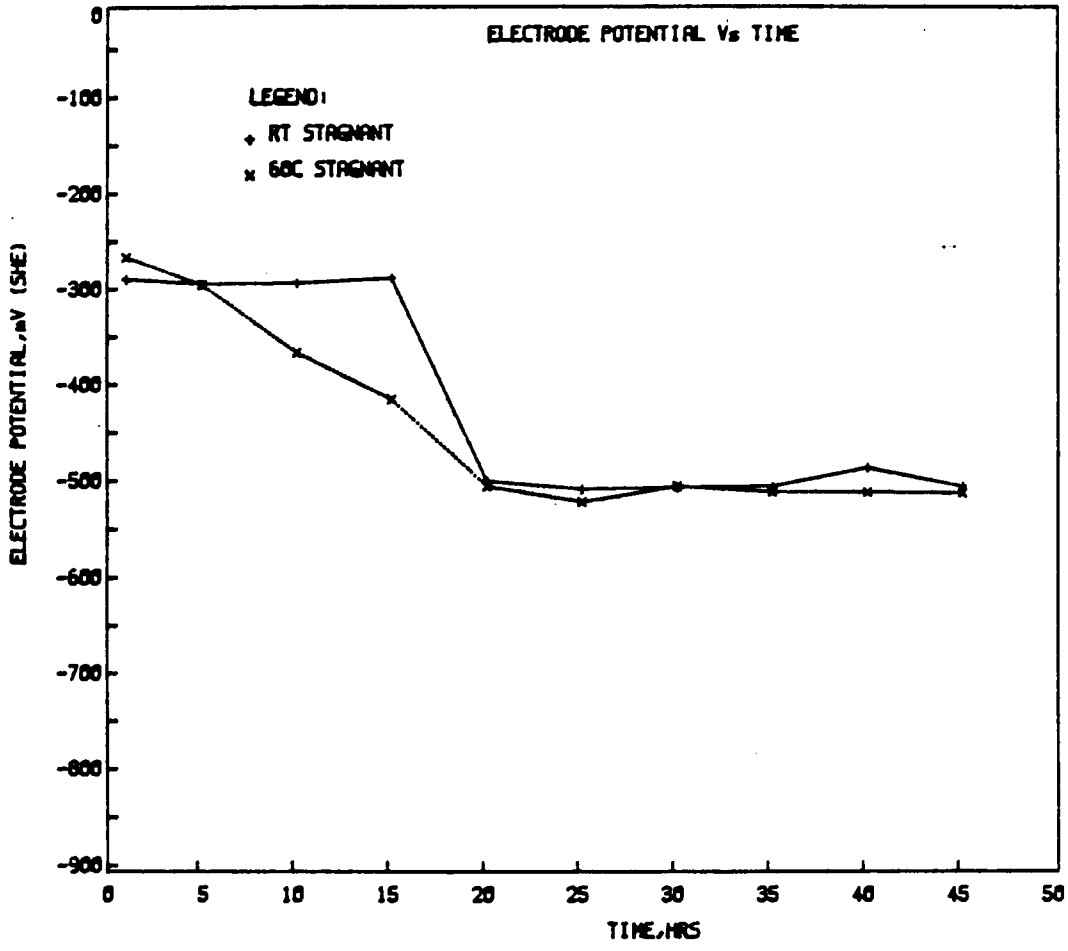


Figure 24. The behavior of iron in 600PPM $HCO_3^-$ at room and 60°C temperature.

Galvanic Coupling

Iron-zinc couples were investigated in the electrolytes shown in Table 4, identified by number 1,2,3,6 and 7. As mentioned earlier, (see Experimental Program) couples were effectively shorted through a zero resistance ammeter, and the potential and currents recorded automatically using a microprocessor. Figure 25 and Table 5 show the potential of the coupled metals as a function of time during exposure to the bicarbonate environment saturated with air, using an air sparge, at room temperature. The initial corrosion potentials at the zinc and at the iron in the above solution were -700 and -400 mV respectively. There is a rapidly increasing potential of the zinc, during the initial five hours of exposure. By four hours, the potentials of zinc and iron were -441 and -449 mV. At this time a potential reversal occurs, (Figure 25) and a current comparable in magnitude to that previously flowing from iron to zinc flowed in the opposite direction, i.e., with iron as anode and zinc as cathode (Table 5).

Similar specimens were exposed to the same bicarbonate environment but under stagnant conditions. Based on Table 5 the initial corrosion potentials at the zinc and the iron were -759 and -504 mV; the potentials as a function of time are plotted in Figure 26. Reversal of polarity occurred after twenty two hours of immersion, the potentials then becoming -423 and -433 mV. This gradual increase in the electrode potential of zinc was accompanied by a steady decrease and final reversal in the cell current (Table 5).

TABLE 4

EFFECT OF AERATION AND TEMPERATURE ON THE CORROSION OF ZINC IN VARIOUS ELECTROLYTES

| No. of Environments | Solution | Type of Test | Temperature | Duration (days) | Loss in Weight (MPY) |
|---|---|---|---|---|---|
| 1 | 600PPM $HCO_3^-$ | Stagnant | Ambient | 7 | 1.340 |
| 2 | 600PPM $HCO_3^-$ | Aerated | Ambient | 7 | 1.040 |
| 3 | 600PPM $HCO_3^-$ | Stagnant | 60°C | 7 | 0.053 |
| 4 | 1% NaCl | Stagnant | Ambient | 7 | 2.600 |
| 5 | 1% NaCl | Aerated | Ambient | 7 | 6.970 |
| 6 | 1% NaCl | Stagnant | 60°C | 7 | 9.740 |
| 7 | Distilled $H_2O$ | Stagnant | Ambient | 7 | 2.100 |

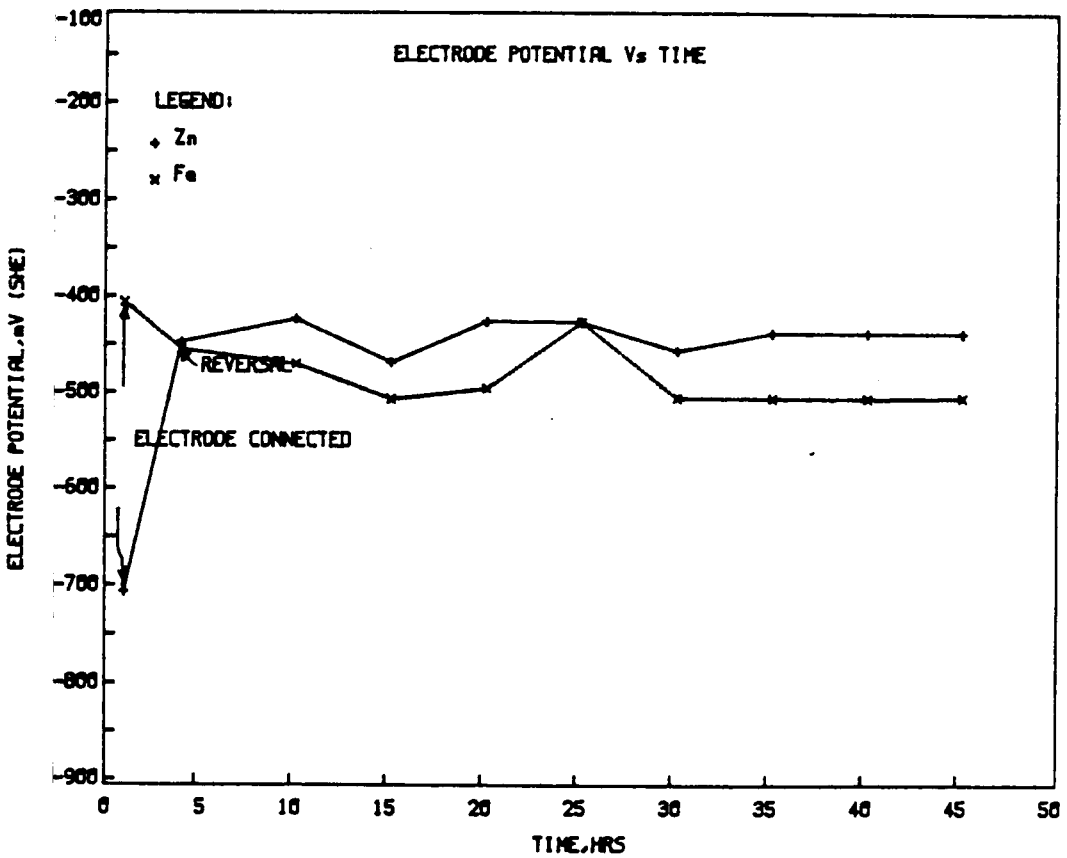


Figure 25. Iron-zinc coupling. Time-potential relationship in bicarbonate, aerated and room temperature conditions. (Iron-zinc ratio 1:1)

TABLE 5

POTENTIAL OF IRON-ZINC COUPLES IN 600PPM $HCO_3^-$ SOLUTIONS

| Duration Time, Hrs. | Aerated Solutions RT $E_{corr.}$ (mV) Fe | Zn | Current .5mA | Aerated Solutions RT $E_{corr.}$ (mV) Fe | Zn | Current .5mA | 60°C, Stagnant Solutions $E_{corr.}$ (mV) Fe | Zn | Current .5mA |
|---|---|---|---|---|---|---|---|---|---|
| 1 | -400 | -700 | 0.0705 | -504 | -759 | 2.0275 | -582 | -596 | 0.0140 |
| 2 | -433 | -580 | 0.0625 | -505 | -615 | 1.7420 | -511 | -519 | 0.0021 |
| 3 | -482 | -531 | 0.0155 | -504 | -591 | 1.1150 | -512 | -519 | 0.0010 |
| 4 | -449 | -441 | -0.8345 | -499 | -580 | 1.0250 | -526 | -521 | -0.0035 |
| 5 | -483 | -446 | -0.9290 | -483 | -559 | 0.9615 | -525 | -522 | -0.0030 |
| 6 | -474 | -440 | -0.9790 | -475 | -541 | 0.5110 | -526 | -524 | -0.0020 |
| 7 | -466 | -427 | -1.1370 | -445 | -540 | 0.3600 | -529 | -528 | -0.0025 |
| 8 | -469 | -431 | -1.0650 | -448 | -530 | 0.2480 | -530 | -528 | -0.0025 |
| 9 | -470 | -430 | -0.9985 | -445 | -575 | 0.2470 | -530 | -528 | -0.0025 |
| 10 | -464 | -417 | -1.1170 | -446 | -571 | 0.1625 | -530 | -528 | -0.0025 |
| 11 | -464 | -420 | -1.0560 | -447 | -572 | 0.1395 | -530 | -528 | -0.0025 |
| 12 | -460 | -422 | -1.0245 | -430 | -514 | 0.1080 | -530 | -528 | -0.0025 |
| 13 | -456 | -409 | -1.1075 | -431 | -512 | 0.1060 | -530 | -528 | -0.0020 |
| 14 | -458 | -419 | -1.0115 | -432 | -522 | 0.0855 | -531 | -530 | -0.0015 |
| 15 | -500 | -462 | -1.0770 | -435 | -515 | 0.0595 | -531 | -529 | -0.0020 |
| 16 | -451 | -415 | -0.9880 | -432 | -514 | 0.0510 | -531 | -529 | -0.0020 |
| 17 | -448 | -410 | -1.0430 | -435 | -514 | 0.0395 | -531 | -530 | -0.0020 |
| 18 | -496 | -410 | -1.0533 | -432 | -490 | 0.0270 | -532 | -533 | -0.0015 |
| 19 | -496 | -415 | -1.0530 | -437 | -480 | 0.0120 | -531 | -530 | -0.0015 |
| 20 | -489 | -419 | -1.0650 | -437 | -450 | 0.0025 | -530 | -529 | -0.0010 |
| 21 | -479 | -420 | -1.0650 | -433 | -437 | 0.0010 | -535 | -535 | -0.0015 |
| 22 | -479 | -420 | -1.0600 | -433 | -423 | -0.0010 | -532 | -531 | -0.0015 |
| 23 | -472 | -420 | -1.0700 | -436 | -421 | -0.0295 | -531 | -530 | -0.0015 |
| 24 | -480 | -420 | -1.0690 | -438 | -425 | -0.0120 | -531 | -531 | -0.0015 |
| 25 | -420 | -420 | -1.0700 | -441 | -428 | -0.0195 | -530 | -529 | -0.0015 |
| 26 | -480 | -430 | -1.0760 | -437 | -433 | -0.0320 | -530 | -529 | -0.0015 |
| 27 | -481 | -430 | -1.0700 | -435 | -427 | -0.0260 | -531 | -528 | -0.0015 |
| 28 | -480 | -430 | -1.0710 | -435 | -422 | -0.0300 | -530 | -529 | -0.0015 |
| 29 | -491 | -429 | -1.0700 | -435 | -423 | -0.0395 | -531 | -528 | -0.0015 |
| 30 | -499 | -450 | -1.0700 | -433 | -423 | -0.0400 | -531 | -529 | -0.0015 |
| 40 | -499 | -431 | -1.0720 | -431 | -422 | -0.0350 | -530 | -529 | -0.0014 |
| 45 | -498 | -431 | -1.0710 | -434 | -419 | -0.0450 | -530 | -528 | -0.0015 |
| 50 | -499 | -431 | -1.0720 | -435 | -423 | -0.0615 | -530 | -528 | -0.0005 |

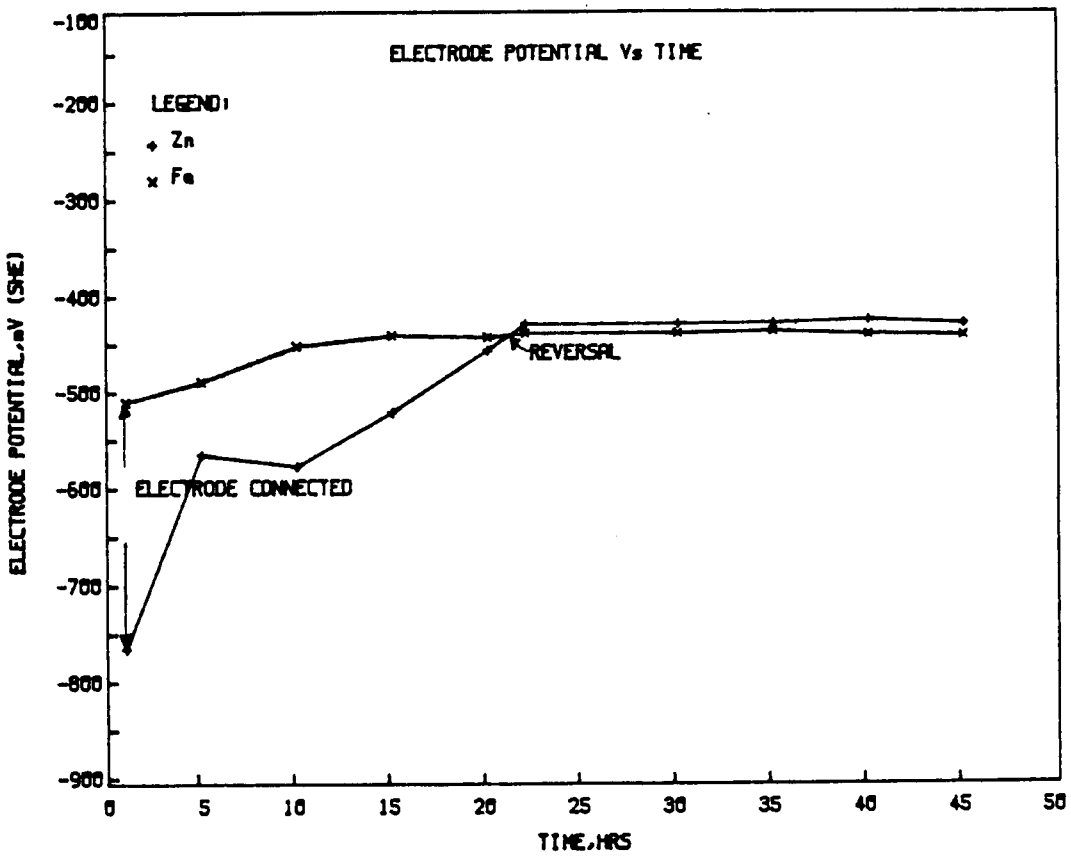


Figure 26. Iron-zinc coupling. Time-potential relationship in bicarbonate, stagnant and room temperature conditions. (Iron-zinc ratio 1:1)

In the corresponding galvanic cell at 60°C, the initial potentials at the zinc and the iron are -596 and -582 mV, i.e., the zinc is slightly anodic (Table 5 and Figure 27). The reversal of polarity occurred at about the same time as for the aerated condition. The cell current, however, was very low and remained at almost a constant value.

Figure 28 and Table 6 show the potential-time behavior of iron-zinc galvanic couples in distilled water at room temperature under stagnant conditions. The corrosion potentials at the zinc and iron are initially -691 and -313 mV respectively, with no reversal of potential for the entire test period. However, inspection during and after the test indicated that the iron was irregularly covered with a corrosion product. The fluctuations in both potential and current may then be attributed to successive acts of formation and breakdown of corrosion product films on the zinc and iron surfaces.

The behavior of the iron-zinc couple in the 1% NaCl environment at room temperature and under stagnant conditions is shown in Figure 29 and Table 6. The initial corrosion potentials at the zinc and iron are -786 and -775 mV, and remain constant throughout the test; there is no reversal of polarity. The current essentially remains high and constant. The electrode potential of the iron is depressed well below the corrosion potential of uncoupled iron and the surface remains bright and free from corrosion product throughout the test period. It is evident that the difference in potential is very small due to the low resistivity of the solution (Table 3) (page 68).

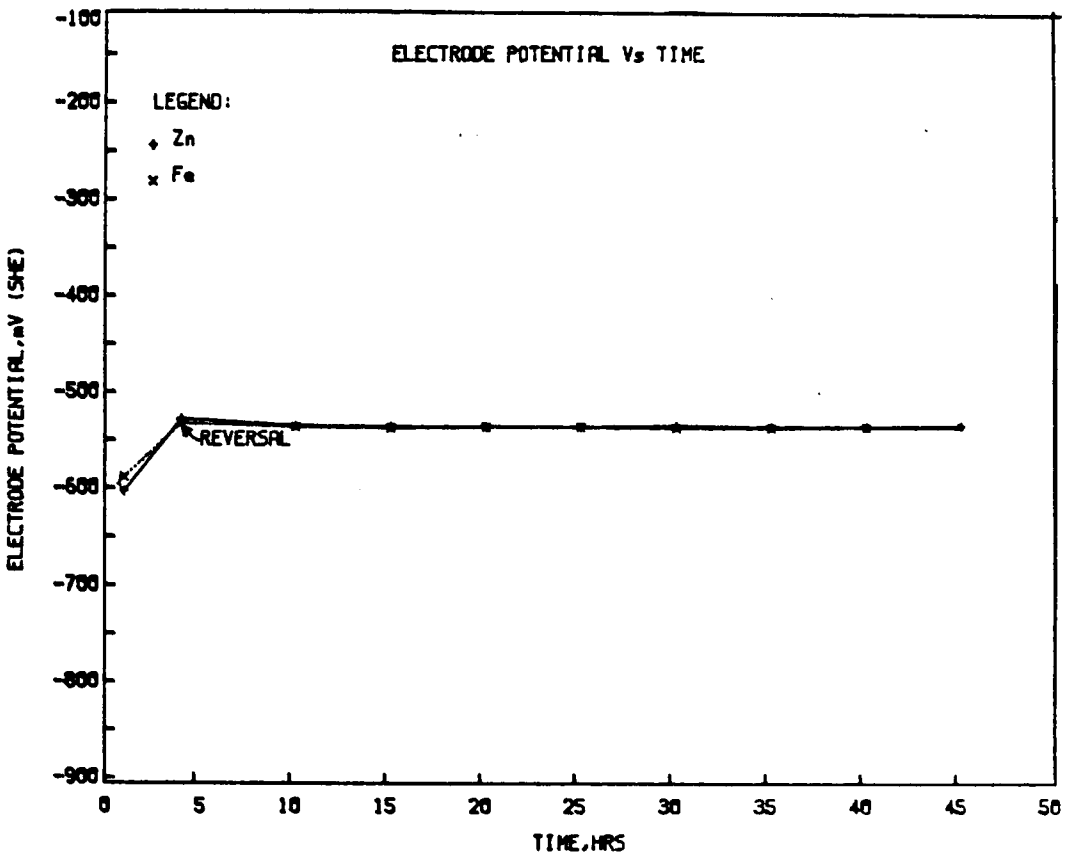


Figure 27. Iron-zinc coupling. Time-potential relationship at 60°C in 600PPM $HCO_3^-$ solution. (Iron-zinc ratio 1:1)

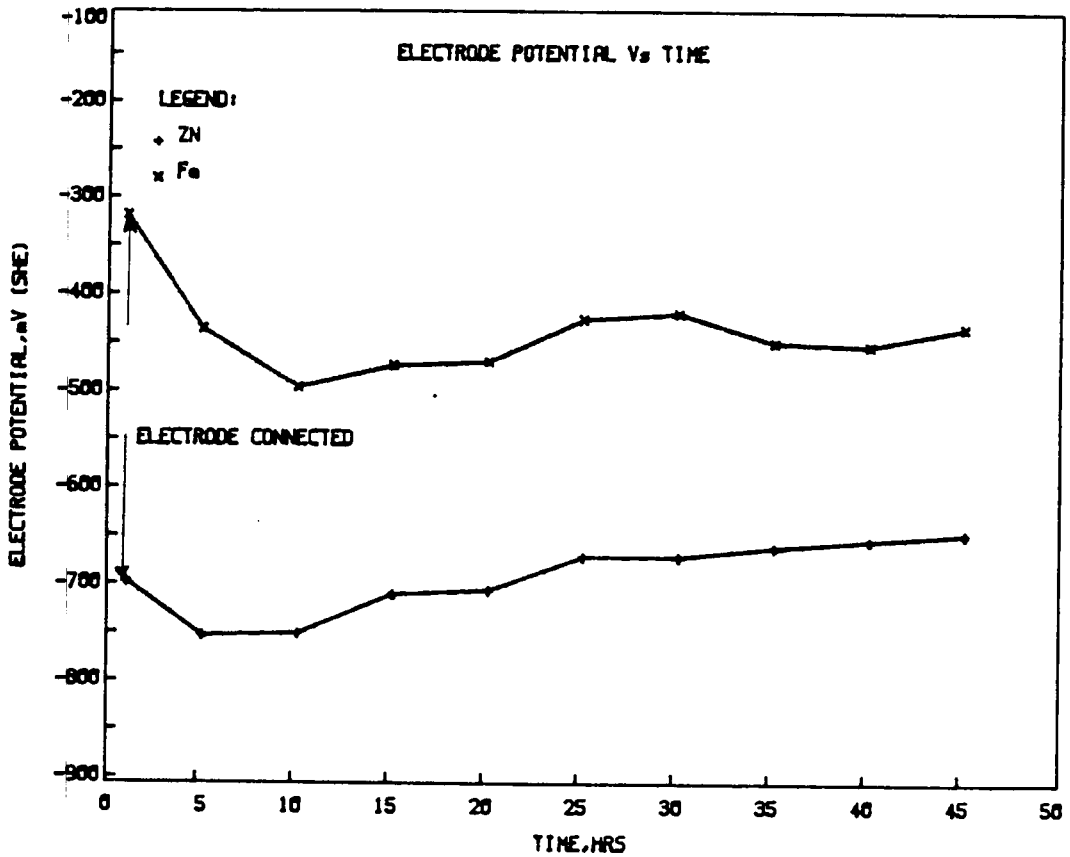


Figure 28. Iron-zinc coupling. Time-potential relationship in distilled water, RT, stagnant conditions. (Iron-zinc ratio 1:1)

TABLE 6

POTENTIAL OF IRON-ZINC COUPLES IN DISTILLED WATER AND 1% NaCl SOLUTIONS

| Duration Time, Hrs. | Distilled Water Stagnant | | | Sodium Chloride Solution Stagnant | | |
|---|---|---|---|---|---|---|
| | $E_{corr.}$ (mV) Fe | Zn | current .5mA | $E_{corr.}$ (mV) Fe | Zn | current .5mA |
| 1 | -313 | -691 | 1.0000 | -775 | -786 | 1.5055 |
| 2 | -417 | -735 | 1.2000 | -776 | -786 | 1.5090 |
| 3 | -449 | -754 | 1.1188 | -774 | -781 | 1.5285 |
| 4 | -450 | -753 | 1.1850 | -774 | -779 | 1.5325 |
| 5 | -430 | -747 | 1.1800 | -758 | -779 | 1.4605 |
| 6 | -425 | -765 | 1.1810 | -775 | -778 | 1.5540 |
| 7 | -430 | -756 | 1.1770 | -776 | -777 | 1.5580 |
| 8 | -464 | -748 | 1.1700 | -715 | -780 | 1.5440 |
| 9 | -487 | -752 | 1.1800 | -772 | -779 | 1.5285 |
| 10 | -490 | -745 | 1.1700 | -772 | -780 | 1.5290 |
| 11 | -480 | -741 | 1.1500 | -771 | -785 | 1.4870 |
| 12 | -484 | -732 | 1.1460 | -773 | -780 | 1.5090 |
| 13 | -487 | -732 | 1.1400 | -771 | -780 | 1.5045 |
| 14 | -470 | -715 | 1.1400 | -772 | -781 | 1.4930 |
| 15 | -467 | -704 | 1.1400 | -773 | -779 | 1.5140 |
| 16 | -461 | -705 | 1.3750 | -773 | -780 | 1.5065 |
| 17 | -462 | -705 | 1.1300 | -773 | -781 | 1.5215 |
| 18 | -461 | -701 | 1.3300 | -773 | -778 | 1.4610 |
| 19 | -462 | -702 | 1.1770 | -772 | -779 | 1.5045 |
| 20 | -463 | -700 | 1.1300 | -775 | -779 | 1.5095 |
| 25 | -419 | -665 | 1.1000 | -773 | -778 | 1.4980 |
| 30 | -413 | -665 | 1.1275 | -772 | -777 | 1.4938 |
| 35 | -443 | -655 | 1.1200 | -774 | -779 | 1.5665 |
| 40 | -446 | -648 | 1.1150 | -771 | -779 | 1.5612 |
| 45 | -427 | -641 | 1.1000 | -772 | -777 | 1.5312 |
| 50 | -444 | -640 | 1.1000 | -767 | -776 | 1.5725 |

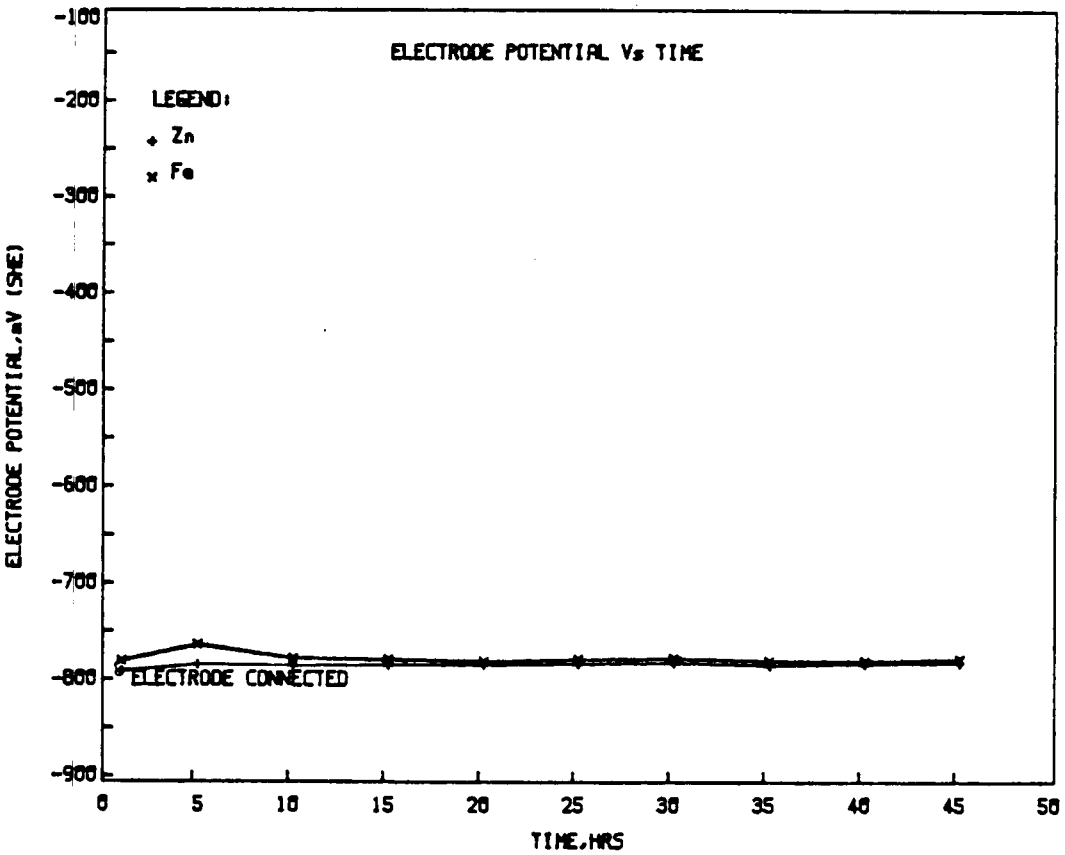


Figure 29. Iron-zinc coupling. Time-potential relationship in 1% NaCl, 60°C and stagnant conditions. (Iron-zinc ratio 1:1)

From the above data one can see that the reversal depends on both electrolyte composition, temperature, aeration and deaeration. Of these factors, it is evident that the bicarbonate solution at higher temperature appears to provide the greatest probability of reversal.

The sodium chloride environment proved to be more effective in preventing the reversal reaction. The addition of NaCl establishes potentials near -775 mV with the potential of iron remaining slightly higher, by about 5 mV, for weeks. At this potential, the iron is completely protected and remains free of corrosion product. The results shown in Figure 25-29 are in general agreement with those of Haney (19).

Weight Loss Measurement

Table 7 shows weight loss and corresponding average calculated penetration rates (MPY) for zinc in bicarbonate and sodium chloride environments for one, two and three-week stagnant exposures at room temperature. Note, from Table 7, that the solution with sodium chloride had a pH of 4.92, largely due to dissolved carbon dioxide; the bicarbonate leads to the higher pH of 8.13. The weight loss per unit area is shown as a function of time in Figure 30. It is evident that the rate of attack of zinc increases with increasing time in the sodium chloride solution. It was also observed that the potential of the zinc remains approximately -900 mV throughout the three week test period. This greater attack compared to the bicarbonate solution is consistent with the complete absence of any

TABLE 7

BEHAVIOR OF ZINC IN VARIOUS SOLUTIONS

| No. of Electrode | | | Duration (days) | Loss in Weight of zinc, $mg/cm^2$* | Penetration rate of zinc, MPY** |
|---|---|---|---|---|---|
| 1 | 600PPM $NaHCO_3$ | 8.13 | 7 | 3 | 1.350 |
| 2 | 600PPM $NaHCO_3$ | | | | |
| 3 | 600PPM $NaHCO_3$ | | 14 | 6 | 1.401 |
| 4 | 600PPM $NaHCO_3$ | | | | |
| 5 | 600PPM $NaHCO_3$ | | 21 | 9 | 1.490 |
| 6 | 600PPM $NaHCO_3$ | | | | |
| 7 | 1% NaCl | 4.92 | 7 | 5 | 2.350 |
| 8 | 1% NaCl | | | | |
| 9 | 1% NaCl | | 14 | 17 | 4.440 |
| 10 | 1% NaCl | | | | |
| 11 | 1% NaCl | | 21 | 55 | 9.090 |
| 12 | 1% NaCl | | | | |

* Surface area approximately ~3 $cm^2$.

**Averaged over the indicated time in days.

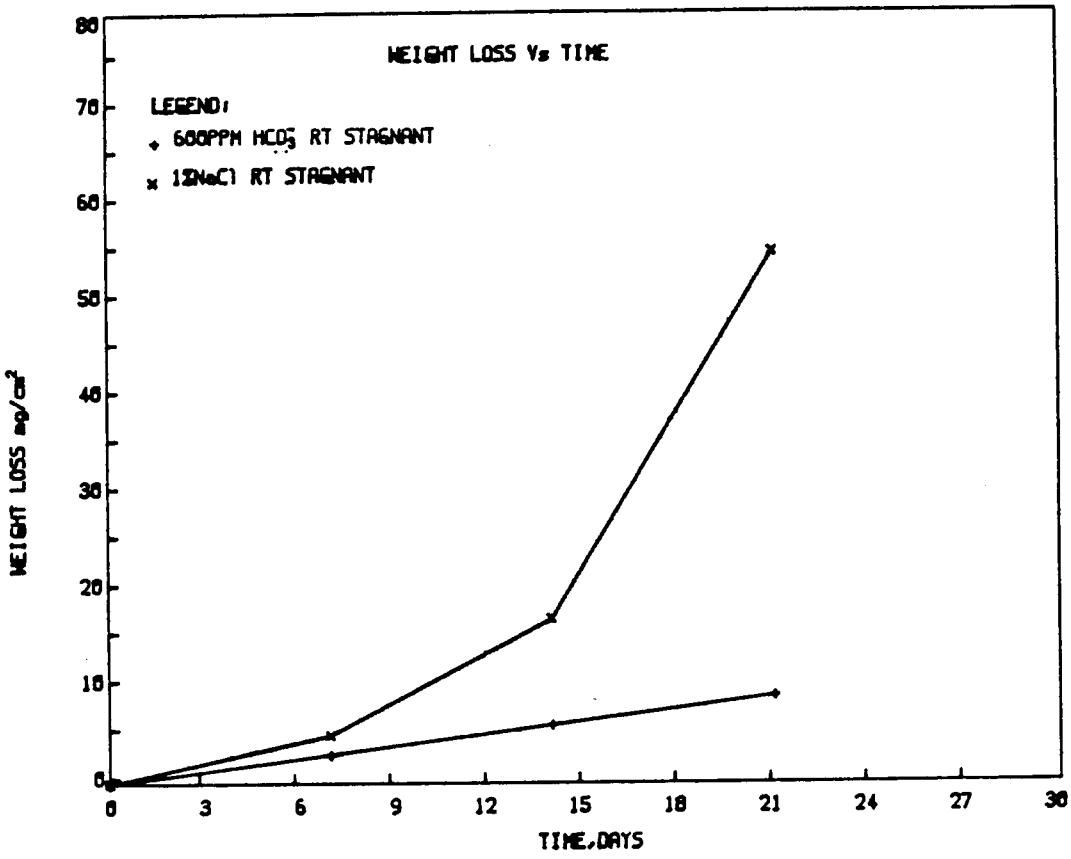


Figure 30. Dissolution of zinc in water containing 600PPM $HCO_3^-$ and 1% NaCl solutions.

adherent film. On the zinc surface, the increased attack is related to pitting, as will be shown and is in agreement with Evans (33) who, noting that chlorides have the ability to penetrate metallic oxide films, attributed the increased corrosion rate of zinc to an increased number of anodic sites on the zinc surface. Figure 30 shows that in the bicarbonate solution, however, the rate of dissolution of zinc remained almost uniform over a period of 21 days. For zinc in bicarbonate solution, however, the potentials were found to increase progressively from -900 mV to as high as -60 mV, the change and rate of change depending on the experimental conditions.

The data in Figure 21 (page 59) indicate that the higher zinc potentials are associated with the presence of bicarbonate and has been correlated to the formation of an adherent type of film on the zinc surface; in such solutions the zinc becomes progressively more cathodic as the temperature is increased.

From Table 7, it is evident that the degree of protection afforded by the corrosion product and scale varies according to the pH of the electrolytes.

The results of exposure of zinc to several environments for a period of one week are shown in Table 7. As is shown, the loss in weight are, in general, considerably greater for environment 6. Comparing environments 4 and 5, as with other common metals, the corrosion rate of zinc increases with aeration. In environment 1, 2 and 3, the loss in weight decreases with increasing temperature and aeration. This appears to be a direct consequence of the more protective corrosion film which reduces the extent of corrosion.

Surface Examination

After stagnant immersion in the bicarbonate and sodium chloride environments for one, two and three weeks, during which the corrosion potentials were monitored, the morphology of the zinc surface was examined by scanning electron microscopy (SEM). The surface morphology was very dependent on the environmental conditions experienced during the test (Figures 31-37). Figure 31 shows the surface after one week of exposure at room temperature in distilled water containing 600 ppm bicarbonate after the corrosion product was removed using 10% HCL inhibited with 0.5% Rodhine 213. It is evident that localized attack has occurred and is selectively along a specific crystal plane of the zinc, probably the basal plane (0001).

The appearance of the uncleaned and cleaned surfaces after two and three weeks of exposure is shown in Figures 32, 33 and 35. Figure 32a and b shows small clumps of corrosion product irregularly covering the surface. At three weeks the clumps have become larger and spherical wtih fibrous protrusions (Figure 34a and b). These cover the whole surface uniformly. After removing the corrosion product, the attack was observed to have initially been localized, with the localized attack spreading with time. Within the localized region the attack was selective along specific crystal planes. The progressive coverage of the surface and the underlying attack on the substrate metal during three weeks of the stagnant exposure at room temperature is evident from this series of figures.

Figures 36 and 37 show specimens exposed to the same bicarbonate solution except that the temperature was raised to 60°C and

a)

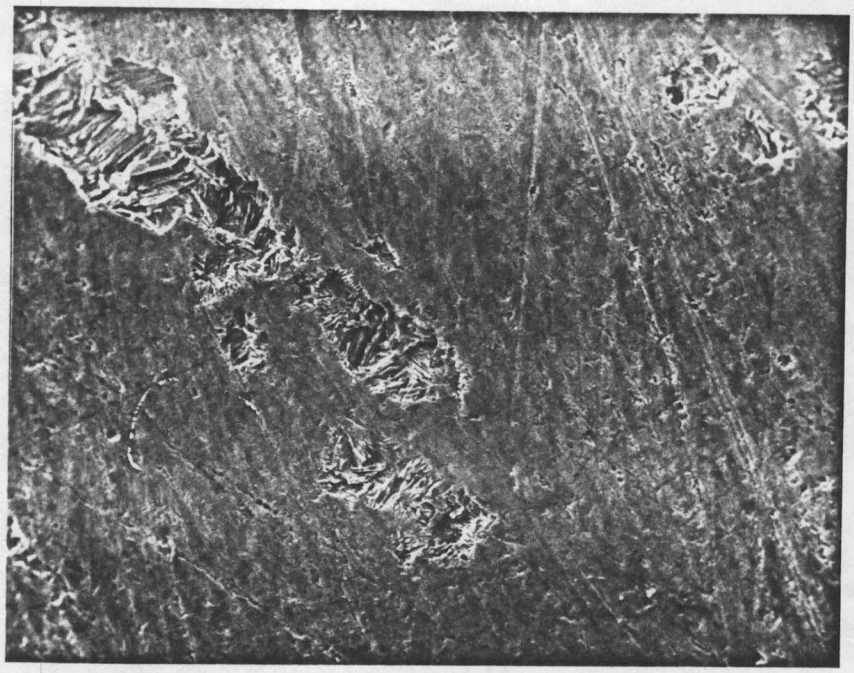

b)

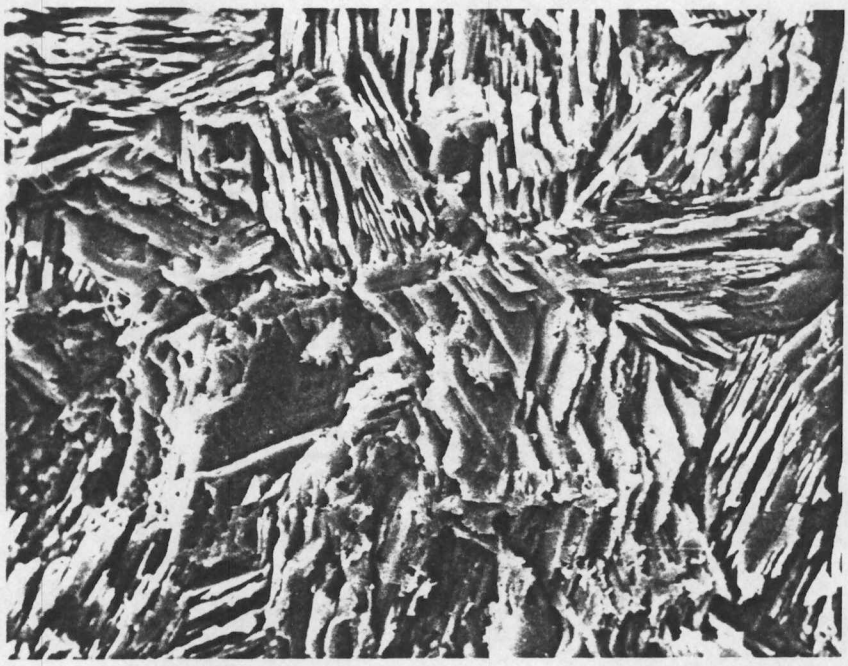

Figure 31. Surface of zinc specimen after removal of corrosion product. (One week, 600PPM $NaHCO_3$, RT, stagnant-- a) 200X b) 2000X.)

a)

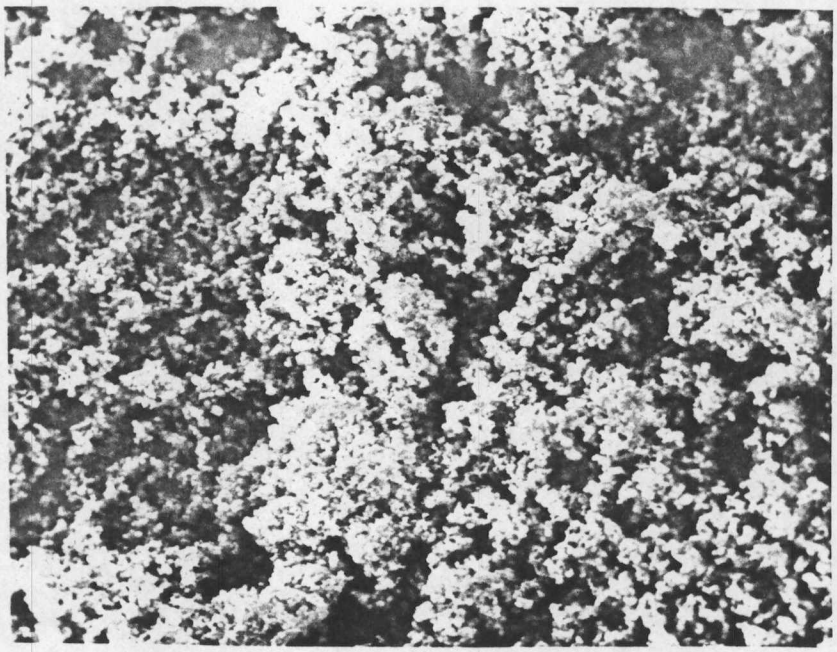

b)

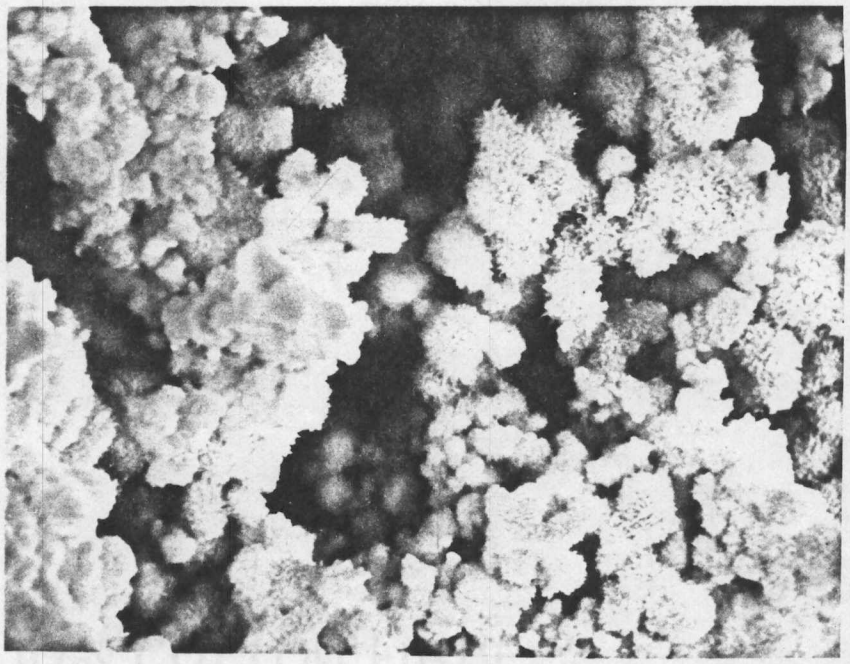

Figure 32. Surface of zinc specimen before removal of corrosion product. (Two weeks, 600PPM $NaHCO_3$, RT, stagnant-- a) 200X b) 2000X.)

a)

b)

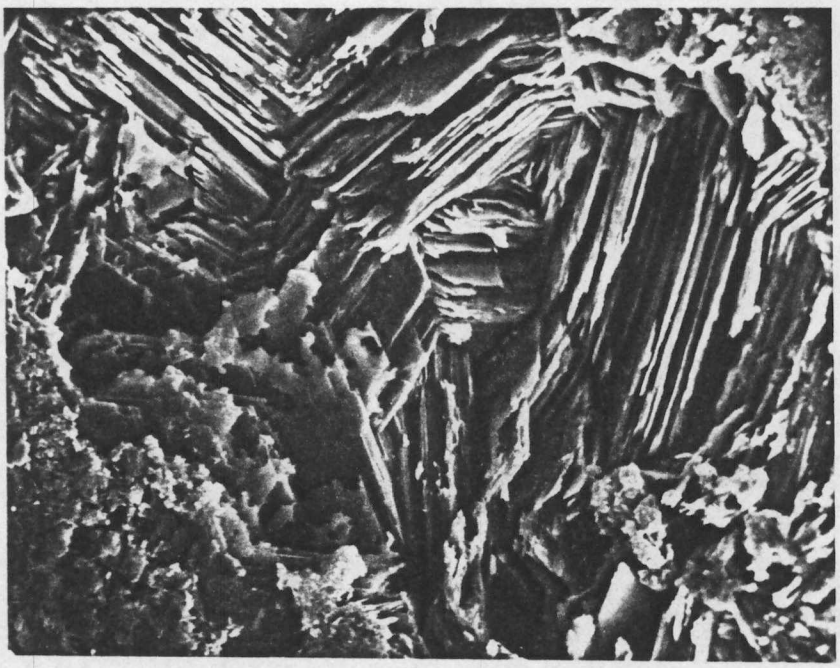

Figure 33. Surface of zinc specimen after removal of corrosion product. (Two weeks, 600PPM $NaHCO_3$, RT, stagnant-- a) 200X b) 2000X.)

a)

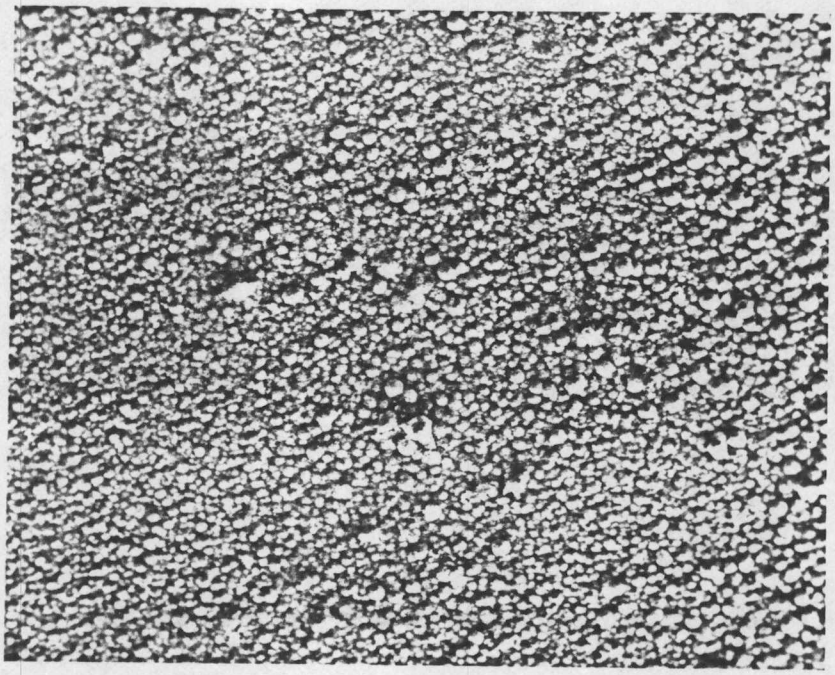

b)

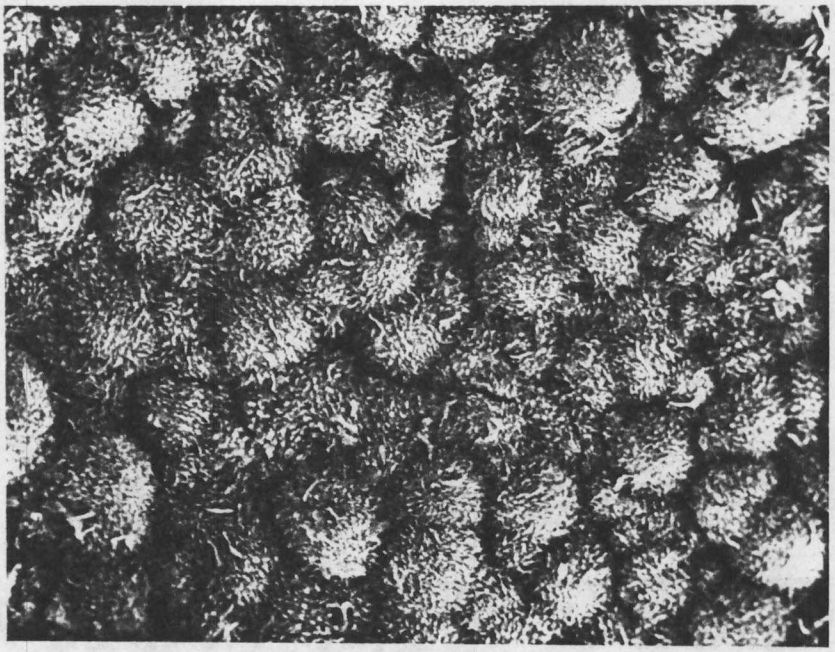

Figure 34. Surface of zinc specimen before removal of corrosion product. (Three weeks, 600PPM $NaHCO_3$, RT, stagnant-- a) 200X b) 2000X.)

a)

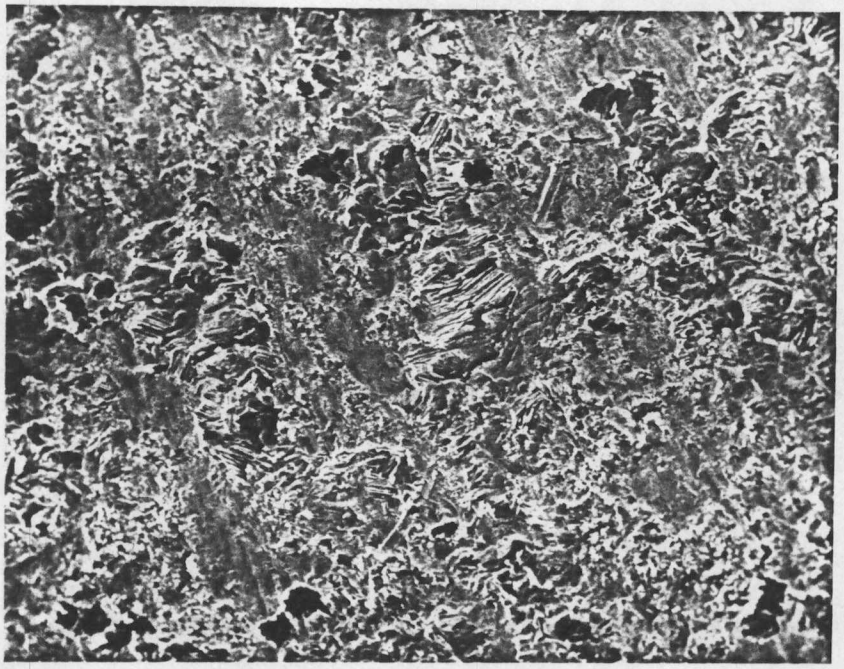

b)

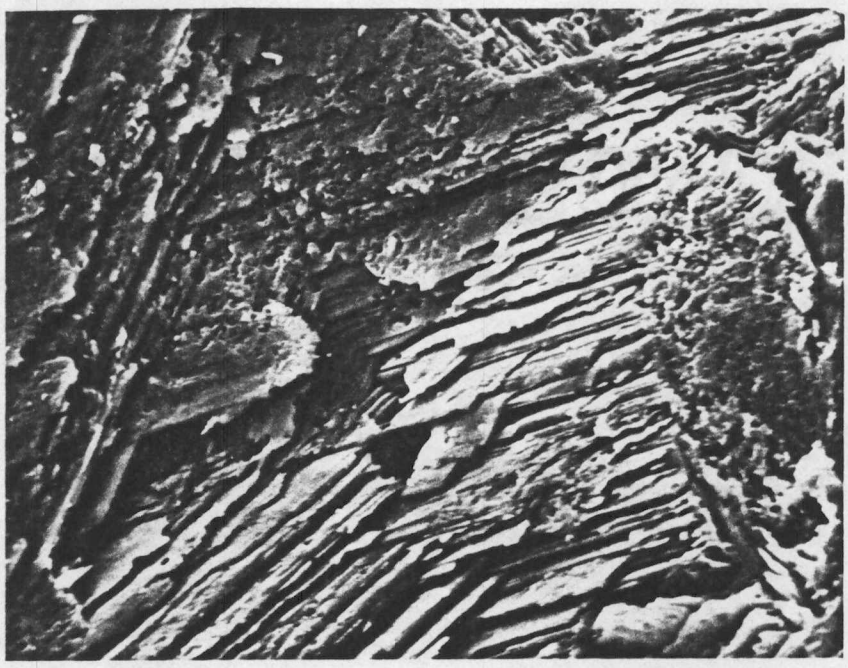

Figure 35. Surface of zinc specimen after removal of corrosion product. (Three weeks, 600PPM $NaHCO_3$, RT, stagnant-- a) 200X b) 2000X.)

a)

b)

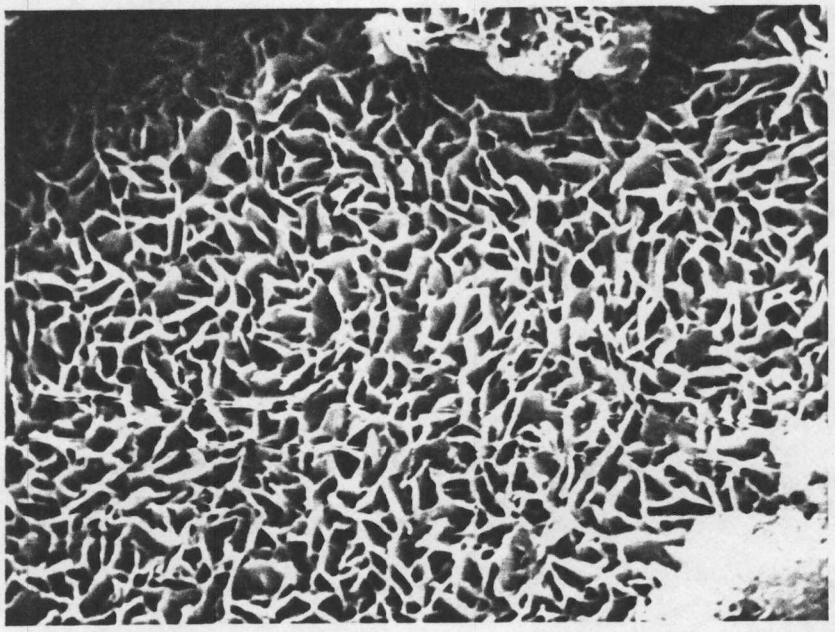

Figure 36. Surface of zinc specimen before removal of corrosion product. (One week, 600PPM $NaHCO_3$, 60°C, stagnant-- a) 200X b) 2000X.)

a)

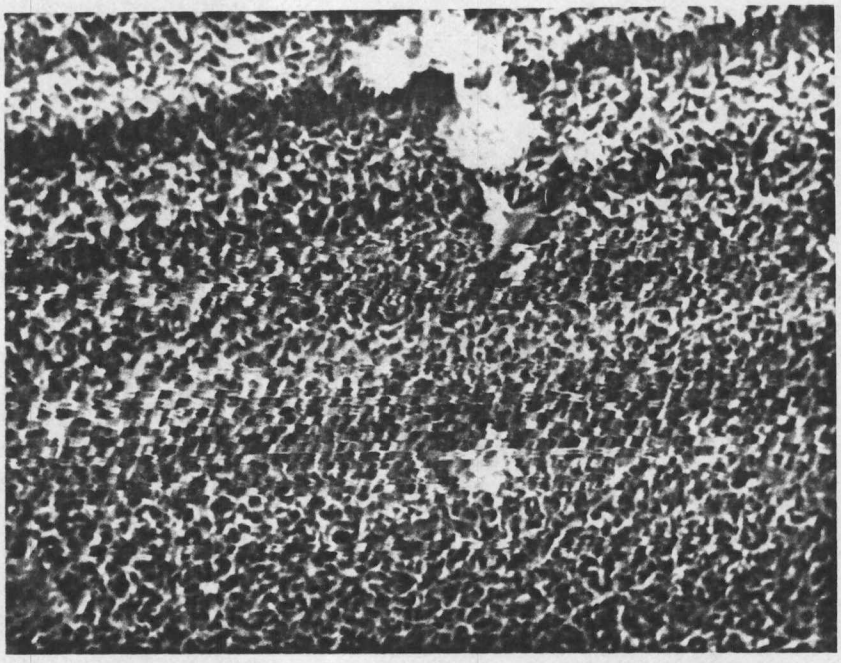

b)

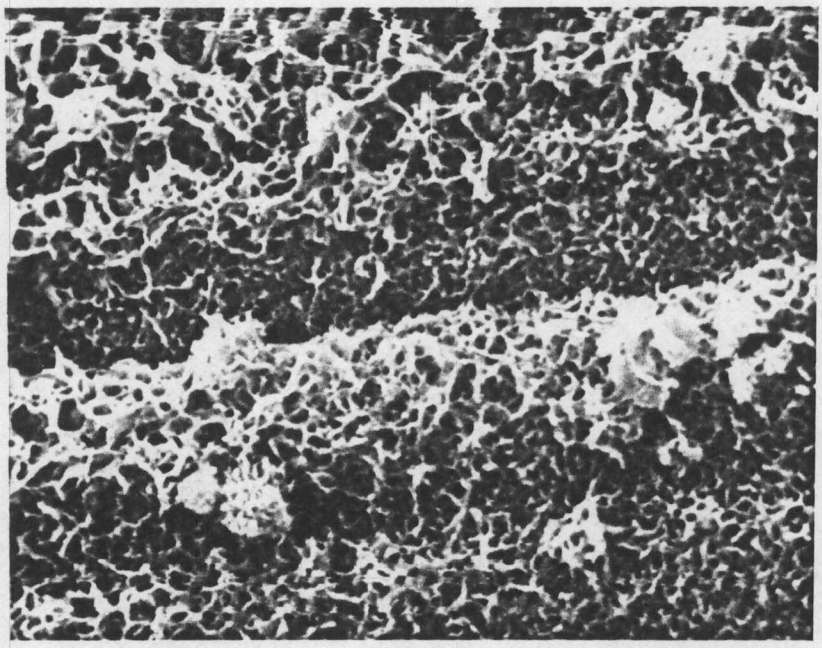

Figure 37. Surface of zinc specimen before removal of corrosion product. (One week, 600PPM $NaHCO_3$, 60°C, aerated-- a) 200X b) 2000X.)

tests conducted under stagnant aerated and deaerated conditions. As is shown in Figure 36, the surface after one week under stagnant conditions, is irregularly covered by a dense cellular type structure. Aeration leads to a finer morphology (Figure 37), with more uniform coverage of the surface. Deaeration however, leads to the surface morphology shown in Figure 38 which appears to be markedly different when compared to that in Figures 36 and 37. The deposit is flaky and loose.

The morphology on deaerated exposure at room temperature (Figure 39), is quite different when compared to that in Figures 36 and 37. The corrosion deposit appears to be flaky, and does not show any cellular structure.

From the SEM observations, the time-potential data in Figure 21 (page 59), and weight loss data in Table 4 (page 71), a reasonable correlation can be made between the corrosion rate and the zinc potential in relation to electrolyte composition, temperature, time, aeration and deaeration.

It is evident from the SEM photographs that the high temperature, aerated bicarbonate environment forms the most adherent, nonporous and corrosion product with a cellular structure. This is consistent with the low weight loss which was observed. Although there is a correlation with the increase in corrosion potential, it is not evident as to why the surface conditions observed resulted in higher corrosion potentials. The problem of understanding this behavior will be considered later in relation to polarization measurements.

a)

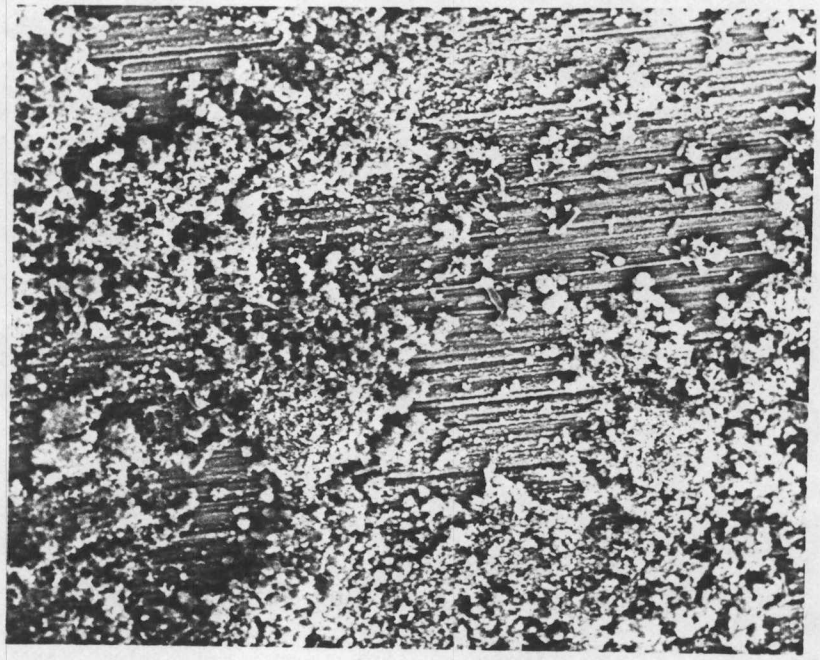

b)

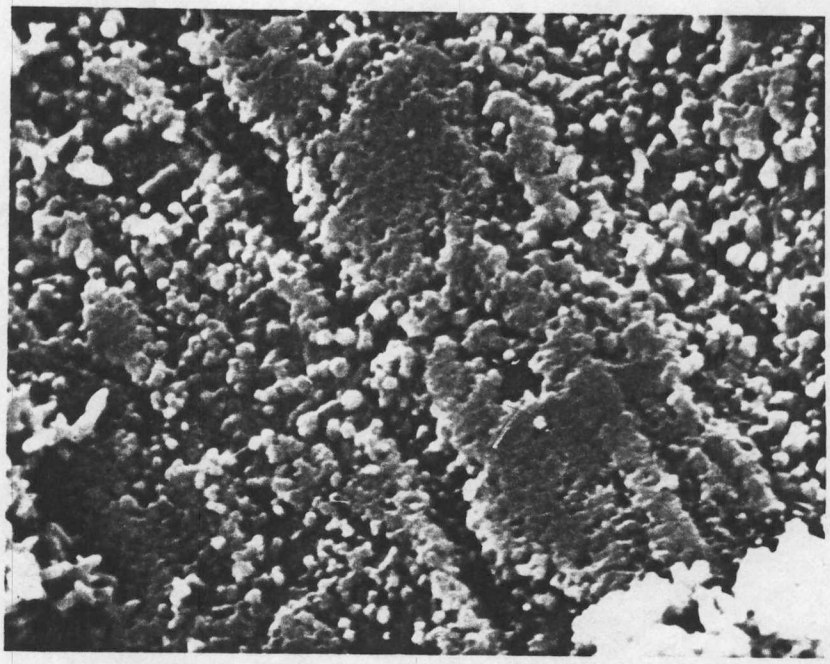

Figure 38. Surface of zinc specimen before removal of corrosion product. (One week, 600PPM $NaHCO_3$, 60°C, deaerated-- a) 200X b) 2000X.)

a)

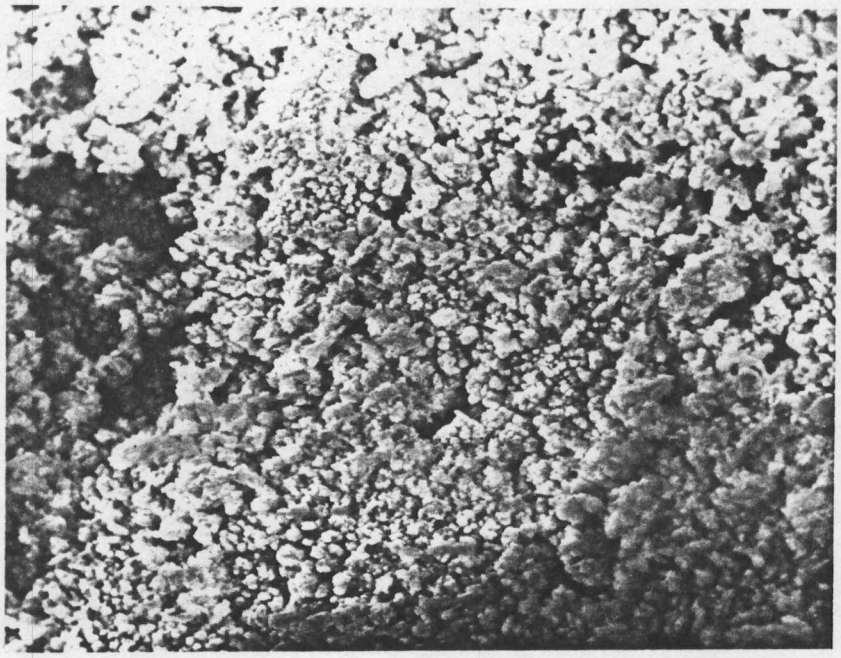

b)

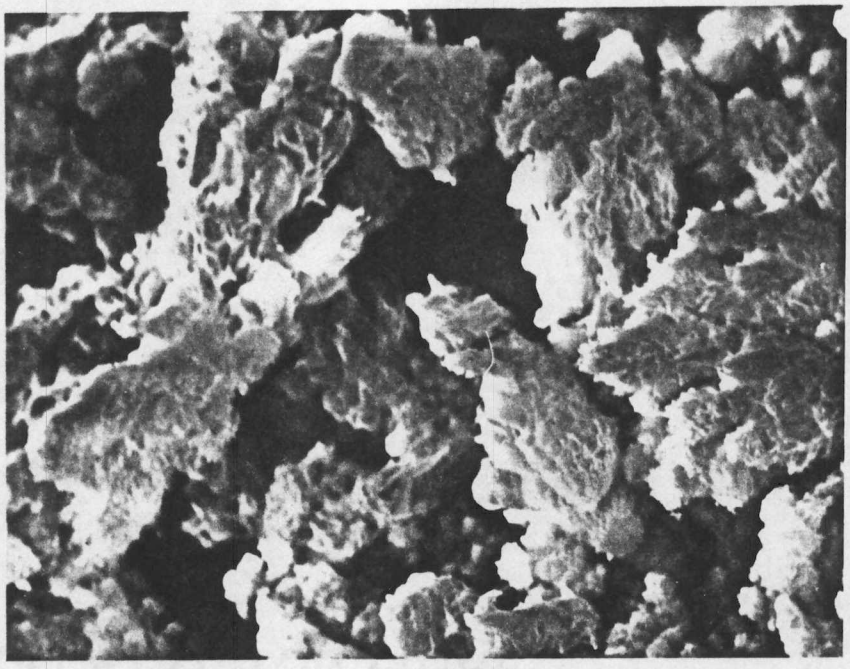

Figure 39. Surface of zinc specimen before removal of corrosion product. (One week, 600PPM $NaHCO_3$, RT, deaerated-- a) 200X b) 2000X.)

The higher corrosion rates in the chloride environment correlates with SEM studies. Figure 40a is a low magnification SEM photograph of a sample exposed in 1% NaCl, under stagnant and room temperature. It indicates uniform but irregular attack over the entire surface. At higher magnification (Figure 40b), the highly crystallographic nature of the attack is evident. Examining the surface before removing the corrosion product revealed, as shown in Figure 41, a non-uniform, non-adherent corrosion product. As is shown in Figure 42, upon removing the corrosion product one can see heavily attacked regions, within which severe pitting was developing. After three weeks of exposure under stagnant conditions, the surface was covered with a dense but irregular corrosion product (Figure 43). The higher magnification photographs of Figure 44b, indicates that several pits of attack will continue at all surfaces of zinc since the corrosion product, zinc chloride is soluble. It was shown in Table 7 that the losses in weight of zinc are, in general, considerably greater in sodium chloride solution. The presence of chloride also decreased the higher potential tendencies, as is shown by the time potential curves in Figure 21 (page 59).

Results and views similar to these have been expressed by Hoxeng and Prutton and others (19,23,24,38).

X-ray analysis of the corrosion product was made directly on the surface of the zinc bicarbonate containing solution. Comparison of the experimental diffraction pattern with patterns of five different types of hydroxide, zinc carbonate and zinc bicarbonate within

a)

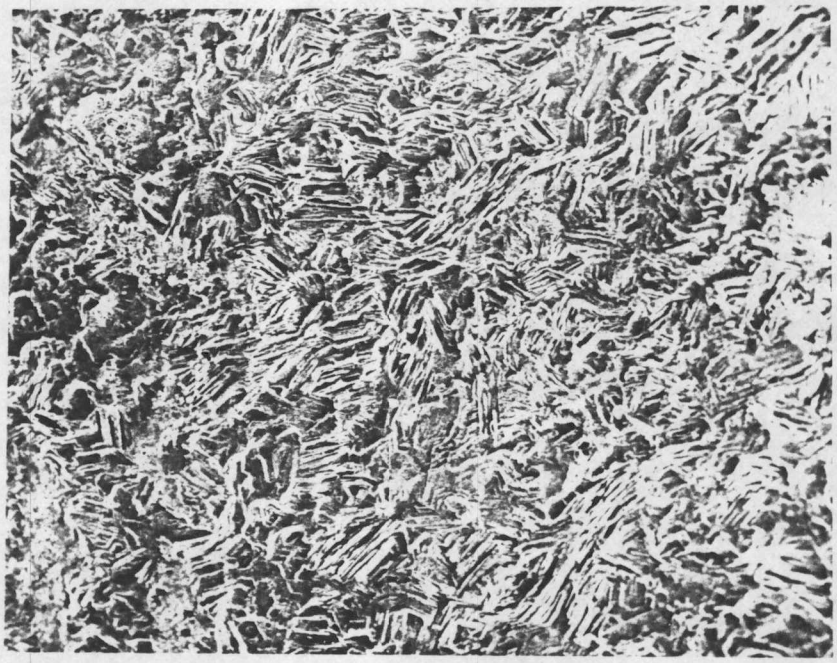

b)

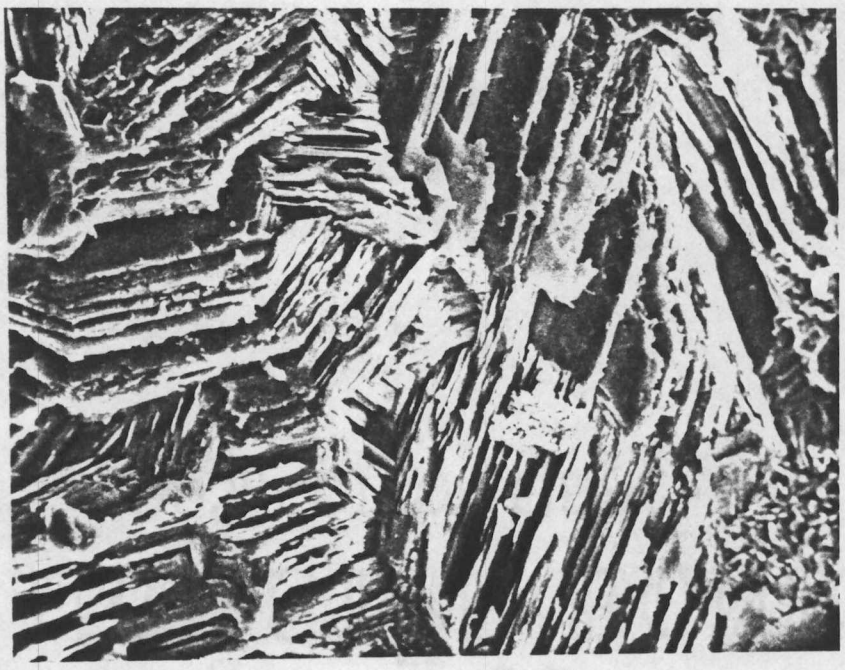

Figure 40. Surface of zinc specimen after removal of corrosion product. (One week, 1% NaCl, RT, stagnant-- a) 200X b) 2000X.)

a)

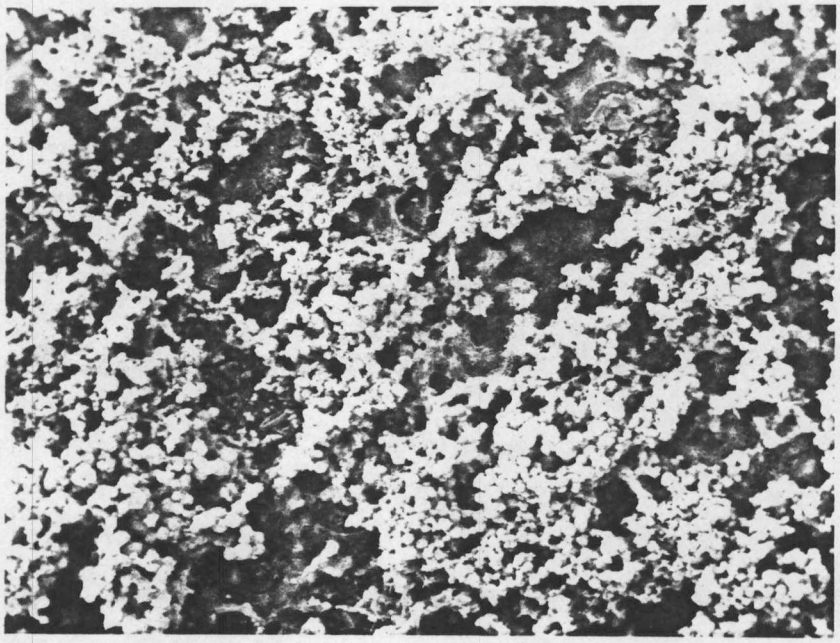

b)

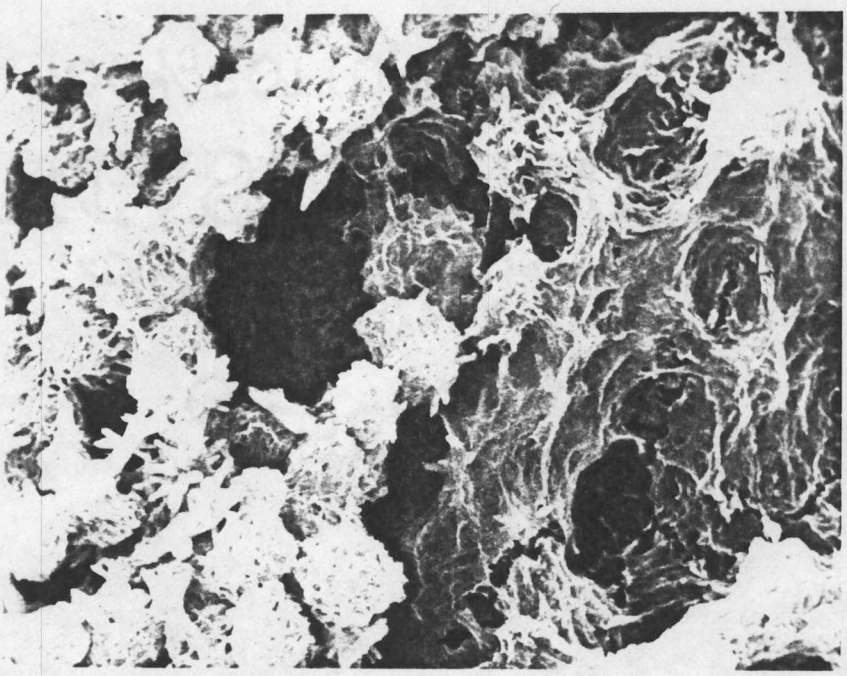

Figure 41. Surface of zinc specimen before removal of corrosion product. (One week, 1% NaCl, RT, stagnant-- a). 200X b) 2000X.)

a)

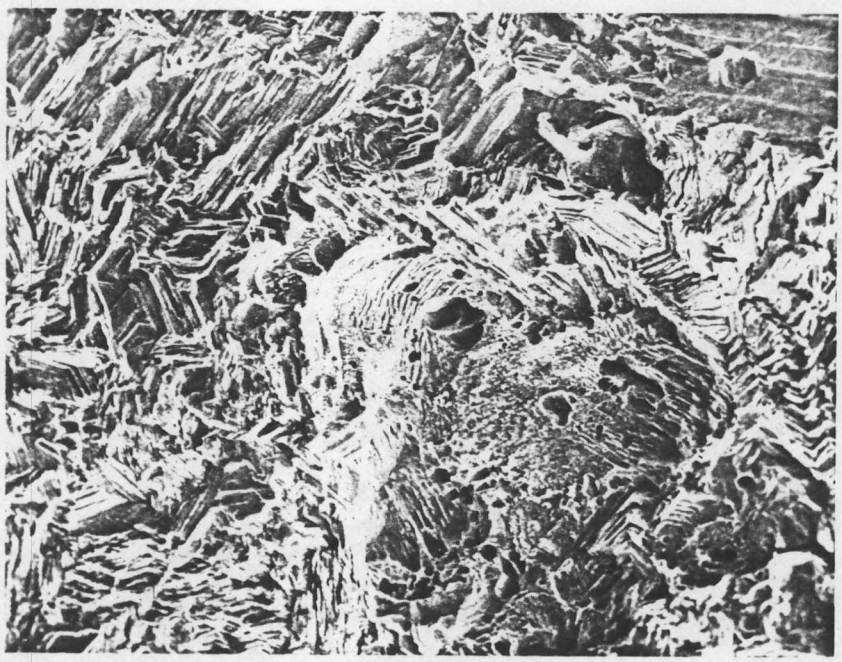

b)

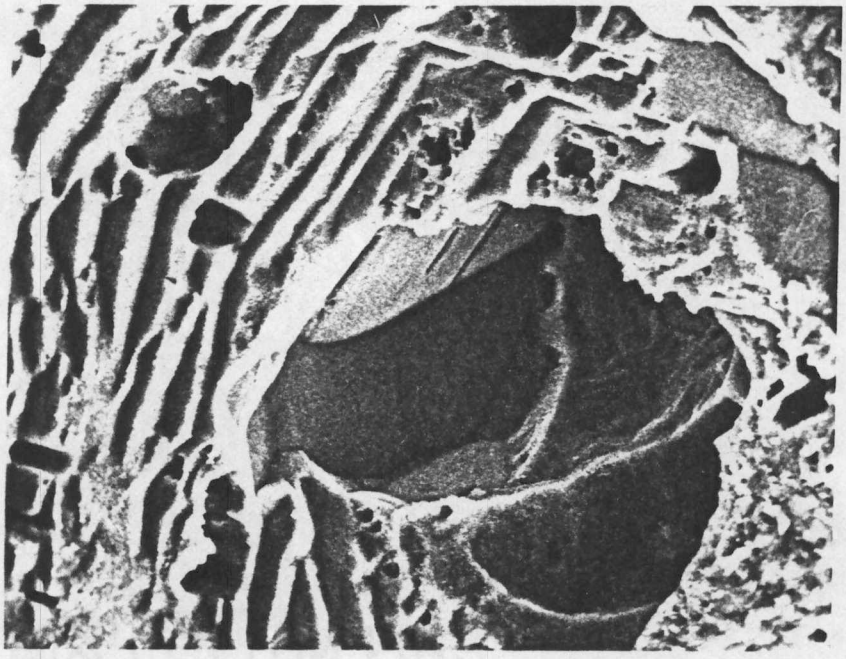

Figure 42. Surface of zinc specimen after removal of corrosion product. (Two weeks, 1% NaCl, RT, stagnant-- a) 200X b) 2000X.)

a)

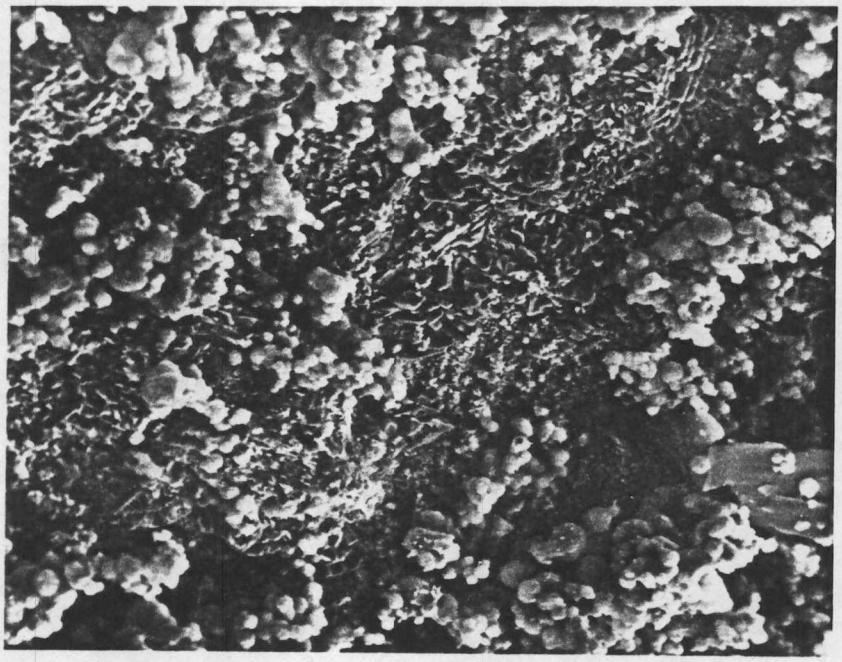

b)

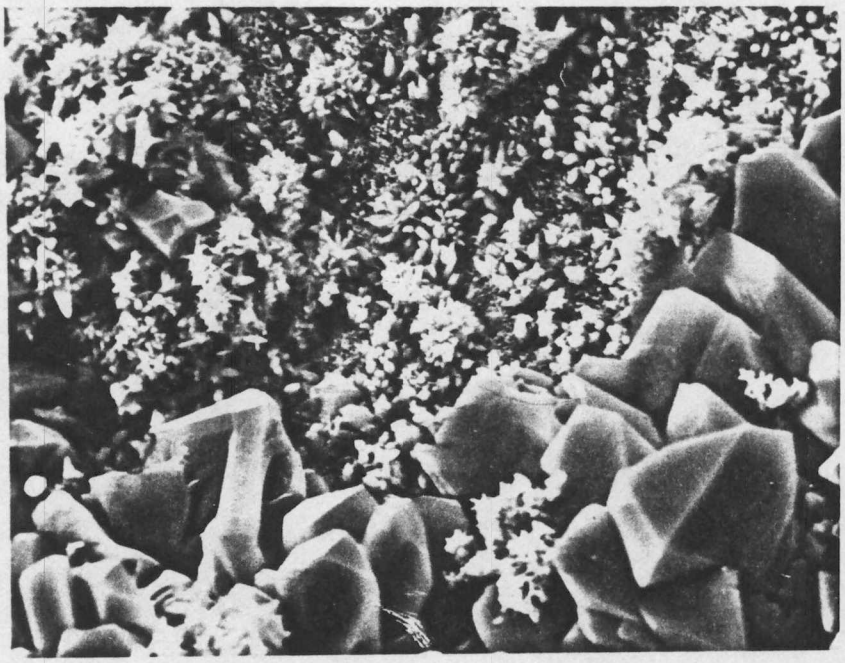

Figure 43. Surface of zinc specimen before removal of corrosion product. (Three weeks, 1% NaCl, RT, stagnant-- a) 200X b) 2000X.)

a)

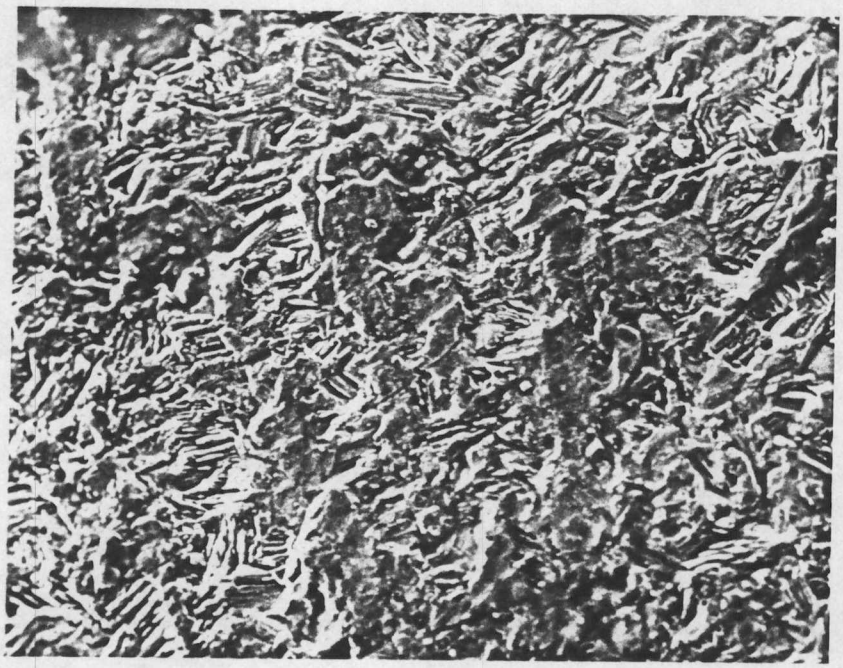

b)

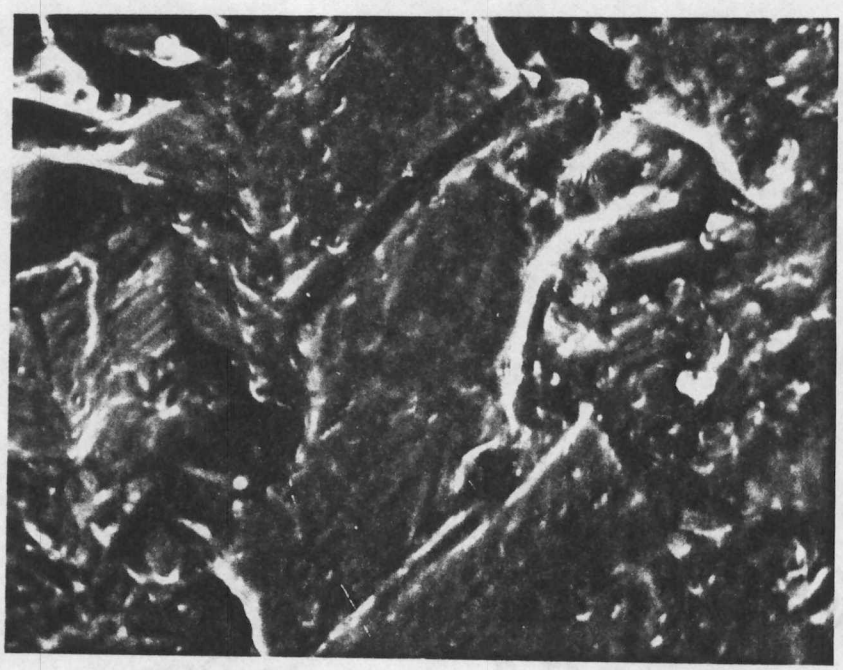

Figure 44. Surface of zinc specimen after removal of corrosion product. (Three weeks, 1% NaCl, RT, stagnant-- a) 200X b) 2000X.)

the file of diffraction data was made. Agreement or any identification was obtained indicating that the corrosion product contained of these compounds. However, the analysis showed well defined diffraction peaks for zinc oxide.

It is likely that the ZnO identified as the corrosion product actually forms by dehydration of $Zn(OH)_2$ and is therefore not the original corrosion product. In order to examine the presence of $Zn(OH)_2$ as the initial corrosion product, a series of x-ray diffraction pattern measurements were undertaken immediately after withdrawing the specimens from the test solutions.

The resulting diffraction patterns showed an irregular arrangement of broad diffraction peaks, thus any attempt to identify $Zn(OH)_2$ were unsuccessful. The nature of the observed diffraction effect is indicative of amorphous or imperfect structure. This structure could have resulted from the jelly like nature of the corrosion product.

## Polarization Studies on Zinc

It was pointed out in the Literature Review that relatively little has been published on polarization curves for zinc as a basis for interpreting its corrosion behavior in near neutral environments. Since the corrosion potential and current are determined by the intersection of the anodic polarization curve for the metal and the sum of cathodic polarization curves for all cathodic reactions, measurements of the polarization, cathodically and anodically, from the corrosion potential can provide information on the corrosion

mechanisms involved. In the case of zinc, with its quite negative half-cell potential and frequently observed corrosion potentials below -700 mV, the polarization of the cathodic reactions must be large. For example at pH 7, the equilibrium half cell reactions for hydrogen ion reduction is -413 mV and for oxygen reduction, +8 mV. Therefore, if the corrosion potential is -7 mV, the hydrogen reaction is polarized by about -3 mV and the oxygen reaction by 1500 mV. These polarizations place the oxygen reaction well into the diffusion polarizations range at any pH and also for the hydrogen reduction for pH values above approximately 5. Furthermore, there is reason to assume that in these lower potential ranges, the dominant cathodic reaction can be the direct reduction of water according to the reaction $2H_2O + 2e \rightarrow 2OH^- + H_2$. Important as the reactions are, relatively little has been published on variables affecting the reduction of water as a function of the substrate on which the reduction occurs and of the ionic species in the environment.

In the present research a large number of polarization measurements were made on zinc in the several environments investigated to better understand observations that were being made of changes of potential as a function of time, temperature and environment. In addition, cathodic polarization measurements were made on several metals, particularly platinum, to provide information on the cathodic reactions that might be involved in the potential range of interest. While the potentiostatic measurements have provided insight into the corrosion mechanisms responsible for the weight loss, potential-time, and surface morphology observations, a satisfactory understanding of

the measurements has not developed. Rather, these measurements have served to demonstrate that the corrosion mechanisms are quite complex and the present results shed some light on the information available in the literature.

Anodic polarization curves for the zinc in distilled water with a pH of 4.35 due to dissolved carbon dioxide are shown in Figure 45. Other conditions of measurement are shown in the figure. The curves were initiated after one, eight and fifteen hours in the polarization cell prior to measurement. The corrosion potentials for these times were -540, -320 and -70 mV indicating an increase of corrosion potential with time, consistent with the potential-time curves shown in Figure 21. Assuming a Tafel slope for the zinc of 5 mV per log decade, intersection of a line tangent to the anodic curves with this slope and extrapolated to the corrosion potential, yields corrosion currents in the range 4-9 microamperes which, on taking the apparent surface area as 4 sq. cm., results in a corrosion current density of 1-5 microamperes/sq.cm. or a corrosion penetration rate of about 0.5 MPY. The relative positions of the anodic curves are surprising in that they are essentially displaced vertically. The fact that the corrosion potential increased with time suggested that a protective film was forming and that a transition from an active to passive state was occurring. However, none of the curves show the usual form for this transition. Rather the curves continue to rise indicating progressively increasing corrosion rates under potentiostatic control. In addition, the curves suggest that, for example, holding at -700 mV should result in a shift in current

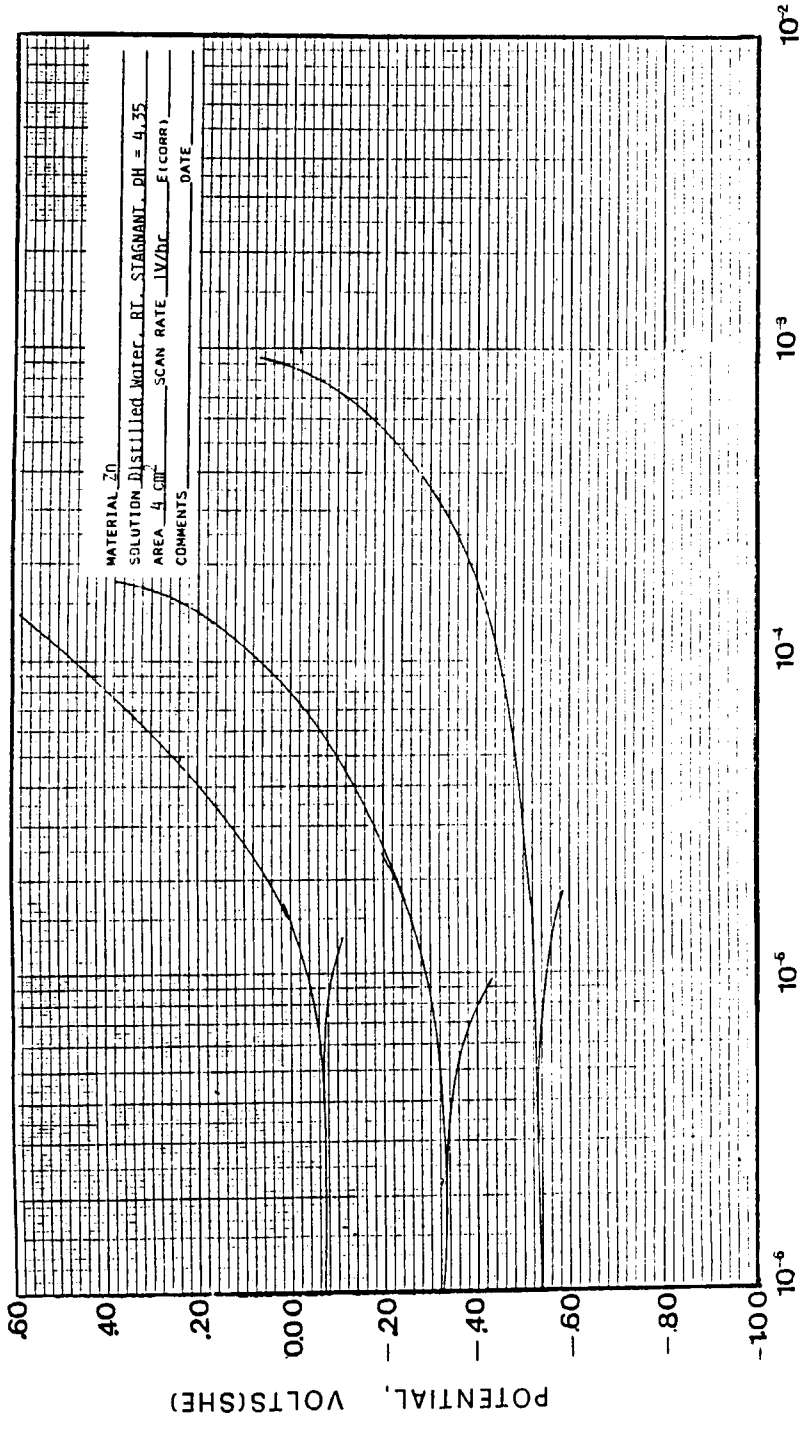


Figure 45. Effect of distilled water on the polarization behavior of zinc.

from $2 \times 10^{-3}$ after one hour in the cell to $1.4 \times 10^{-5}$ amperes after 15 hours. Further, on holding at a potential such as -800 mV, the potential should have shifted from anodic to cathodic in this time. These shifts were not observed. Rather, if the anodic scan was stopped, the current remained essentially constant at the particular potential.

The polarization behavior of zinc in 1% NaCl (pH 4.3) at room temperature for aerated stagnant and deaerated conditions is shown in Figure 46. Under aerated and stagnant conditions, the corrosion potential is -800 mV; under deaerated conditions (nitrogen purge) the corrosion potential is slightly lower, about -910 mV. The anodic polarization curves exhibit approximate Tafel behavior to remarkably high current densities (>10-2 amperes per sq. cm.) with slopes from 40 to 70 mV per log decade, which are reasonable values for metals. Thus the magnitude of the zinc polarization is small over a rather large current density range and is relatively independent of the degree of aeration. In contrast, the cathodic exhibit almost immediate diffusion polarization characteristics (no defineable Tafel range) with a tendency towards limiting current densities increasing with the degree of aeration. Following the procedure for estimating corrosion current density, for the aerated environment the estimated current density is approximately $8 \times 10^{-4}$ amperes per sq. cm., for the stagnant environment about $5 \times 10^{-4}$ and for the deaerated condition, about $2 \times 10^{-5}$ amperes/$cm^2$. These values are considerably higher than for the distilled water environment and are

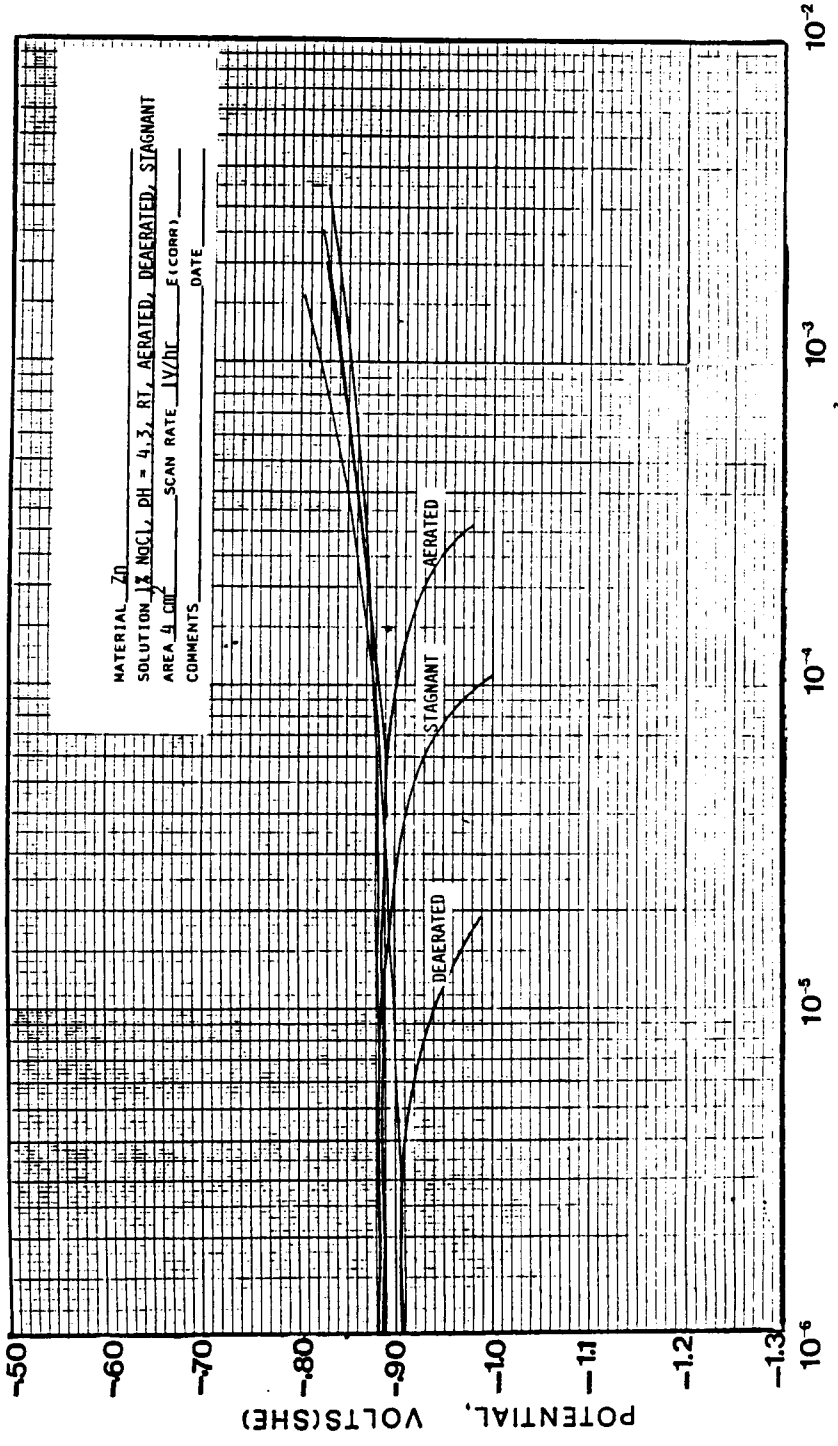


Figure 46. Polarization curves for zinc under aerated, stagnant and deaerated conditions.

consistent with the lower resistivity of the 1% NaCl solution and the absence of any significant corrosion product film, the later being substantiated by the SEM observations.

The corrosion potential measurements as a function of time and the corrosion potential observed on making polarization measurements on zinc in chloride environments indicated values closer to the equilibrium half-cell potential than is observed for most metals in this environment. Specifically, reference to Pourbaix diagram for zinc shows that the equilibrium half-cell potential should be near -900 mV in the range of pH = 5; the observed corrosion potential is in the same range -800 to -850 mV. Therefore, the corrosion potential is less than 100 mV positive to the equilibrium value. In contrast, the equilibrium potential for iron is near -650 mV in this range but the corrosion potentials are approximately -30 mV. In these cases, exposure was made under stagnant conditions with the solution in contact with air. It was also pointed out with reference to Figure 46 that the polarization curves for the zinc in the chloride environment have extended Tafel ranges and the corrosion rates derived from the polarization curves are higher than observed experimentally by weight loss.

A large number of polarization measurements were made in aerated, deaerated and stagnant environments containing 600 ppm bicarbonate ion at room temperature and 60°C. The objective was to better understand, in terms of electrochemical behavior, the rapid increase in corrosion potential of the zinc with in time discussed previously

shown in Figure 47. It was pointed out initially that the pH of this environment is much more basic than either the distilled water (pH 4.35) or the 1% NaCl environment (pH 4.3). If the polarization measurements in the bicarbonate solution are initiated within one hour, the starting corrosion potential is near -800 mV as shown in Figure 46. An anodic curve rises rapidly with no indication of an active-to-passive transition. The cathodic curve has been included for this run and has the form of diffusion controlled reaction leading to a limiting current of $10^{-3}$ amperes ($2.5 \times 10^{-4}$ amperes/$cm^2$). However, after eight hours exposure in the test cell, the corrosion potential has increased to -500 mV, Figure 47. The anodic curve determined starting with this potential is similar in shape to that observed with one hour exposure and again there was no indication of passive transition.

After 15 hours in the polarization cell prior to determining the anodic curve, the corrosion potential increased to -325 mV. The subsequent anodic polarization curve has the same slope as the two curves for test at a higher potential.

This behavior was consistently observed in the bicarbonate solution both at room temperature and at 60°C, the value of the initial corrosion potential increasing more rapidly with time. Otherwise, sets of curves similar to those in Figure 47 were observed.

Some estimates of corrosion rate in the bicarbonate solution were made from the polarization curves for comparison to the weight loss measurements (Table 7). From Figure 47, the corrosion current

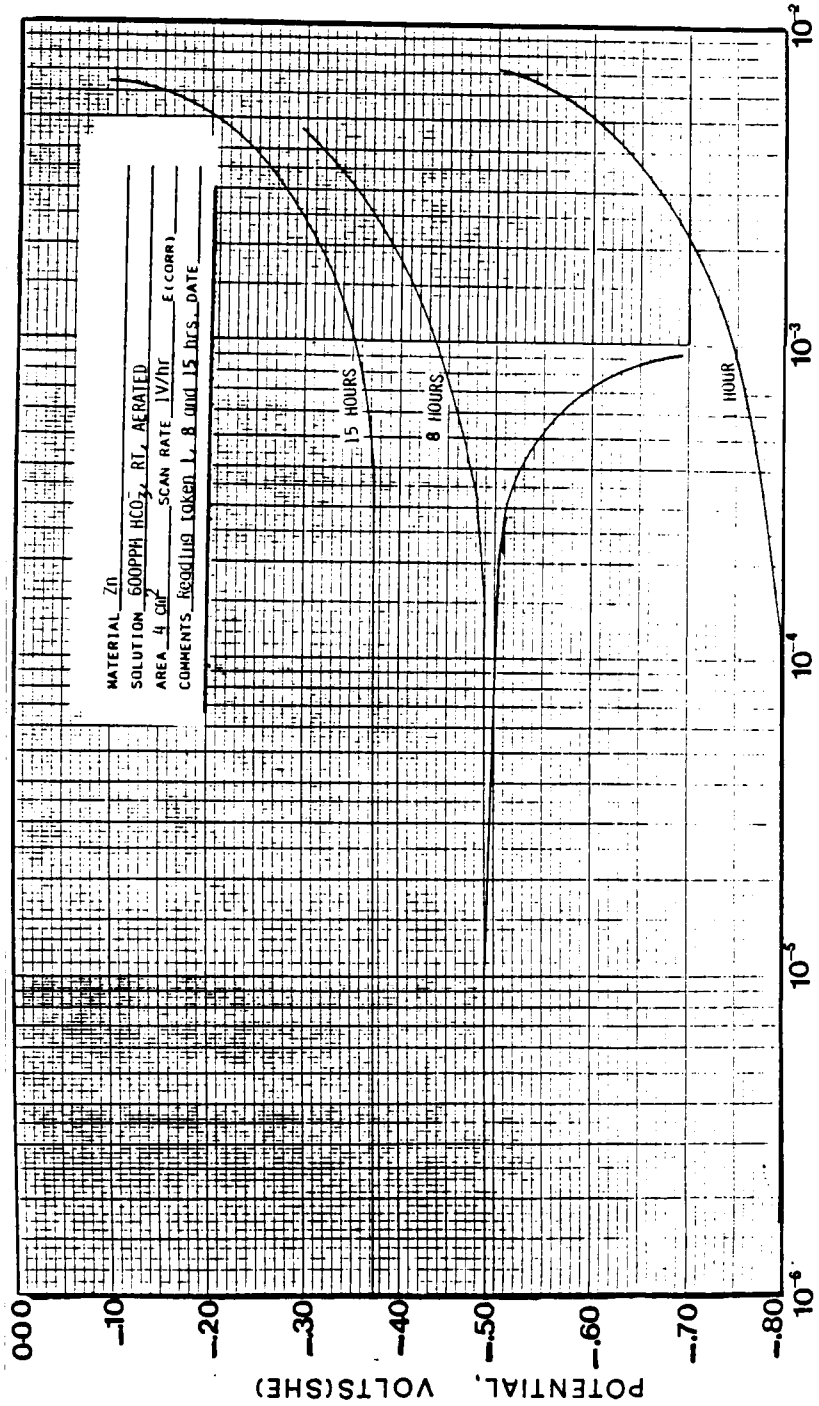


Figure 47. Effect of bicarbonate on the polarization behavior of zinc.

density is estimated to be $10^{-4}$ amperes/$cm^2$ (sample area of 4 $cm^2$), corresponding to a corrosion rate of about 60 MPY. This value is much larger than that determined by weight loss, the latter being 1.4 MPY averaged over a three-week period.

It has not been possible to develop a reasonable correlation between the polarization, potential-time and weight loss measurements, and the SEM observations for the zinc exposed to the bicarbonate. First, it is emphasized that the real nature of the film is not known. X-ray investigations made in this study and discussed earlier indicated the presence of zinc oxide on dried samples. On the other hand, samples removed from the environment and quickly transferred for x-ray examination while the film was still moist produced only broad peaks, indicating amorphous or, at most, poorly developed crystalline material. This makes it difficult to draw very heavily on discussion in the literature proposing that the film is either the oxide, hydroxide, or a carbonate. Evans (33) has proposed that the corrosion behavior of zinc may be controlled by the semi-conducting properties of zinc oxide. However, he is not very specific beyond a general statement and neither Evans or other investigators have presented polarization curves to support an explanation of the corrosion behavior over the pH range investigated in this research. Zinc oxide is a semiconductor and various aspects of its electrochemistry is reported by Morrison (41).

A rather simple model can be advanced consistent with the shift in the anodic polarization curves of Figure 47. It appears that the zinc oxide may be a reasonable electron conductor under the

circumstances involved. While the pure dry oxide is a well defined semiconductor, impurities and defects cause a considerable spread in the energy levels in the material until it behaves as a normal conducting material with reasonable low resistance. Assuming that this is the behavior of the corrosion product film, then as the film forms and spreads, access of the zinc surface to the environment is decreased and assuming that the surface of the oxide can function as a surface supporting the cathodic reaction, then the anode to cathode area is decreasing during corrosion. The effect is represented schematically in Figure 48 where, for a given cathodic polarization curve, the anodic curve is moved progressively to the left proportional to the decrease in the anodic area. The intersections of the shifted anodic curves with the cathodic curve thus lead to an increase in potential. The shift in potential and, in particular the shift in corrosion current will depend in a sensitive way on the shape of the cathodic curve. If this curve is steep, as would be the case with strong diffusion control, then the corrosion current does not change very much with shift in the anodic curve. This follows directly from the fact that under these conditions, the corrosion is under diffusion control of oxygen or some other species. Actually, two factors may move the cathodic curve to smaller values. First, if the corrosion process still involves oxygen reaching the surface, then the film will inhibit this diffusion. A second factor is the decrease in the kinetics of the cathodic reaction on the oxide surface.

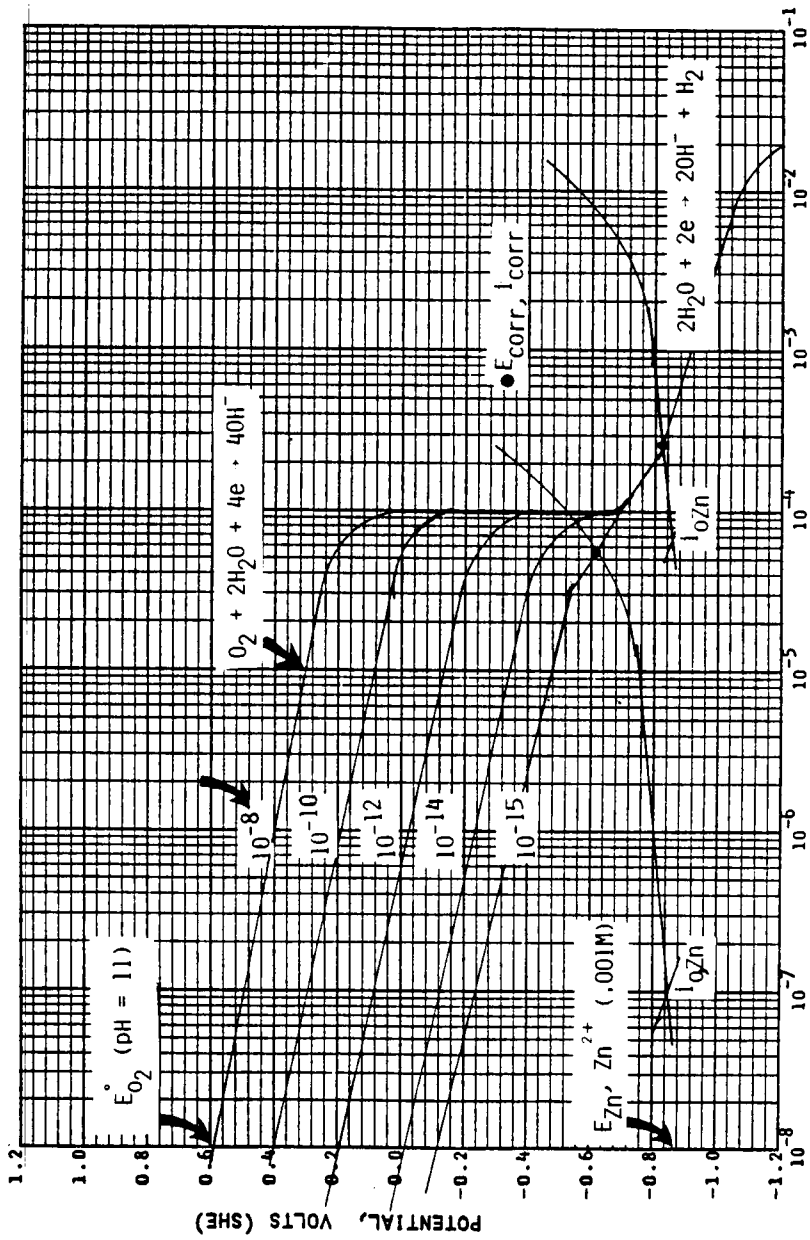


Figure 48. Schematic polarization curves showing influence of relative positions of anodic and cathodic curves on corrosion potential and current.

The above model is also consistent with the cellular structure of the corrosion product film, assuming that its main structural features, observed by SEM on a dried surface, existed when exposed to the environment. The model is also consistent with the observation of some pitting when the film is removed and that the weight losses are reasonably low. The model is not consistent with the observed cathodic polarization curve. The model predicts the anodic curves shown in Figure 48. The cathodic curve in Figure 47 however, remains in diffusion control down to -0.7 volts where the measurement was stopped. This indicates that the cathodic curve reaction for water occurs at lower potentials than that represented in Figure 48.

Although a qualitative correlation can be made between the SEM observations of corrosion product formation on zinc in the several environments and the polarization behavior, the reactions and mechanisms responsible for either the electrochemical behavior or the film formation remained obscure. To provide some insight into this phenomenon, two additional groups of measurements were conducted. One consisted of a series of measurements of the polarization behavior of the zinc over pH range 8-12 in chloride containing solutions. This pH range was selected on the basis of the earlier observations that the pH of the surface of the zinc was of the order of ten in environments having a bulk pH equal to 5-8. Therefore, useful information might be derived from measurements in solutions having bulk pH values equivalent to the interface pH during the corrosion process. The

second set of polarization measurements was pursued to both identify and obtain kinetic information on the cathodic reactions that might be responsible for the corrosion. In some cases, the solution was made 0.001M in $ZnCl_2$ in order to have a specific zinc ion concentration from which the equilibrium half-cell potential could be calculated using the Nernst equation. The pH was adjusted by additions of sodium hydroxide. Another reason for these measurements was based on the Literature Review in which essentially no reference was found in which electrochemical mechanisms were proposed to explain the corrosion potential of the zinc in neutral chloride environments. Since the corrosion potential and current density depends upon both the anodic polarization behavior of the metal and on polarization of supporting cathodic reactions, a series of measurements were undertaken to provide this information.

The cathodic polarization curve on platinum for the stagnant environment containing 0.001M $ZnCl_2$ and pH equal to 11 is shown in Figure 49. A small Tafel range is observed near +0.15 volts corresponding to the reaction $O_2 + 2H_2O + 4e = H_2O$ with an equilibrium half-cell potential near +0.58 volts. At this pH, the exchange current density for the reaction is very low (<10-11) and if any reducible species exist in solution, an open circuit initial potential much lower than this is observed; in this case about +0.25 volts. In the potential range 0.0 to -0.6 volts the current density is very near $10^{-4}$ amps/$cm^2$ which is well established as the limiting diffusion current density for dissolved oxygen. The curve below -0.6 volts is generally assumed to be the direct reduction of water according to

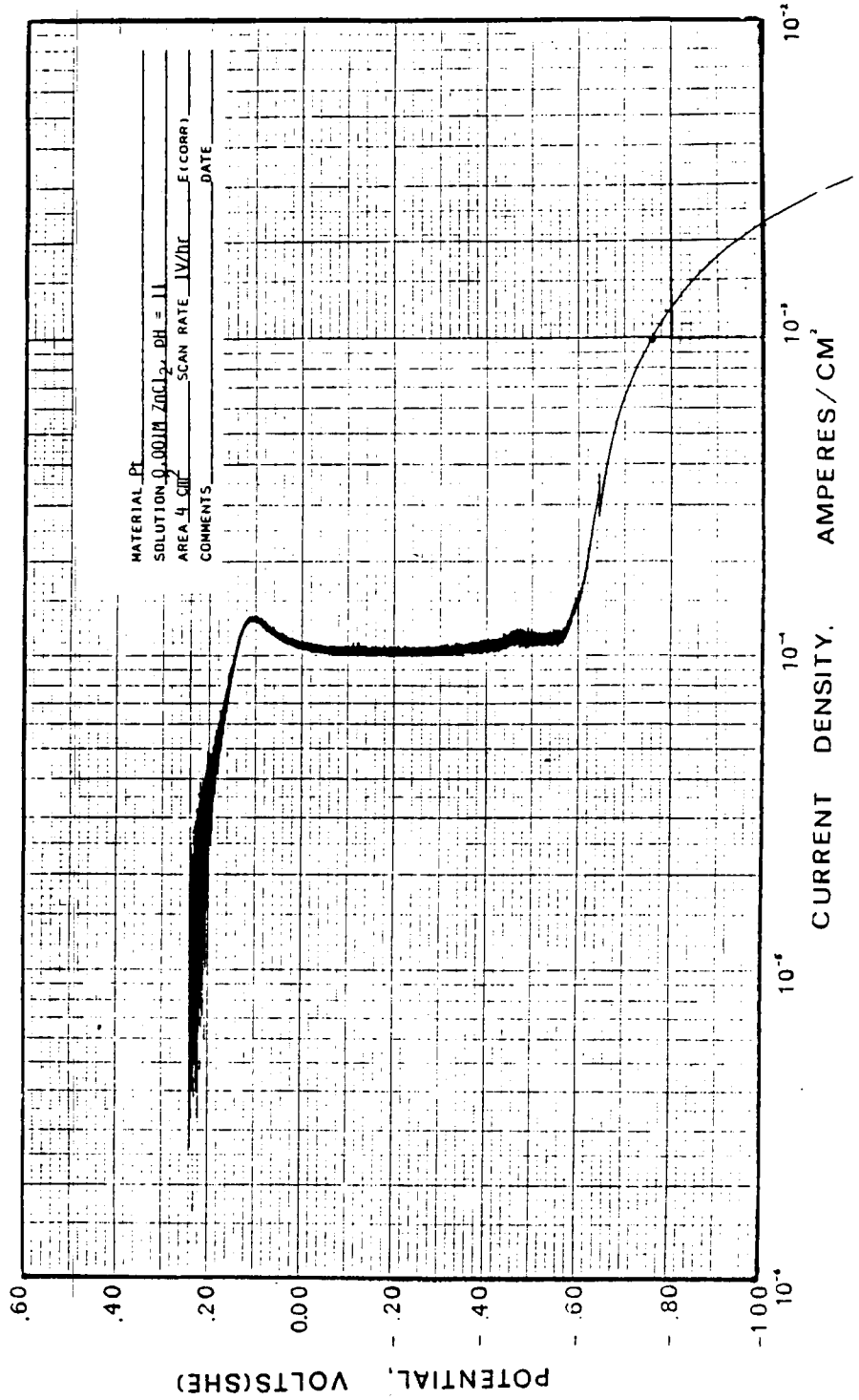


Figure 49. Potentiostatic cathodic polarization curve of platinum.

$2H_2O + 2e = 2OH^- + H_2$. The upper part of this section of the curve shows linear Tafel behavior while the lower part represents a tendency for diffusion control, possibly that of diffusion of hydroxyl ions on the surface.

Figure 50 shows the cathodic curves in the same environment but as recorded on zinc, monel, iron, copper, and platinum. While it was beyond the scope of this investigation to study this behavior in detail, particularly with respect to reproducibility of the curves, they do show that the cathodic polarization involving the reduction of dissolved oxygen and water in the pH range which can exist on the stagnant surface of zinc is very sensitive to the substrate on which the reaction occurs. In the higher potential range shown in the figure, evidence for limiting oxygen diffusion control near $10^{-4}$ amps/cm$^2$ is seen for monel, iron, platinum, and copper. It is significant that the curve for zinc does not exhibit oxygen diffusion control. In fact, a corrosion potential for the zinc of -0.6 volts is observed with both anodic and cathodic polarization curves plotted. This corrosion potential is higher than the corrosion potential of about -0.9 volts shown in Figure 46 (page 106) for 1% NaCl at pH equal to 4.3 and is attributed to the lower chloride and higher pH in Figure 50 permitting formation of a protective corrosion product film. On the other hand, at pH equal to 12, the corrosion potential suddenly decreases to the very low value of -1.12 volts as shown in Figure 5 (page 18). In this case, the anodic curve is again very flat to high current densities, similar to that observed at pH equal to 4.3 in

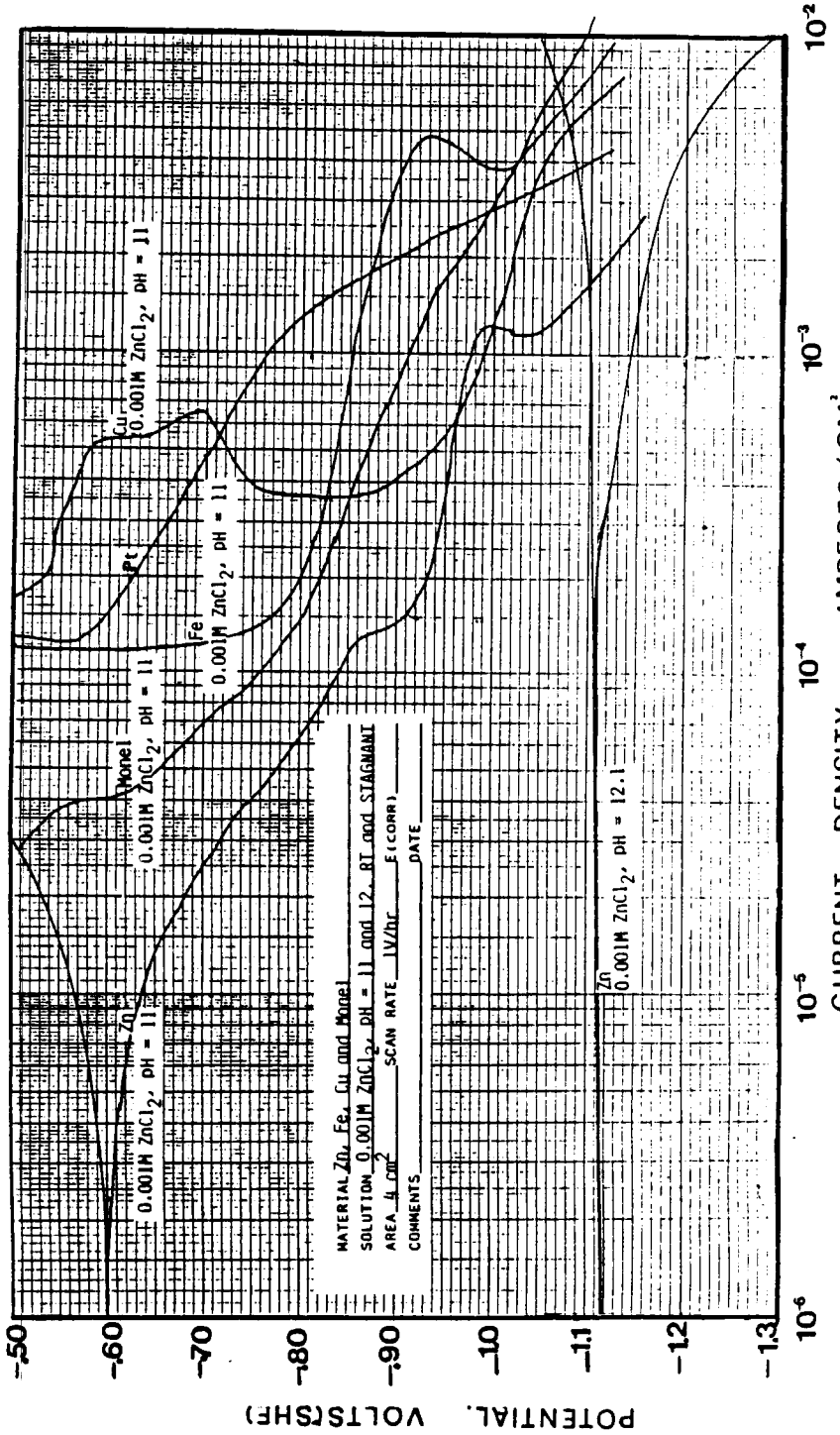


Figure 50. Effect of pH on the cathodic polarization of Zn, Fe, Cu and Monel.

Figure 46, but the cathodic curve extends to higher current densities, and in fact, in the current density range of the cathodic polarization curves observed on the metals indicated in the figure at pH, equal to 11.

These cathodic curves are consistent with extremely low but substrate dependent values of the exchange current densities for the oxygen reaction. The effect of the exchange current density is shown schematically in Figure 51. At pH equal to 11, the equilibrium half-cell potential for oxygen reduction is +0.58 volts as shown. Tafel curves are drawn with a slope of -0.1 volts/log decade for assumed current densities of $10^{-8}$ down to $10^{-15}$ amps/cm$^2$. The limiting diffusion current density is $10^{-4}$ amps/cm$^2$ and the lower part of the curve is due to the direct reduction of water. Just as the substrate can affect the position of the Tafel region for the oxygen reaction, such an effect is expected for the Tafel region for water reduction. Variations in the Tafel region for water reduction however, are not represented in Figure 51. However, variations in the limiting diffusion current density are not represented. These can be due to surface films through which oxygen must diffuse.

Two anodic curves that might be representative of zinc with exchange current densities of $10^{-4}$ and $10^{-7}$ amps/cm$^2$ are also shown. Since the corrosion potential and current is the intersection of pairs of anodic and cathodic curves, it is evident that the values of the latter will be very sensitive to the exact shape and position of the respective curves. On a clean surface with high zinc exchange current density, the intersection will be in the Tafel region for

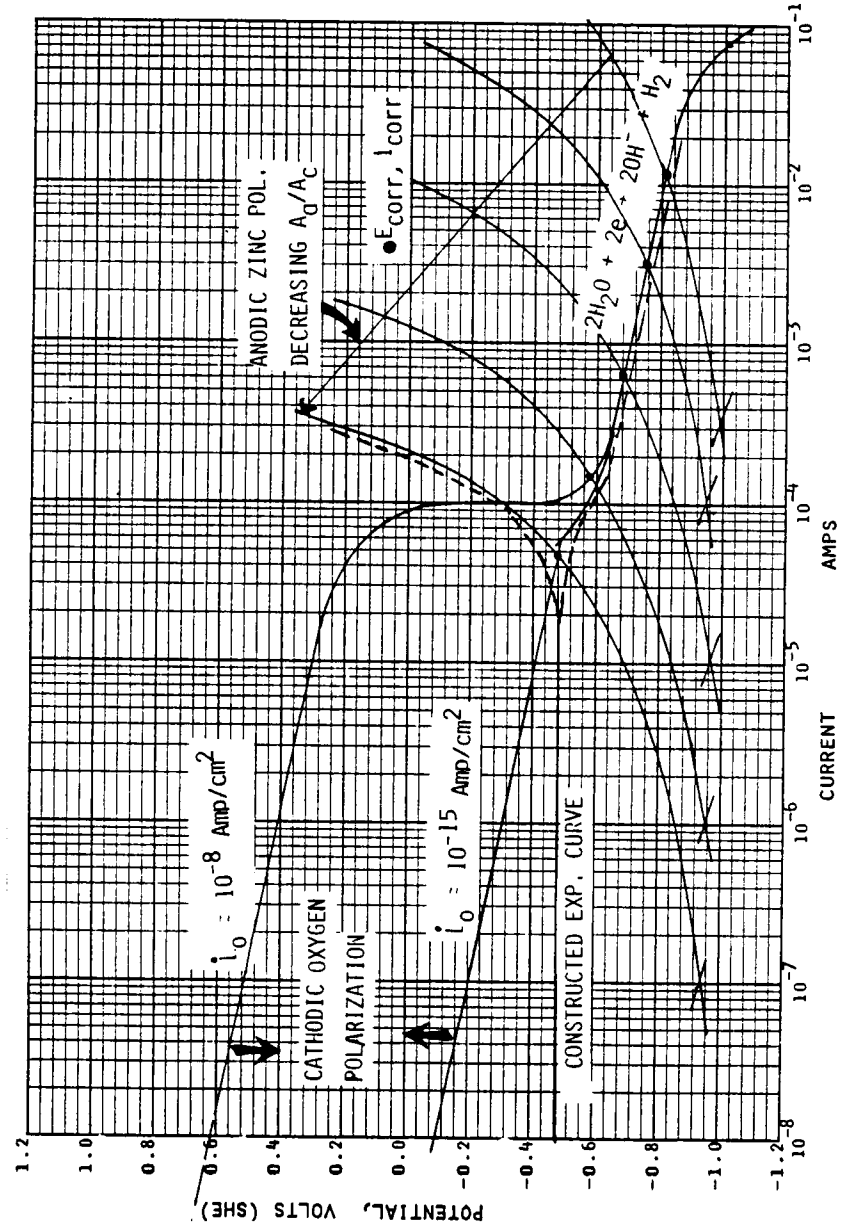


Figure 51. Schematic polarization curves showing effects of anodic/cathodic area ratio on corrosion potential and current (●).

reduction of water, and the direct reduction of water will be the dominant cathodic reaction responsible for the corrosion. On the other hand, any factors shifting the anodic zinc curve to a position representative of the second anodic curve in Figure 51 will result in higher corrosion potentials. The latter situation is plotted schematically in Figure 52 as one of the anodic-cathodic pairs of curves from Figure 51. Also represented is the experimental anodic and cathodic curves expected under these conditions. It is evident that the experimental actually determined for zinc in 0.001M $ZnCl_2$ at pH equal to 11 in Figure 50 and the schematic curve of Figure 52 are similar.

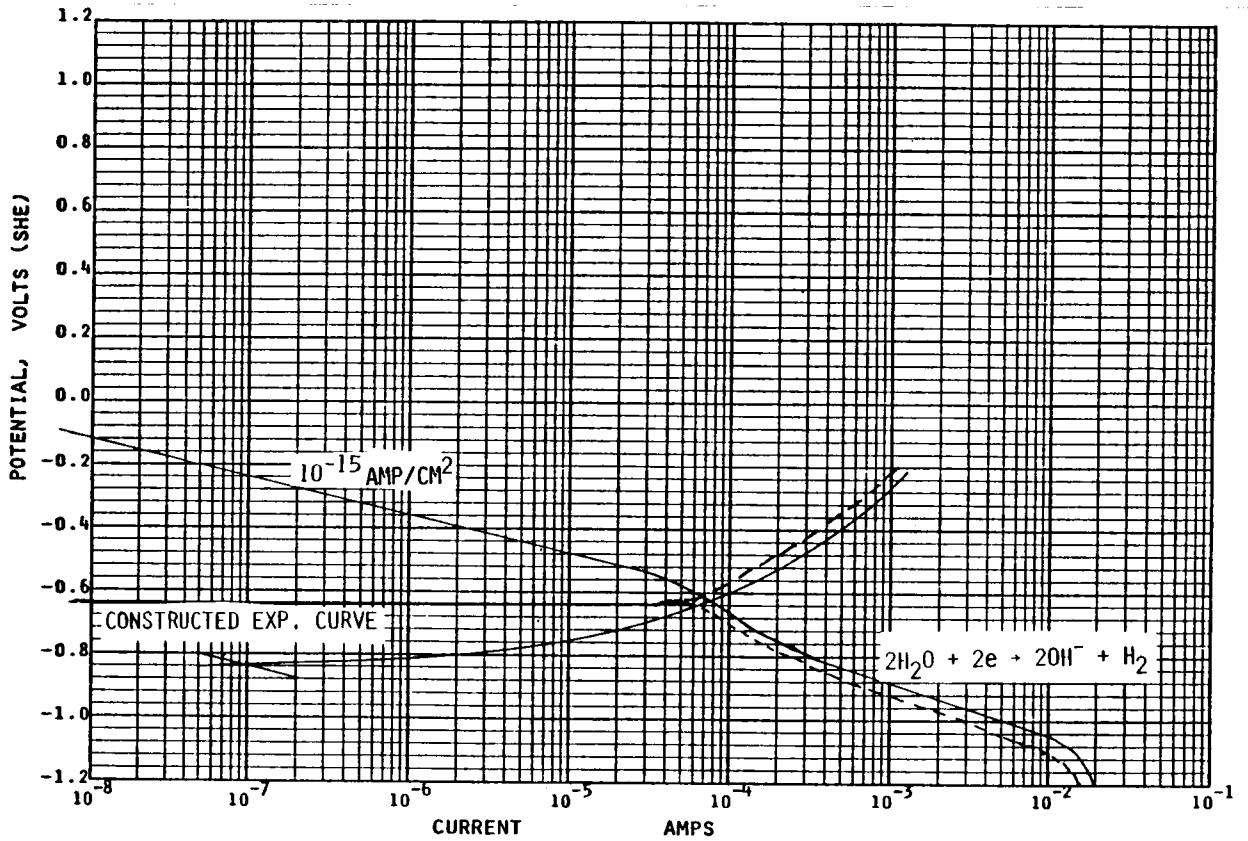


Figure 52. Schematic polarization curves in relative position consistent with observed polarization curves for zinc in solution of 0.001 M $ZnCl_2$ and pH = 11 (see Figure 50).

# CHAPTER 5

## CONCLUSIONS

The results of this investigation allow the following conclusions to be made:

1. The reversal of the zinc potential from anodic to cathodic relative to iron in iron-zinc couples was confirmed in $HCO_3^-$, $CO_3^=$, and $NO_3^-$ solutions. The reversals were attributed to a large increase in the potential of zinc.
2. The time for reversal decreased from 22 hours under deaerated conditions to four hours under aerated conditions. The increase in potential of the zinc was attributed to the formation of a corrosion product film which exhibited a different x-ray pattern when moist but on drying was identified as zinc oxide. Polarization measurements did not produce typical curves of transition to a passive state.
3. The higher zinc potentials are usually accompanied by a severed and highly localized pitting type corrosion.
4. Of the variables studied, no potential reversal occurred in the case of 1% NaCl environment. Whether or not higher zinc potentials are obtained depends both on electrolyte composition and other environmental conditions such as temperature and the degree of aeration. Of these factors, electrolyte composition is the most important.
5. The weight loss measurement showed an increasing rate of attack with increasing time in sodium chloride solutions.

However, in bicarbonate solutions the rate of dissolution of zinc remained almost constant over a three-week period.

6. The corrosion product and substrate morphologies were very dependent on the environment. The oxide film, from bicarbonate solutions, before removing the corrosion product revealed a dense cellular type of structure with protrusions. However, in chloride solutions, the corrosion deposit appears to be flaky, and does not show any cellular structure. Upon removing the corrosion product, after exposure in any environment, a highly localized and crystallographic attack was observed.

7. Potentiostatic polarization measurements provide insight into the corrosion mechanisms responsible for the weight loss, potential-time and surface morphology observations. From the measurements, schematic polarization curves can be constructed predicting the increase in corrosion potential of zinc with time in bicarbonate solution. Schematic curves consistent with experimental observations in chloride solutions indicate a sensitive pH dependence on oxygen diffusion or direct reduction of water being rate controlling cathodic reactions. However, a satisfactory understanding of the measurements did not develop. The polarization measurements did demonstrate that the corrosion mechanisms are quite complex, particularly identification of the cathodic reactions. A factor may be that the very negative

corrosion potential of zinc forces the cathodic reactions to occur at large deviations from their equilibrium potentials. The complexity of the polarization behavior observed in the current research may explain the limited information in the literature on the understanding of the corrosion of zinc in near neutral environments based on electrochemical measurements.

# LIST OF REFERENCES

# LIST OF REFERENCES


1. Uhlig, H., Corrosion Handbook, John Wiley and Sons, Inc., 1948.

2. Henthrone, M., "Corrosion and the Process Plant," J. Chemical Engineering, 1971-1972.

3. Stansbury, E.E., "A Set of Supplement Notes to Met. 3150, Corrosion," Dept. of Chem. and Met. Engineering, Univ. of Tennessee, 1983.

4. Fontana, M.G., and Greene, N.D., Corrosion Engineering, McGraw-Hill Book Co., 1967.

5. "Applachian Underground Corrosion Short Course Notes," West Virginia University, 1982.

6. Morgan, J.H., Cathodic Protection, Leonard Hill Limited, N.W.I., 1959.

7. Steigerwald, R.F., "Electrochemistry of Corrosion," Corrosion, Vol. 24, p. 10, 1968.

8. Stern, M., and Geary, A.L., "Electrochemical Polarization I," J. Electrochemical Soc. Vol. 104, p. 56, 1957.

9. Greene, N.D., "The Classical Potentiostat," Corrosion, Vol. 15, p. 369, 1959.

10. Greene, N.D., "Predicting the Behavior of Corrosion Alloys by Potentiostatic Polarization Methods," Corrosion, Vol. 18, p. 136, 1962.

11. Kurr, G.W., "Cathodic Protection," Materials Performance, Vol. 18, p. 33, 1979.

12. Alvarez, M.G., and Galvele, J.R., "Pitting of High Purity Zinc and Pitting Potential Significance," Corrosion, Vol. 32, p. 285, 1976.

13. Hurlen, T., "Corrosion of Zinc," Acta Chem. Scand., Vol. 16, p. 1347, 1962.

14. Dirkse, T.P., "The Behavior of Zinc Electrode in Alkaline Solutions," J. Electrochemical Soc., Vol. 27, p. 1452, 1980.

15. Dirkse, T.P., "The Behavior of Zinc Electrode in Alkaline Solutions," J. Electrochemical Soc., Vol. 126, p. 1456, 1979.

16. West, J.M., Electrodeposition and Corrosion Processes, D. Van Nostrand Company Limited, Princeton, New Jersey, 1965.

17. Leidheiser, H., Momose, R., and Granata, R.D., "Inhibition of the Cathodic Reaction on Zinc in Aerated 3% Solution," Corrosion, Vol. 38, p. 178, 1982.

18. Leidheiser, H., and Suzuki, I., "Towards a More Corrosion Resistant Galvanized Steel," Corrosion, Vol. 36, 1980.

19. Haney, E.G., "The Zinc-Steel Potential Reversal in Cathodic Protection," Materials Performance, Vol. 14, p. 44, 1982.

20. Hoxeng, R.B., and Prutton, C.F., "Electrochemical Behavior of Zinc and Steel in Aqueous Media," Corrosion, Vol. 5, p. 330, 1949.

21. Bauer, H., and Schikorr, G., "Study of Zinc in Tap Water," Trans. Electrochemical Soc. Vol. 76, p. 247, 1947.

22. Laque, F.L., and Cox, G.L., "Some Observations of the Potentials of Metals and Alloys in Sea Water," Corrosion Science, p. 671, 1947.

23. Maconachie, J.E., Trans. Electrochemical Soc., Vol. 66, p. 220, 1934.

24. Gilbert, P.T., "Paper Presented at Pittsburgh International Congress on Surface Reactions," 1948.

25. Uhlig, H.H., Corrosion and Corrosion Control, 2nd Edition, John S. Wiley and Sons, 1971.

26. Uhlig, H., Triadis, D., and Stern, M., J. Electrochemical Soc., Vol. 102, p. 59, 1955.

27. Pourbaix, M., Atlas of Electrochemical Equilibria in Aqueous Solutions, NACE, 1974.

28. Pourbaix, M., Lectures on Electrochemical Corrosion, Plenum Press, New York, 1973.

29. Delahay, P., Pourbaix, M., and Rysselberghe, P.V., "Potential-pH Diagram of Zinc and Its Application to the Study of Zinc Corrosion," Corrosion, Vol. 98, p. 101, 1951.

30. LaQue, F.L., and Copson, H.R., Corrosion Resistance of Metals and Alloys, Reinhold Publishing Corp., NY, 1963.

31. Hoxeng, R.B., "Electrochemical Behaviour of Zinc and Steel in Aqueous Media--Part II," Corrosion, Vol. 6, p. 308, 1950.

32. Hoare, J.P., The Electrochemistry of Oxygen, John Wiley and Sons, New York, 1968.

33. Evans, U.R., Metallic Corrosion and Passivity and Protection, Longmans, Greer Co., New York, p. 359, 1946.

34. Powers, R.W., "Film Formation and Hydrogen Evolution on the Alkaline Zinc Electrode, J. Electrochemical Soc., Vol. 118, p. 685, 1971.

35. Nagy, Z., and Bockeis, J.O.M., "On the Electrochemistry of Porous Zinc Electrodes in Alkaline Solutions," J. Electrochemical Soc., Vol. 119, p. 1129, 1972.

36. Hurlen, T., "On the Kinetics of the $Zn/Zn^{2+}$ aq. Electrode," Acta. Chem. Scand., Vol. 16, p. 4, 1962.

37. Maconachie, J.E., "Effect of Electrolyte Composition," Trans. Electrochemical Soc., Vol. 66, p. 22, 1934.

38. Schikorr, G., "Corrosion Behavior of Zinc Coatings in the Atmosphere," Werkstoffe U. Corrosion, Vol. 15, p. 543, 1964 (in German).

39. Newberry, E., "Discussion of Maconachie's Papers," Trans. Electrochem. Soc., Vol. 66, p. 220, 1934.

40. Cox, G.L., "The Electrochemical Behavior of Zinc in Distilled Water," Industrial and Eng. Chem., Vol. 23, p. 902, 1931.

41. Morrison, S.R., Electrochemistry at Semiconduction and Oxidized Metal Electrodes, Plenum Press, New York, 1980.

42. Slunder, C.J., and Boyd, W.K., Zinc--Its Corrosion Resistance, International Lead Zinc Research Organization, Inc., 1971.

43. Wahlauist, H.W., Use of Zinc for Cathodic Protection, Vol. 1, p. 119, 1945.

44. Despic, A.R., "Kinetics and Mechanism of Deposition of Zinc from Zincate in Concentrated Alkali Hydroxide Solutions," Chemical Acta, Vol. 21, p. 63, 1976.

45. Breiter, M.W., "Film Formation and Reduction on Zinc Electrodes in Concentrated Potassium Hydroxide Solutions," J. Electrochemical Soc., Vol. 117, p. 738, 1970.

46. Bockris, J.O.M., and Nagy, Z., "On the Deposition and Dissolution of Zinc in Alkaline Solutions," J. Electrochemical Soc., Vol. 119, p. 285, 1972.

47. McKubrie, M.C.H., and Macdonald, D.D., "The Dissolution and Passivation of Zinc in Concentrated Aqueous Hydroxide," J. Electrochemical Soc., Vol. 128, p. 524, 1981.

48. Coates, G.E., "Concentration Polarization in Acid Solutions," J. Electrochemical Soc., p. 484, 1945.

49. Defrancq, J.N., "Zinc and Zinc-Lead Alloys in Domestic Water," British Corrosion Journal, Vol. 17, p. 125, 1982.

50. Brown, R.H., and Mears, R.R., "The Electrochemistry of Corrosion," Trans. Electrochemical Soc., Vol. 74, p. 495, 1935.

51. Pryor, M.J., and Keir, D.S., J. Electrochemical Soc., Vol. 104, p. 269, 1957.

52. Stern, M., "Electrochemical Polarization," J. Electrochemical Soc., Vol. 104, p. 645, 1957.

53. Greene, N.D., France, W.D., and Wilde, B.E., "Electrode Mounting for Potentiostatic Anodic Polarization Studies," Corrosion, Vol. 21, p. 275, 1965.

54. Stern, M., "Surface Area Relationship in Polarization and Corrosion," Corrosion, Vol. 14, p. 329, 1959.

55. Vetter, K.J., Electrochemical Kinetics, New York Academic Press, 1967.

56. Greene, N.D., Experimental Electrode Kinetics, Rensselaer Polytechnic Institute, Troy, New York, 1965.

57. Foroulis, Z.A., "Proceedings of the Fifth International Congress on Metallic Corrosion," 1942.

58. Whitman, W., Russell, R., and Altieri, V., Industrial Engineering, Vol. 16, p. 665, 1924.

59. Speller, F.N., Corrosion--Causes and Prevention, Third Ed., McGraw-Hill Book Co., New York, 1951.

60. Fontana, M.G., and Staehle, R.W., Advances in Corrosion Science and Technology, Vol. 4, Plenum Press, New York, 1970.

61. Hill, R.F., and Harries, D.R., Chemical and Process Engineering, 1960.

62. Brasunana, A.S., and Stansbury, E.E., "Symposium on Corrosion Fundamentals," The University of Tennessee Press, pp. 84-92, 1956.

63. Baboian, R., France, W.D., Rowe and Rynewics, L.C., Galvanic and Pitting Corrosion, ASTM 576, 1974.

64. Shams El Din, A.M., and Kuhn, A.T., "Pitting Corrosion of Zinc in Aqueous Solutions," British Corrosion, Vol. 15, p. 208, 1980.

65. Hubbard, D.J., and Shanahan, C.E.A. Br., Corrosion, Vol. 8, pp. 270-275, 1973.

# VITA

Mussie Wossene was born in Addis Ababa, Ethiopia on December 9, 1954. He completed his elementary and high school education in Addis Ababa.

The author came to the United States in the winter of 1974 and earned his Bachelor of Science degree in the field of Chemistry at Southeastern Oklahoma State University in 1977. He was initially employed with Johnson and Johnson Company, Arlington, Texas. In September 1979 he joined Exxon Petrochemical Company, Houston, Texas. In winter, 1982, he entered the Graduate School of The University of Tennessee, Knoxville.

The author is a member of the American Chemical Society, the National Association of Corrosion Engineers, the Metallurgical Society of AIME and the American Welding Society.